126p

An Analysis of the Second Project High Water Data

Report No. 02.01
(NASA Contract NAS 10-841)
Launch Operations Center
National Aeronautics and Space Administration

(NASA CR-52970; Rept. 02.01)

~~Dr.~~ David D. Woodbridge,
~~Dr.~~ James A. Lasater,
~~Mr.~~ Bennett M. Fultz,
~~Mr.~~ Richard E. Clark, and
~~Miss~~ Nancy Wylie

October ~~25,~~ 1963 126 p Refs

No code:
Corp. author:
International Space Corporation
1080 "B" Street
P. O. Box 395
Melbourne, Florida

An Analysis of the Second Project High Water Data

Report No. 02.01

Contract NAS 10-841

Launch Operations Center

National Aeronautics and Space Administration

Dr. David D. Woodbridge
Dr. James A. Lasater
Mr. Bennett M. Fultz
Mr. Richard E. Clark
Miss Nancy Wylie

October 25, 1963

International Space Corporation
1080 "B" Street
P. O. Box 395
Melbourne, Florida

ABSTRACT

10645

An analysis has been performed of the optical, ELF-VLF, radiofrequency, and radar data obtained in conjunction with the second Project High Water experiment. The results of the analysis have been combined with laboratory studies of the release of water at reduced pressures and telemetry performance evaluation. Extensive cross correlations were found and these cross correlations present a consistent representation of the physical conditions present in the ionosphere. The results of this analysis are divided into three (3) categories which are: (a) the expansion of the water-ice cloud, (b) the development of an onboard fire, and (c) ionospheric attenuations of telemetry and radar transmissions. The release of the water caused the development of a "cloud" which expanded turbulently with an initial average expansion rate velocity of 1.05 km/sec; however, expansion rate velocities as high as 3.60 km/sec were observed. Extensive cooling was also encountered with the water release. The estimated temperature of the cloud was -110°C. Conclusive evidence was found that an onboard fire developed following Project High Water. This onboard fire persisted during the major portion of the descent time. Definite evidence was found that inhomogeneous regions in the ionosphere produce severe attenuations of telemetry and radar transmissions. The attenuation effects were found to be both frequency and directional sensitive. Electromagnetic observations provided a technique for establishing the location of the inhomogeneous regions of the ionosphere.

Author

TABLE OF CONTENTS

LIST OF FIGURES

TABLE

LIST OF TABLES

1.0 INTRODUCTION

Early in 1962 NASA established "Project High Water" to investigate the sudden release of large quantities of water into the upper atmosphere. The primary objectives of these experiments were to obtain information on the behavior of liquids released in the ionosphere and the localized effects on the ionosphere produced by the injection of large quantities of water. The data obtained in the two (2) Project High Water experiments have yielded an extensive amount of information concerning the complex phenomena associated with the sudden release of liquids in the ionosphere. The detailed analysis of data obtained during the second Project High Water experiment (i.e., the third Saturn I vehicle test or SA-3) presented in this report demonstrates that the objectives of the Project High Water were achieved. In addition, the Project High Water has provided essential information relevant to a number of problems vital to manned explorations of space.

This presentation is based on an analysis of (motion picture) photographic data, radar tracking data, "RF noise" observations, WWV reception data, and ELF-VLF spectral observations conducted during the SA-3 Project High Water. These data were combined with SA-3 telemetry evaluations and laboratory studies of water released at simulated ionospheric conditions. Since an extensive amount of data was analyzed, it was necessary to restrict the original data contained in

this presentation to only that which illustrated significant aspects of the study.

The second Project High Water data (SA-3) yielded the following results:

1. Detailed knowledge of the dispersal of large quantities of liquids in space. This permits the determination of first order engineering parameters associated with an abort or explosion in space.

2. Data on the time interval radar track and telemetry will be lost following an abort or explosion in space.

3. Cognition of the interactions between water and the ionospheric environment.

4. Conclusive evidence of a fire in the tankage section of the Saturn vehicle following Project High Water.

5. Direct evidence of inhomogeneous regions in the ionosphere. Degredation of telemetry and radar beacon dropouts correlated with vehicular encounters with these inhomogeneous regions.

A large portion of the results of Project High Water have direct applications to operational problems. However, a considerable amount of valuable scientific knowledge was also obtained concerning liquid behavior at reduced pressures and concerning ionospheric inhomogeneities.

2.0 RELEASE OF LIQUIDS IN THE IONOSPHERE

Studies of the release of large quantities of water in the ionosphere are of considerable practical importance as well as theoretical significance. One of the more obvious aspects is that an abort (or explosion) of a liquid propelled spacecraft in the ionosphere must necessarily result in the release of large quantities of liquids into the ionosphere. Therefore, the behavior of a liquid following the release has two pertinent phases. The behavior of liquid propellants immediately following the release will determine the "mixing efficiency" and the explosion hazard associated with an ionospheric abort. The initial liquid behavior will also have produced telemetry and tracking effects since a liquid forms a visible cloud before it vaporizes. A second important aspect is the "long term" effects produced by the nonequilibrium conditions created. A wide variety of speculations were advanced prior to the Project High Water experiments, especially as to electromagnetic effects. Both attenuations and enhancements (or emissions) of electromagnetic signals have been found to be associated with the second Project High Water experiment (i.e., SA-3).

2.1 PROJECT HIGH WATER EXPERIMENTS

Two (2) Project High Water operational experiments have been performed. The first water release occurred in April 1962 at an altitude of 105 km (SA-2), and the second release was in November 1962 at an altitude of 165 km (SA-3). The US Standard Atmosphere (1962) gives the atmospheric pressure at

105 km at 1.3×10^{-4} torr (mm of Hg), and 2.4×10^{-6} torr at 165 km.

In the second Project High Water experiment, a total of 87,414 kg of water was released. This water was ballast in the upper stages of the third Saturn I vehicle (SA-3); the S-IV dummy second stage carried 41,102 kg, and the S-V dummy third stage carried 46,312 kg (Ref. 1). The water release was achieved by activating the vehicle destruct system. In the case of the dummy second stage, the water was contained in an inner tank. This inner tank was ruptured and four (4) 56 inch by 80 inch ports were simultaneously cut in the outer tank.

Although the same quantity of water is believed to have been released at 165 km, the visible cloud persisted for a much longer period of time with the 105 km release. The shorter persistence of the visible cloud was predicted (by the authors) on the basis of previous theoretical and laboratory studies (Ref. 2, 3).

From a scientific standpoint, the Project High Water experiment provided data that can not be obtained in any other manner. At the present time, it is not possible to duplicate ionospheric conditions in the laboratory. Certain aspects (e.g., pressure) can be attained, but the complex ion-electron, solar radiation, and volumetric conditions are beyond present technological capabilities. Laboratory studies under known and controlled conditions are manditory for the proper interpretation of the Project High Water data.

However, the detailed dynamics of the "cloud" can only be ascertained from large-scale, unconfined experiments. The internal cloud dynamics are the dominant factor in the mixing efficiency and telemetry/tracking effects, whereas the external dynamics control the dispersal rate and ionospheric interactions. The external cloud dynamics and ionospheric interactions contributed data which permits an improved representation of the ionospheric structure. Although information concerning the ionosphere is rapidly being developed, knowledge is still imperfect. For example, present techniques and theories do not provide an adequate representation of either the vertical or horizontal inhomogeneities.

2.2 IONOSPHERIC RELEASE OF WATER

The release of large quantities of water into the ionosphere presents many interesting phenomena. Laboratory studies have shown that the initial process which occurs following the (vacuum) release is the body of water disintegrating into a multiplicity of fine droplets of water (Ref. 2). Evaporative cooling (due to the reduced pressure conditions) rapidly converts the droplets into ice. The ice particles then sublime. Extensive cooling in the vicinity accompanies the water release. Therefore, the initial processes of the phenomena result in the conversion of the water from the liquid phase into the vapor phase.

In the second Project High Water experiment, the visible cloud expanded to a diameter of approximately 9 km. Therefore, the condensed phases of water (i.e., liquid or solid)

traversed an ionospheric volume of the order of 400 km^3. The water vapor will pervade a much larger region since it will continue to diffuse after the condensed phases disappear.

Interactions between the water and the ionospheric environment will be initiated with the release. The specific reactions which occur will depend on the physical state of the water present. That is, the reactions between the liquid/solid phases and the ionospheric environment will not be identical with the reactions between water vapor and the ionospheric environment. Thus, the release of water into the ionosphere initiates a complex series of physical and chemical phenomena. Ultimately, the water (vapor) will become dissociated by the action of energetic ionospheric particles (electrons and ions) and solar radiation (ultraviolet). The end result of the complex series of physical/chemical processes will be the creation of positive ions and electrons.

Charged particles (electrons and ions) in a magnetic field possess an intrinsic spin. Under the conditions of their creation, the number of charged particles in the higher energy spin states will exceed equilibrium distribution. Therefore, as the excess number of particles tend toward the lower energy states, they will radiate energy. The frequency of this radiation will be determined by the quantum conditions of the individual particles (Ref. 4). Radiations from positive particles (ions) in the earth's magnetic field will have frequencies in the extra-low-frequency (ELF) and the very-low-frequency (VLF) portion of the electromagnetic

spectrum, and radiation from electron spin transitions in the earth's magnetic field will have frequencies in the megacycle range.

2.3 HYDRODYNAMICS OF EXPANDING LIQUIDS

Formulation of a theory for liquid expansion at reduced pressures can be developed from hydrodynamic-thermodynamic considerations. This approach provides an expression for the density of the expanding liquid. A number of physical parameters such as surface temperature, vapor pressure, viscosity, and initial density are relevant to the expansion. For the initial formulation of a theory for the expansion of liquids at reduced pressures, phase changes have been neglected. Future theoretical investigations should incorporate these important effects. The ability of any density expression to predict the rate of rarefaction of a specific liquid depends on the values chosen for the above-mentioned parameters.

Consider a spherical mass of fluid initially at rest in a region of zero pressure. At time t=0 the restraining membrane is instantaneously removed allowing the fluid to expand into the evacuated region. It is assumed for reasons of simplicity that the expansion is spherically symmetric. Vaporization effects are neglected, and the expansion is considered adiabatic. Euler's equation for hydrodynamic flow is

$$\rho \frac{d^2\vec{r}}{dt^2} = \rho\vec{g} - \nabla P \qquad (1)$$

where

$\rho = \rho(r, t)$ density

$\vec{r}$ = position vector
$\vec{g}$ = gravitational acceleration
P = pressure of the flow

The equation of continuity from hydrodynamics is

$$\frac{\partial \rho}{\partial t} + \nabla \cdot (\rho \dot{r}) = 0 \qquad (2)$$

Equation (2) represents the flow through a volume bounded by an arbitrary surface in the flow region. Since the fluid flow is due to the expansion, it is certainly a nonequilibrium event. Therefore, equation (2) for this problem must be re-interpreted as

$$\frac{\partial \rho}{\partial t} + \nabla \cdot (\rho \dot{r}) = -k\rho \qquad (2')$$

where k is the "growth factor". (Note that the upper bound for the growth factor is k=0.) Insertion of the First Law of Thermodynamics gives

$$Q = S\frac{dT}{dt} + P\frac{d(1/\rho)}{dt} \qquad (3)$$

where

Q = energy added
S = specific heat
T = absolute temperature
P = pressure of the flow
ρ = density

For an adiabatic expansion, Q=0 and equation (3) becomes

$$Q = 0 = S\frac{dT}{dt} + P\frac{d(1/\rho)}{dt} \qquad (3')$$

The divergence of a function in spherical coordinates can be expressed as

$$\nabla \cdot F = \frac{1}{r^2}\frac{\partial (r^2 F_r)}{\partial r} + \frac{1}{r \sin\phi}\frac{\partial (F_\phi \sin\phi)}{\partial \phi} + \frac{1}{r \sin\theta}\frac{\partial F_\theta}{\partial \theta} \qquad (4)$$

where

r = radius of a sphere
ϕ = azimuth angle
θ = elevation angle
F = function

Applying this concept in equation (2'), the div(ρr) for the spherically symmetric event is

$$\nabla\cdot(\rho r) = \frac{1}{r^2}\frac{\partial(r^2\rho\dot{r})}{\partial r} = \frac{1}{r^2}(2r\rho\dot{r}) + \frac{r^2}{r^2}\dot{r}\frac{\partial\rho}{\partial r} + \rho\frac{\partial\dot{r}}{\partial r} \quad (5)$$

Now if $(\partial\rho)/\partial r = \rho r$ during the initial phases of the expansion, and $\partial\dot{r}/\partial r = 0$, then

$$\nabla\cdot(\rho r) = \frac{2\rho\dot{r}}{r} + \dot{r}\rho r \quad (5')$$

Equation (2') thus becomes

$$\frac{\partial\rho}{\partial t} + \frac{2\rho\dot{r}}{r} + \dot{r}\rho r + \rho k = 0 \quad (6)$$

Solving equation (3') for the pressure and setting $S\frac{\partial T}{\partial t} = Z$

$$P = \frac{-Z}{\frac{d(1/\rho)}{dt}} = \frac{Z\rho^2}{\dot{\rho}} \quad (7)$$

The gradient of a function $\underline{f}$ in spherical coordinates may be expressed as

$$\nabla f = \mu_r\frac{\partial f}{\partial r} + \mu_\phi\frac{1}{r}\frac{\partial f}{\partial\phi} + \mu_\theta\frac{1}{r\sin\phi}\frac{\partial f}{\partial\theta} \quad (8)$$

where the μ's are the spherical unit vectors. Thus, the gradient of P becomes

$$\nabla P = \nabla\left(\frac{Z\rho^2}{\dot{\rho}}\right) = 2Z\rho\frac{\partial\rho}{\partial r}\dot{\rho}^{-1} - Z\rho^2\dot{\rho}^{-2}\frac{\partial\dot{\rho}}{\partial r} \quad (9)$$

As previously $\partial\rho/\partial r = \rho r$ and $\partial\rho/\partial r = 0$. Thus,

$$\nabla P = \frac{2Z\rho^2 r}{\dot{\rho}} \quad (9')$$

Equation (1) thus becomes

$$\frac{d^2r}{dt^2} - g = -\frac{2Z\rho^2 r}{\dot{\rho}} \qquad (10)$$

Assuming the intrinsic acceleration of the expansion is constant, set

$$\frac{d^2r}{dt^2} - g = a$$

Adding equations (6) and (10) produces

$$\dot{\rho}a + 2Z\rho r + \dot{\rho} + \frac{2\rho\dot{r}}{r} + \dot{r}\rho r + \rho k = 0 \qquad (11)$$

Applying the Bernoulli separation method and assuming the density may be represented in a product of a position function and a time function, then

$$\rho = \rho(r, t) = R_{(r)}\, T_{(t)} \qquad (12)$$

Substituting equation (12) in (11) yields:

$$R_{(r)}\frac{\partial T_{(t)}}{\partial t}(a) + 2Z\frac{\partial R_{(r)}}{\partial r}T_{(t)} + R_{(r)}\frac{\partial T_{(t)}}{\partial t} + \frac{2R_{(r)}\,T_{(t)}\,\dot{r}}{r} + \dot{r}\,T_{(t)}\frac{\partial R_{(r)}}{\partial r} + k\,R_{(r)}\,T_{(t)} = 0 \qquad (13)$$

Dividing by $R_r T_r$

$$\frac{a}{T}\frac{\partial T}{\partial t} + \frac{2Z}{R}\frac{\partial R}{\partial r} + \frac{1}{T}\frac{\partial T}{\partial t} + \frac{2\dot{r}}{r} + \frac{\dot{r}}{R}\frac{\partial R}{\partial r} + k = 0 \qquad (14)$$

or

$$\frac{a}{T}\frac{\partial T}{\partial t} + \frac{1}{T}\frac{\partial T}{\partial t} + k = -\left[\frac{2Z}{R}\frac{\partial R}{\partial r} + \frac{\dot{r}}{R}\frac{\partial R}{\partial r} + \frac{2\dot{r}}{r}\right] = \mu \qquad (15)$$

Converting to total differential equations

$$\left(\frac{1+a}{T}\right)\frac{dT}{dt} - \mu = 0 \qquad (16a)$$

$$\left(\frac{2Z+\dot{r}}{R}\right)\frac{dR}{dr} + \frac{2\dot{r}}{r} + k + \mu = 0 \qquad (16b)$$

Solving equation (16a) gives

$$T = T_o \exp\left[\frac{\mu t}{a + 1}\right] \qquad (17a)$$

and equation (16b) gives

$$R = R_o \exp -\left[\frac{k(r-r_1) + \mu(r-r_1) + 2\dot{r}(\ln r - \ln r_1)}{2Z + \dot{r}}\right] \qquad (17b)$$

finally as

$$\rho = \rho(r, t) = R_{(r)}\, T_{(t)} \qquad (12)$$

equations (17a) and (17b) must be multiplied together to give

$$\rho = \rho_o \exp\left[\frac{\mu t}{a + 1} - \frac{k(r-r_1) + \mu(r-r_1) + 2\dot{r}(\ln r - \ln r_1)}{2Z - \dot{r}}\right] \qquad (18)$$

The expansion depends significantly on the function $Z = S\frac{dT}{dt}$.

Expansion of a liquid with a small change in temperature, that is, with no phase change will occur very rapidly. Conversely, high Z (rapid temperature change) implies large changes in internal energy, thus causing slower expansion.

2.4 LABORATORY EXPERIMENTS

Laboratory experiments simulating the release of water into the ionosphere have been carried out in a Space Environment Simulator (SES). One of these tests is briefly described and the results obtained in these studies are summarized (Ref. 2). In the SES studies, small glass bulbs containing from one (1) to five (5) cubic centimeters (cc) of water were broken in the vacuum chamber of the SES. This chamber had a (free space) volume of approximately 3.23×10^7 cc. Thus,

the required sudden and reasonably unrestricted expansion of the water was achieved. These tests were performed with ambient pressures within the SES ranging from 1.1×10^{-4} torr to 2.0×10^{-3} torr. High-speed motion pictures were made of the release phenomena. Temperatures were recorded by means of thermocouples located adjacent to the glass bulbs and the inner wall of the SES. The chamber pressure was continuously monitored throughout the test operations.

Expansion of the water and sublimation of the ice particles were so rapid that the events could not be followed visually (naked eye). However, high-speed motion picture records provided an excellent time-history of the breakup of the water into droplets, the subsequent freezing, and sublimation. Figure 1 shows a set of four frames from the high-speed motion picture records of the release of 3.0 cc of water in the SES. The timing of the frames are, respectively, 1, 10, 20, and 30 milliseconds from the time the glass bulb was ruptured. The pre-release chamber pressure was 1.4×10^{-4} torr. Following the release, the chamber pressure rose to 3.2×10^{-2} torr. The thermocouple adjacent to the bulb recorded a temperature drop of $38^{\circ}C$.

An examination of the film records showed that the water emerged as a multiplicity of minute droplets. These droplets rapidly dispersed. A portion of the droplets were converted to ice particles. Freezing of the droplets probably commenced almost immediately. A significant fraction of the droplets froze within five (5) milliseconds, and after 10 milliseconds, all of the remaining droplets were frozen.

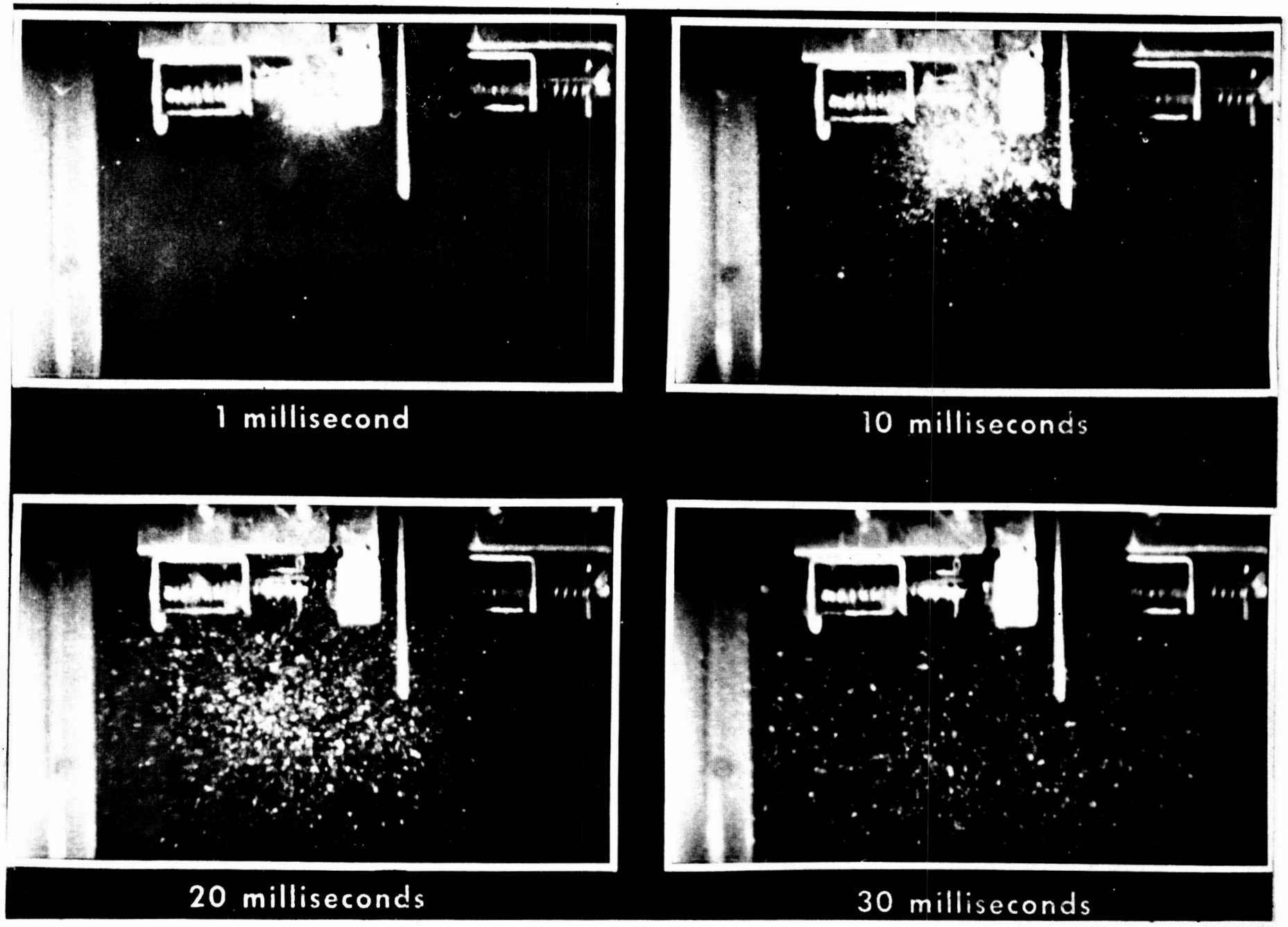

Figure 1: High Speed Photographs of Laboratory Release of 3.0 cc Water at a Pressure of 1.4×10^{-4} torr.

Between 10 and 20 milliseconds there was an apparent "growth" in the size of the ice particles. After 20 milliseconds the particle size rapidly decreased with all (visible) particles absent after 51 milliseconds.

If the increase in the ice particle size represents an increase in the actual particle mass, the increase was a result of the vapor pressure of the ice particle being less than the actual pressure of the water vapor in the vicinity of the particle. The other possible explanation for the increase in size of the particles is that the solid particle expanded to an "open lattice structure". There was no evidence of agglomeration of ice particles. On the basis of the available evidence, it is believed that the increase in the size of the ice particles is a consequence of "condensation" of water vapor on the subcooled ice particles. The same general particle size pattern was repeated in all of the water release studies. It is probable that this same general particle size variation will occur for all liquids which form a solid phase when released.

The rise in pressure (1.4×10^{-4} to 3.2×10^{-2} torr) has more significance when the size of the test sample (3.0 cc) is compared to the volume of the SES (3.23×10^{7} cc). That is, the volumetric ratio is approximately 10^{7}. The pressure rise in the SES was essentially instantaneous with the rupture of the bulb. This pressure rise was experienced with the vacuum pumps operating. Therefore, the sudden release of sizeable quantities of liquids in the ionosphere

or space will produce a pressure effect throughout a tremendous volume.

Thermocouples adjacent to the glass bulb show a high rate of cooling occurred as the water expanded. Temperature records indicate an almost instantaneous drop in temperature with the release of water. The observed temperature drop increased with the size of the water sample. That is, the 3.0 cc sample produced a 38°C drop, and a 66°C drop was recorded with a 4.5 cc sample as shown in Figure 2. Zero time in this figure is the instant the glass bulb was ruptured. The instant the water was released, the equilibrium vapor pressure (15.5 torr) was several orders of magnitude greater than the ambient chamber pressure (1.4×10^{-4} torr). Vaporization of the water cools the droplets until ice is formed. The ice rapidly sublimes because of the great difference between the equilibrium vapor pressure and the ambient pressure. The equilibrium vapor pressure over ice as a function of temperature is shown in Figure 3. As long as the condensed phases of a liquid are present, evaporative or sublimation cooling will occur. When large quantities of a liquid are released, there will be a sharp decrease followed by a slower decline. As a first approximation, the sharp temperature drop will be to a temperature where the equilibrium vapor pressure of the stable condensed phase has a vapor pressure equal to the ambient pressure. Using this approximation, the temperature of the first Project High Water cloud is estimated to have been -80°C, and the second Project High Water cloud is estimated to have been -110°C.

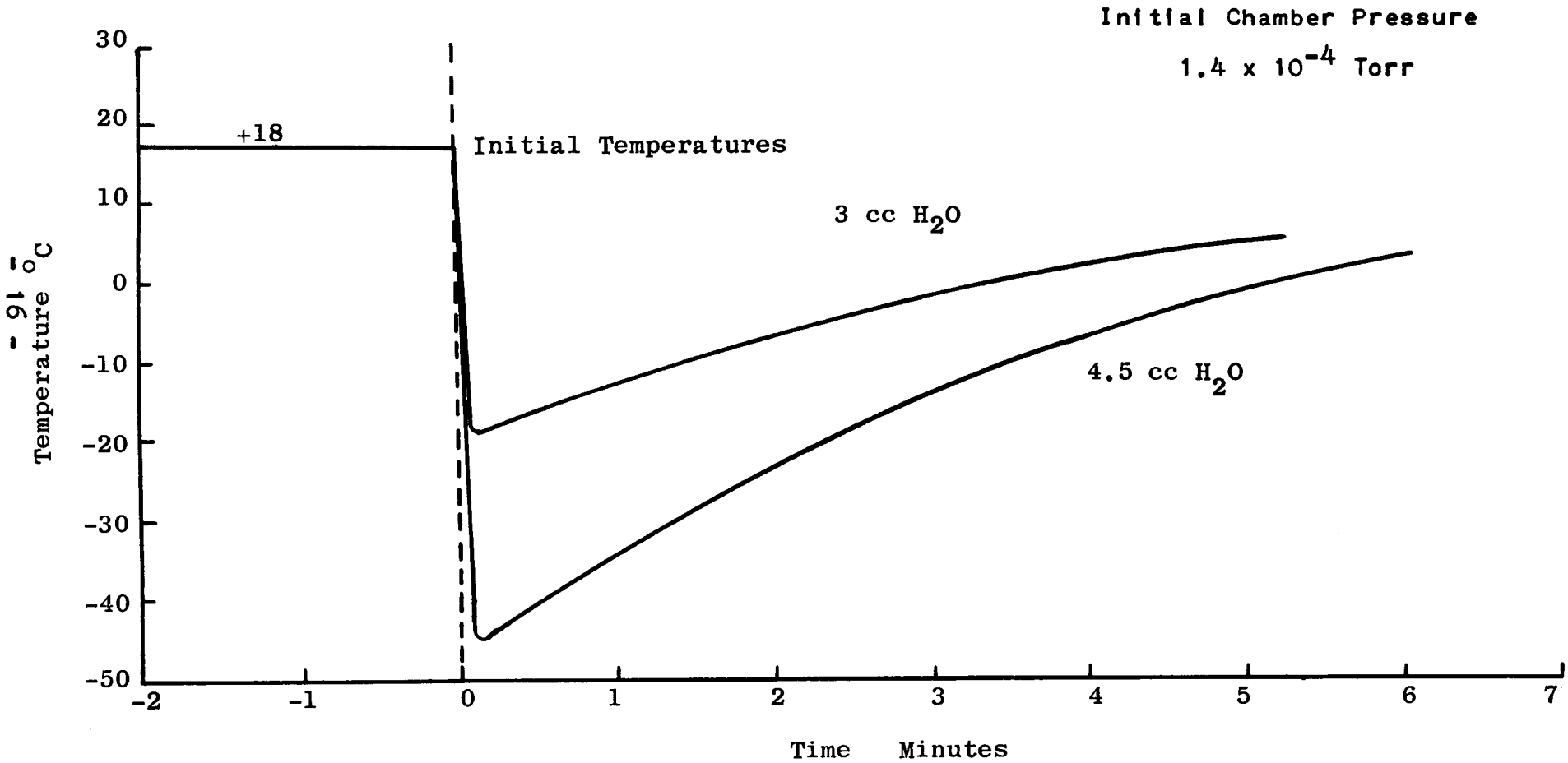

Figure 2. Thermocouple Temperatures

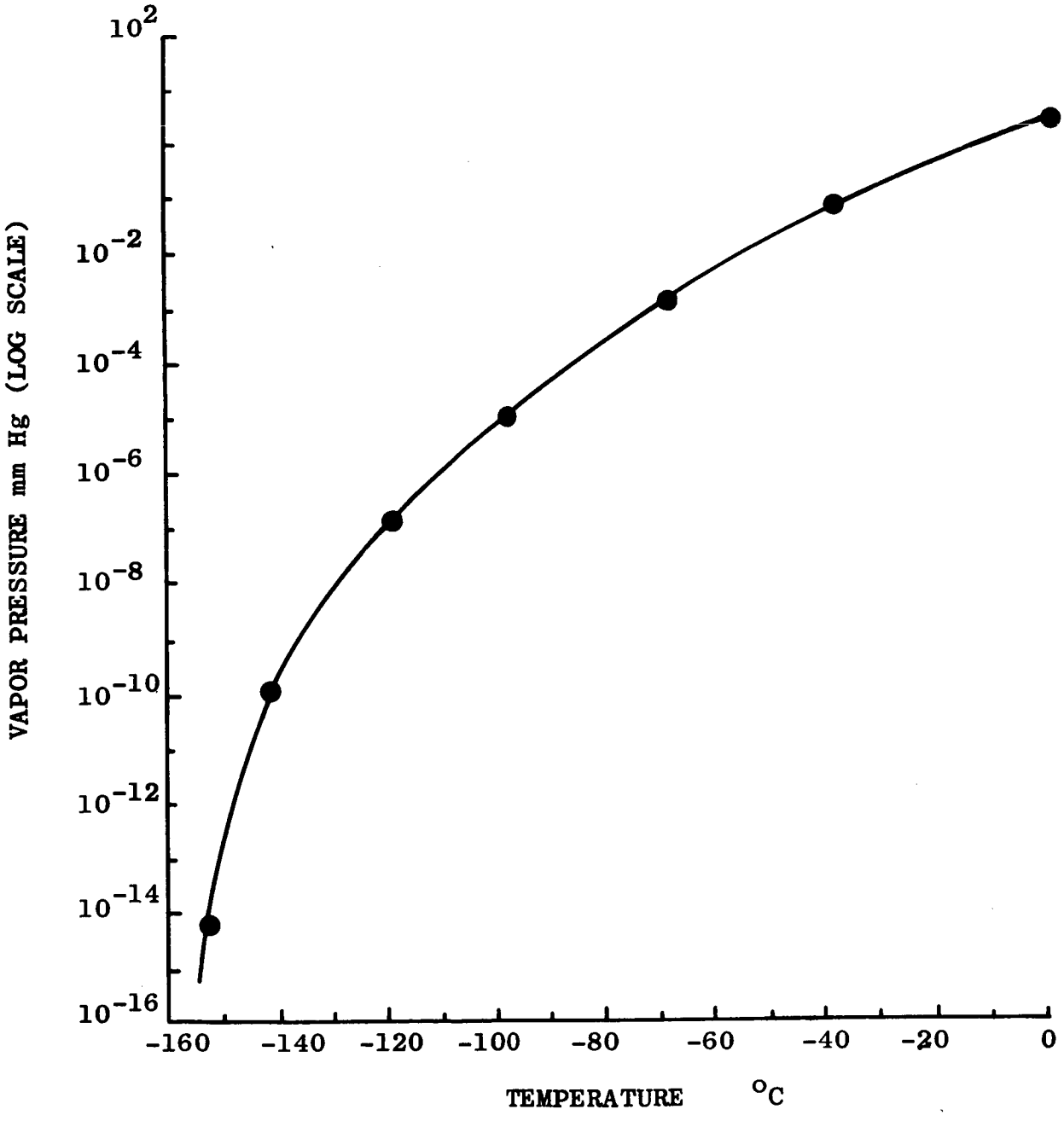

FIGURE 3. VAPOR PRESSURE VS. TEMPERATURE (ICE)

The high-speed motion picture film also demonstrated the existence of a pressure wave associated with the sudden release of liquids at reduced pressure. The film showed a definite upward motion of the ice particles as the pressure wave was reflected off the bottom of the SES chamber. The observed motion of the ice particles can only be accounted for by a pressure wave effect.

3.0 ANALYSIS OF OPTICAL DATA

Cameras located at the Vero Beach tracking site (Vero Beach, Fla.) and atop the Technological Laboratory (AFMTC, Patrick AFB, Fla.) obtained motion pictures of the water release and the tumbling vehicle parts for about 100 seconds after the tanks were ruptured. The Vero Beach site employed a standard 500 inch focal length ROTI with a 35 mm format. The TV Camera System employed at the Technological Laboratories (Tech Lab) has a special design and a discussion of this system is given in Appendix A. The ROTI system (Vero Beach) operated at a camera speed of 48 frames/sec, and the TV Camera System operated at 30 frames/sec.

Weather conditions for the SA-3 launch operations were good. Scattered high, thin cirrus clouds and a few scattered cumulus clouds did, however, slightly obstruct optical viewing. The base of the cumulus clouds was about 1 km. The height of the cirrus clouds was not reported. Ground meteorological conditions just after the launch of the SA-3 vehicle are listed in Table I (Ref. 1).

Table I
Ground Meteorological Conditions

Temperature	24.7°C
Relative Humidity	36%
Wind	SW at 3 m/sec
Pressure	1.03858 kg/cm^2

3.1 SUMMARY OF OPTICAL DATA ANALYSIS

A detailed analysis was made of the second Project High Water motion picture films. This analysis was performed in two (2) phases. Phase I considers the behavior of the water-ice cloud created by the release of the ballast water. Phase II considers the glow that developed in the tankage section of the vehicle.

3.1.1 Summary of Water Release Analysis (Phase I)

An appreciation of the dynamics of the expansion of the water-ice cloud requires several viewings of the motion picture film A number of significant results have been obtained from a careful study of the photographic records. These general conclusions are:

A. The expansion of the water-ice cloud was highly unsymmetrical. This asymmetry in the expansion is a consequence of the procedure employed to rupture the ballast tanks.

B. A considerable amount of turbulent action existed on the interior of the expanding water-ice cloud. Part of the turbulence was a consequence of the asymmetric expansion; however, turbulence would be encountered with a symmetrical expansion.

C. Large gradiations in the cloud density occurred during the expansion. Regions of the cloud were observed to increase in density (for short periods of time) as the expansion progressed.

D. The average expansion velocity of the cloud varied from 0.417 km/sec to 1.88 km/sec. The variation in the average expansion rate did not show a regular trend. This irregularity in the average expansion rate also demonstrates the occurrence of turbulence.

E. Portions of the water-ice cloud had very high expansion rates. The maximum expansion rate found was 3.60 km/sec and a number of cloud portions had expansion rates in excess of 2 km/sec.

F. The water-ice cloud persisted as an actually observable entity for approximately seven (7) seconds.

G. The same general expansion behavior of the cloud was obtained from both sets of film data. In a few instances the same structures are believed to have been observed from both locations.

H. The estimated diameter of the water-ice cloud as an optically observable entity was 10 km.

A detailed description of the more outstanding facets of the water-ice cloud expansion are presented in Section 3.4.

3.1.2 Summary of Glow Phenomena (Phase II)

An analysis was made of the two (2) sets of optical data obtained on the glow phenomena seen aboard the tankage section of the Saturn vehicle after Project High Water. These optical data provided definite indications that the glow observed in the tankage section was an onboard fire. The optical evidence combined with the other data to be presented provides conclusive evidence of an onboard fire. Specifically, the optical data yield the following evidence of an onboard fire:

A. The orange color of the "glow" is that of an oxidizer-deficient hydrocarbon flame.

B. The "glow" was simultaneously observed from two (2) widely separated locations.

C. The "glow" was observed at nearly all possible orientations of the vehicle with respect to

the camera. That is, with the end of the vehicle pointing at the camera, pointing at right angles to the camera, and pointing (almost) away from the camera.

D. The rotation period of the vehicle changed from 7.17 seconds to 7.92 seconds following a sustained orange "glow" from the vehicle. An examination of this sustained "glow" showed that a jet extended in the direction of rotation.

A more detailed discussion of the optical evidence of the on-board fire is presented in Section 3.5.

3.2 CAMERA LOCATION AND ASPECT ANGLE

The TV Camera System located at the Tech Lab, Patrick AFB, Fla. was 20.4 miles from the Saturn launch site (Complex 37), and the ROTI Camera System located at Vero Beach, Fla., was 59.6 miles from the launch site. Figure 4 shows the azimuth angle of the TV Camera System (Tech Lab) as a function of range time. Figure 5 gives the corresponding elevation angle for the TV camera. Azimuth and elevation angles for the ROTI Camera System (Vero Beach) are given in Figures 6 and 7, respectively.

3.3 SOME PRINCIPLES OF OPTICAL DATA ANALYSIS

Photographic results from an operation can produce a considerable amount of quantitative data. A number of physical parameters of an event can be determined if proper photographs are obtained. In general these parameters are:

a. Geometry.

b. Motion.

c. Event Time.

d. Reaction Rates.

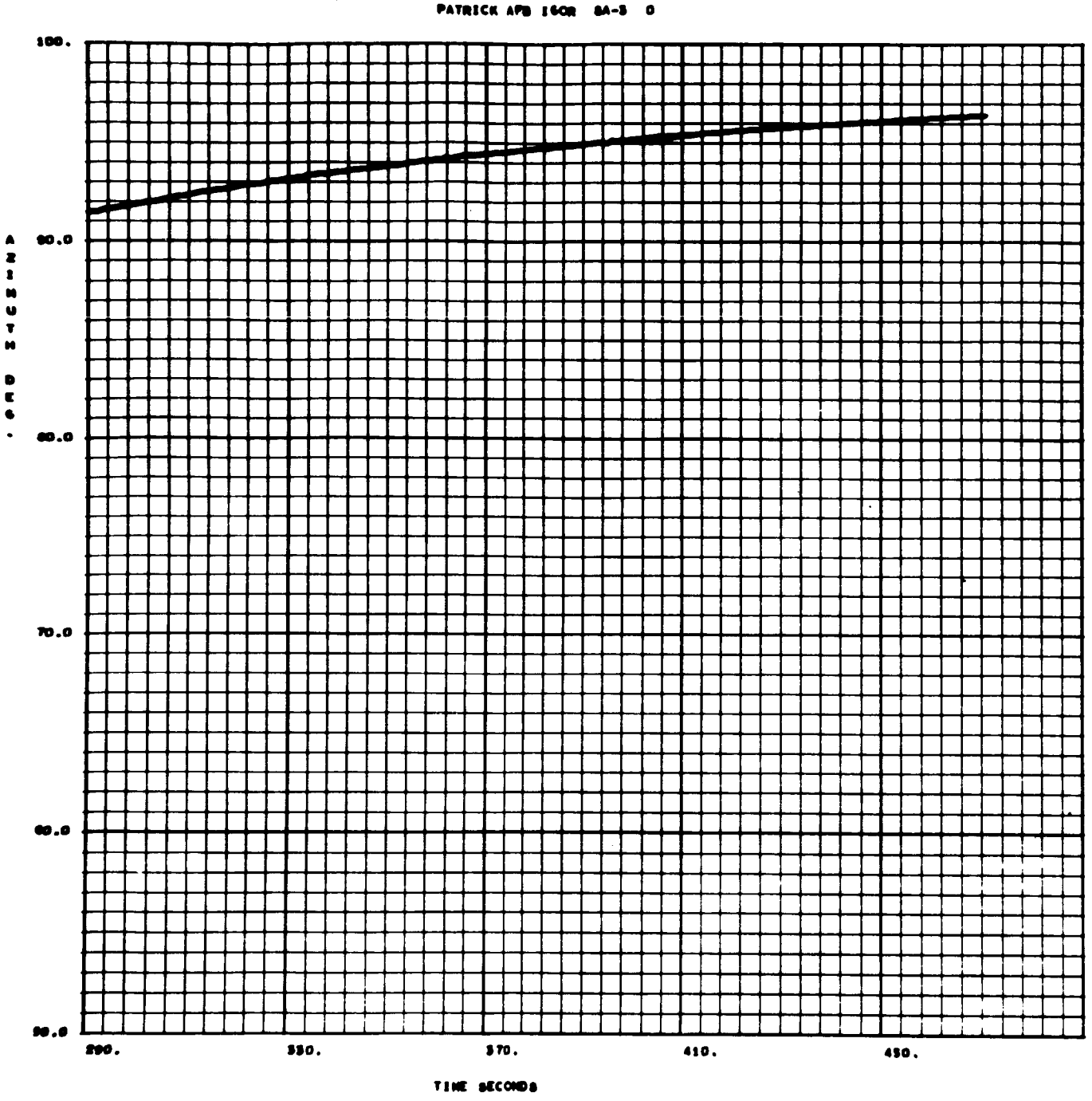

Figure 4: Azimuth Angle of TV Camera System for Project High Water

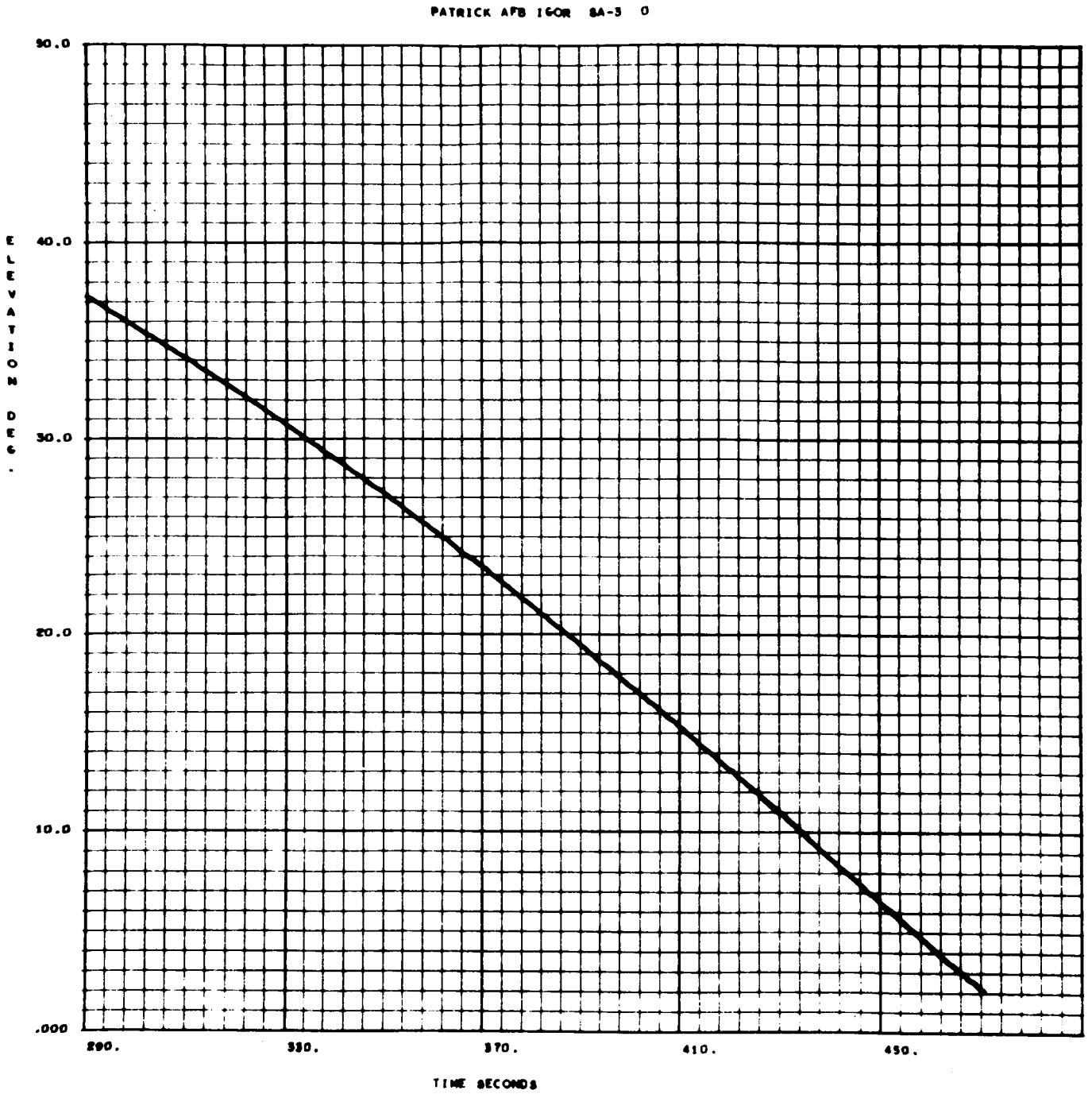

Figure 5: Elevation Angle of TV Camera System for Project High Water

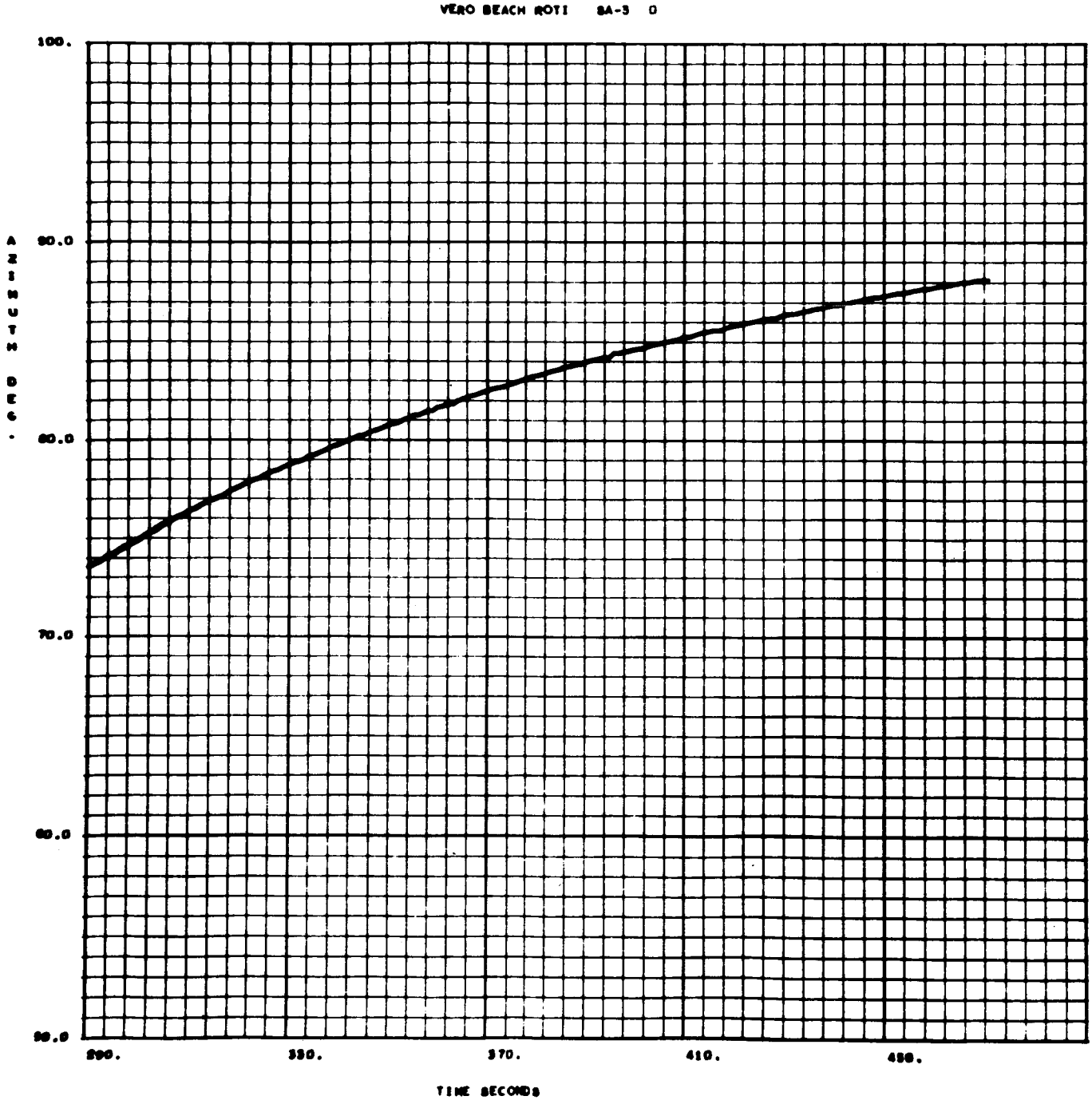

Figure 6: Azimuth Angle of ROTI Camera System for Project High Water

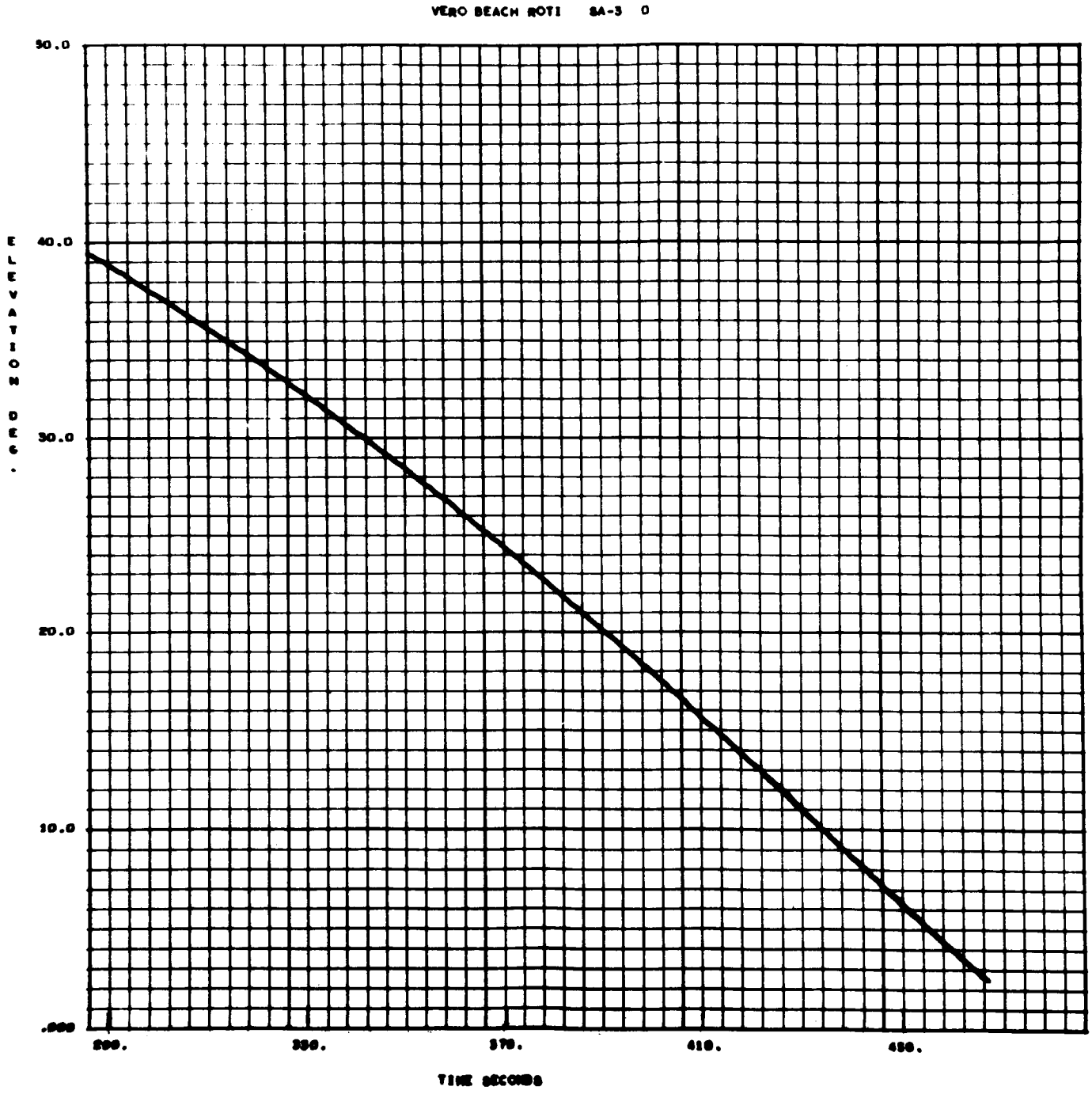

Figure 7: Elevation Angle of ROTI Camera System for Project High Water

Additional parameters can be derived from color photography of an event. For example, color photographs of a flame can yield semiquantitative data on:

a. Temperature.

b. Flame Analysis.

The color of a flame is often indicative of the substances involved in the combustion. Table II shows the characteristic colors of a few chemical elements.

Table II
Flame Colors

Hydrogen	Blue
Carbon	Yellow-Orange
Sodium	Yellow
Barium	Green
Strontium	Red
Chlorine	Green

Thus, flame constituents can often be determined by a trained analysist from observation of the color of a flame.

3.4 WATER-ICE CLOUD EXPANSION

During the release of the water into the ionosphere and for approximately one hundred (100) seconds after the release detonation, both black and white and color photographs were obtained. Both camera systems obtained about ten (10) frames of data on the expanding water-ice cloud before the edges of the cloud became larger than the field of view of the camera. After the release the expanded water-ice cloud obscured the view of the vehicle for approximately seven (7) seconds. This time interval was almost identical in the records of both camera systems.

3.4.1 TV Camera System Film Data

Figures 8 and 9 show eight (8) sequential frames of the data obtained by the TV Camera System located at the Tech Lab (Patrick AFB, Fla.). Figure 8A is an enlargement of the first motion picture frame obtained after the water tanks were ruptured. Figure 8B is the following motion picture frame obtained 0.033 seconds after Figure 8A. In Figure 8B the expanding water cloud is seen. Unsymmetrical characteristics of the expansion are a consequence of the technique employed to rupture the tanks. Thirty-three (33) milliseconds after the photograph 8B, the motion picture frame shown in Figure 8C was obtained. The unsymmetrical expansion of the water-ice cloud is evident. Structural characteristics can be seen that developed into filaments as the cloud expanded. A large center structure is still visible that appears similar to the initial water expansion shown in Figure 8B. A small spike-like structure can be seen at the upper right leading edge of the center part of the expanding cloud. Also a spike-like structure expanding to the left appears at the lower edge of the cloud next to the void area. Both of these spike structures show that rapid expansion and evaporation/sublimation processes were operative. Figure 8D shows the expanding cloud thirty-three (33) milliseconds after the previous picture. The uneven cloud structure is very evident in Figure 8D. A nearly vertical band appears to separate the portion of the water-ice cloud expanding to the right and the portion of the cloud expanding to the left. Comparing Figures 8C and 8D, it is seen that the small spike

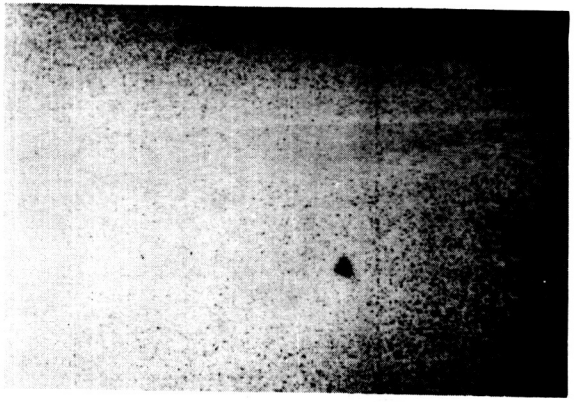

A

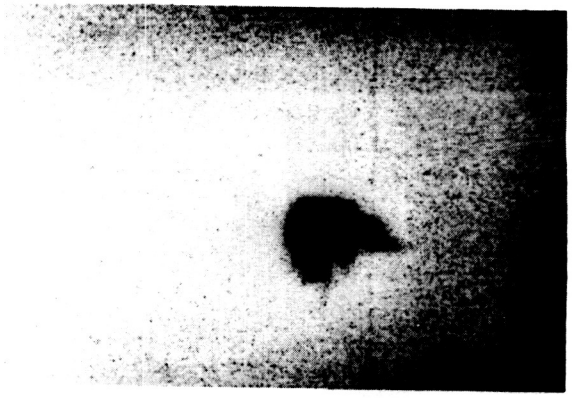

C

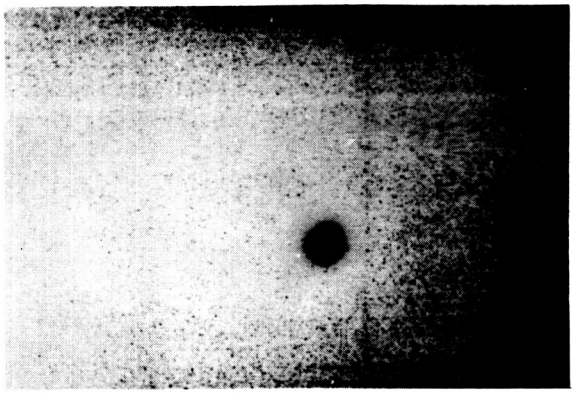

B

D

Figure 8: TV Camera Records of Project High Water - First Series
(1/30 second interval)

A

C

B

D

Figure 9: TV Camera Records of Project High Water - Second Series
(1/30 second interval)

observed (Figure 8C) at the lower left edge of the cloud has expanded in width as well as distance from the center. However, the spike at the upper left still retained the narrow spike-like character. A number of other structures of the cloud can be identified and followed for several frames. In the center of Figure 8D, the small cloud-like structure appears to have partially evaporated. This small structure appears to be the center of the expansion in the initial pictures, but later pictures show that this small structure also expands and forms filaments that radiate outward from a point mid-way between the two most intense clouds present in Figure 8D. Each of these dense cloud structures display an interesting expansion. For example, a small cloud structure develops from the upper edge of the large cloud on the right hand side of Figure 8D that is of particular interest. From this region a jet-like cloud develops that appears to grow in intensity at the expense of the surrounding structure.

Expansion of particular parts of the cloud structure can be definitely traced throughout the 0.132 seconds time covered by four (4) pictures in Figure 9. The jet-like structure (noted above) developed in the 0.033 seconds between Figure 8D and Figure 9A. This jet structure is a dominant feature for five (5) sequential frames (i.e., for 0.165 sec). After this time the jet structure had expanded beyond the field of view of the camera. A small round shaped cloud structure (1 cloudlet) is seen to develop in the lower right hand portion of Figure 9A. This structure appears to become detached from the main cloud, and it can be followed as an

entity in eight (8) consecutive frames (i.e., for 0.264 sec) as evidenced in Figures 9B, 9C, and 9D. The small spike-like structure that was noted in Figure 8C can still be clearly seen to be expanding toward the upper right in Figure 9A. In the time interval between Figures 9B to 9D most of the spike structure dissipates.

Both of the dense cloud structures that were used to determine the center of the expansion develop individual structures and decrease in density as they expand. The small central cloud observed in Figure 8B acquires a diffuse ring shape in Figure 9A. This ring grows in density with time and moves outside the field of view of the camera the sixth frame after that of Figure 9A (i.e., in 0.198 sec). During the time interval that this second ring cloud remains in the field of view, it expands and becomes embedded in the original cloud just before this system moved outside the field of view of the camera.

Figure 10 shows four (4) nonsequential frames. Figure 10A was obtained 0.264 second after the picture shown in Figure 8A and 0.033 second after Figure 9D. The time interval between each of the frames in Figure 10 is 0.099 second. Nearly all of the structures visible in Figure 9D can be seen in Figure 10A. However, the outer edges of many of the structures have expanded beyond the field of view of the camera system. By the time of Figure 10B (0.099 sec from Figure 10A), all of the structures followed from the time of Figure 8D have been obliviated or expanded out of the field

A

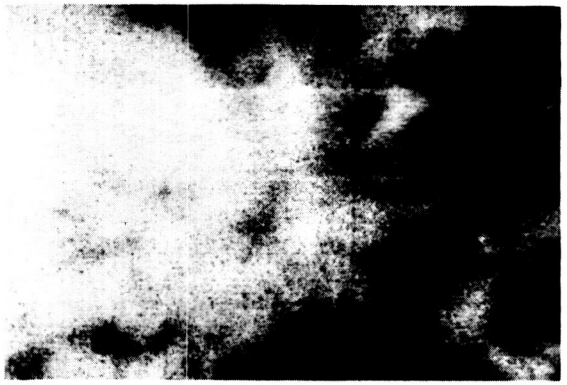

C

B

D

Figure 10: TV Camera Records of Project High Water - Third Series
(3/30 second interval)

of view of the camera system. Both Figures 10C and 10D show only a portion of the cloud since a substantial part of the cloud had expanded beyond the camera's field of view. One of the interesting aspects of Figure 10C to 10D is the evidence of turbulence within the ice cloud. Many of the visible structures possess a circular or spiral character. Also, individual small structures can be seen to move in a circular pattern.

3.4.2 ROTI Camera Film Data

Figures 11, 12, and 13 show twelve (12) consecutive frames of data obtained by the ROTI camera (Vero Beach). Figure 11A is a picture of the Saturn vehicle taken just as the tanks were ruptured to release the water into the ionosphere. The picture shown in Figure 11B was obtained 0.0208 second after the preceeding picture (11A). The first evidence of unsymmetrical nature of the expansion can be seen in Figure 11B. This lack of symmetry in the expansion was also evident in photographs obtained by the TV Camera System (Tech Lab). Figure 11C shows the water-ice cloud 0.0208 second after that shown in Figure 11B. The lack of symmetry of the water-ice cloud is still evident. However, a thin cloud does indicate that some water is expanding in all directions rather than just away from the tank rupture. Nonuniformities in the density of the cloud structure are evident even at this early aspect of the expansion process. A dense structure on the lower right hand side of the cloud in Figure 11C appears to be the center structure observed in Figure 8C. A close examination of Figure 11C reveals a cross-like effect.

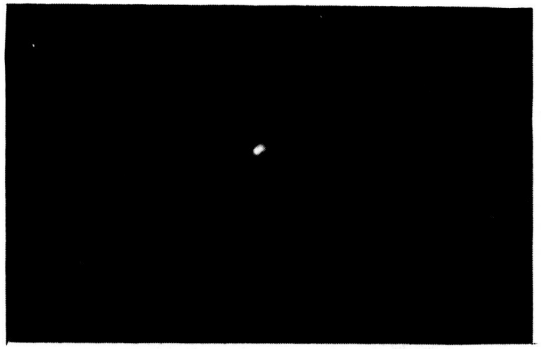

A

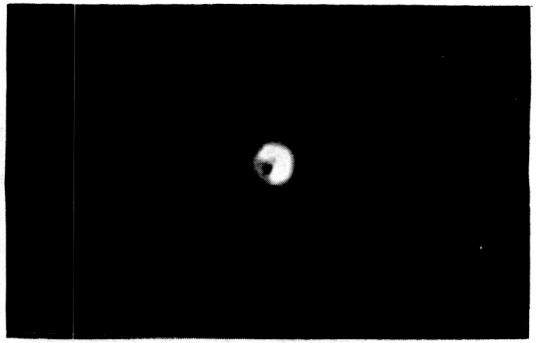

C

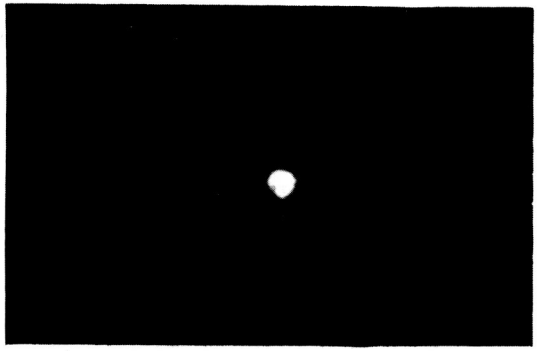

B

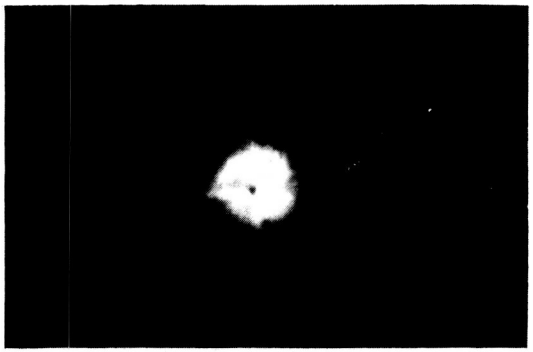

D

Figure 11: ROTI Camera Records of Project High Water - First Series
(1/48 second interval)

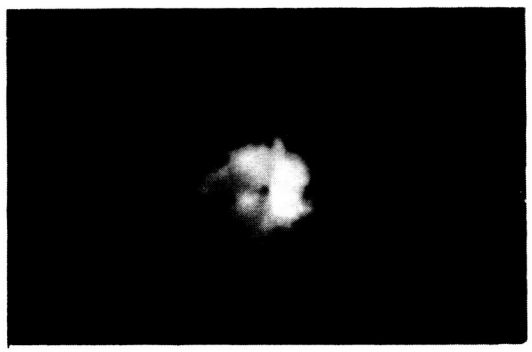

A

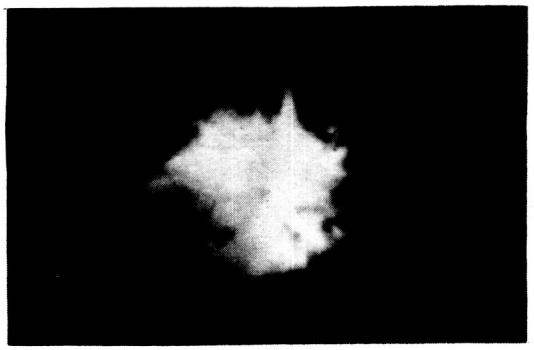

C

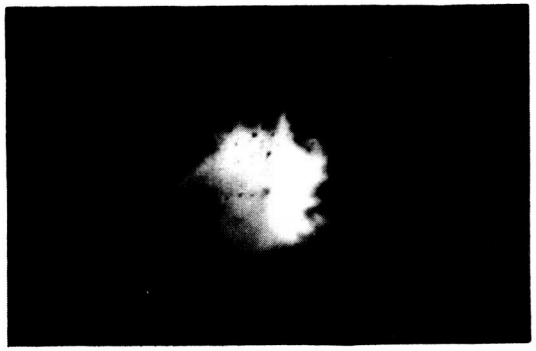

B

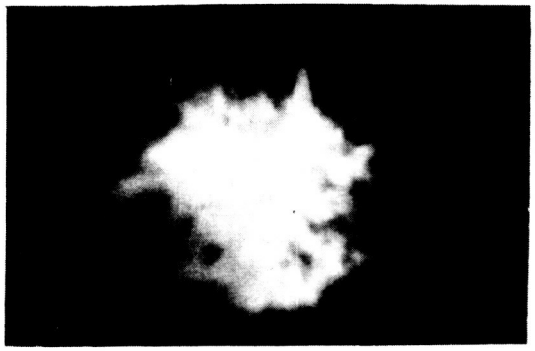

D

Figure 12: ROTI Camera Records of Project High Water - Second Series
(1/48 second interval)

A

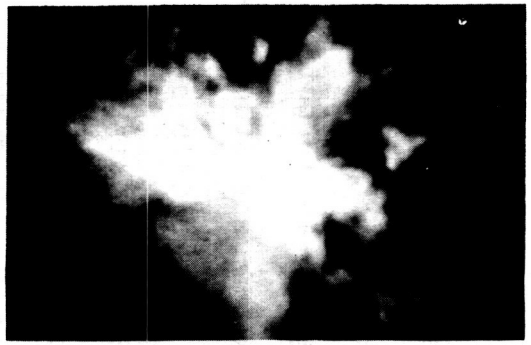

C

B

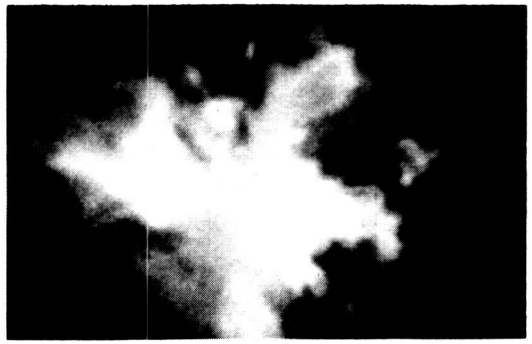

D

Figure 13: ROTI Camera Records of Project High Water - Third Series
(1/48 second interval)

That is, protrusions extend both vertically and horizontally from the center structure in the form of a cross. Traces of this "cross" are found in the subsequent frames. The cause of the cross-like effect has not been established. No spike-like structure appears in Figure 11C as was first observed in Figure 8C. However, the time of Figure 8C was slightly longer than 0.066 seconds after the water tanks were ruptured, while the time of exposure of Figure 11C was only 0.0416 second after the tanks were ruptured. The spike-like structures can be seen to be developing in Figure 11D at both the upper right hand edge of the cloud and the left edge of the cloud. Two dense structures (i.e., main segments of the cloud) appear in Figure 11D as were evident in Figure 8D. The center of expansion appears to be a point mid-way between the two dense structures.

Figure 12 shows four (4) frames of pictures of the expanding water-ice cloud which sequentially follow those shown in Figure 11. Structural characteristics can be traced throughout the four frames. Figure 12A shows many of the structural features that were shown in Figure 8D. Time of exposure of the water release of these two frames is very close. Figure 12A was obtained 0.103 second after the detonation, and Figure 8D was exposed 0.099 second after the water was released. The development of the spike-like structure on the upper edge of the cloud begins to take a definite form by the time Figure 12A was obtained. Figure 12D was obtained 0.165 second after the water was released. Expansion of the cloud structure in the form of filaments also developed in

the twenty (20) milliseconds between the time of exposure of Figures 12A and 12B. Several spike-like structures can be observed on the upper edge of the cloud in Figure 12B. A spike on the right hand edge of the cloud is similar to a spike observed with the TV Camera System on the Tech Lab. An expansion of a narrow band on the left edge of the cloud (Figure 12B) is similar to the spike-like structure in the same location that was photographed with the TV Camera System (Tech Lab). Of particular interest is the sudden development of the dense structure near the center of the cloud. This dense structure has the appearance of a second release of water and may be due to the expansion of the water from the internal tank of the second stage. The motion of several curved structures on the right hand edge of the cloud show the existence of turbulent conditions. Figure 12C shows the cloud's structure 145 milliseconds (0.145 sec) after the water was released. Areas of concentration of the cloud produce a filament structure. Spike-like structures extending upward and to the left are believed to be the same ones observed by the TV Camera System (Tech Lab). The dense structure noted in the center area in Figure 12B has expanded in Figure 12C. This behavior of the dense structure supports the second water release concept noted above in Figure 12B. Figure 12D shows a further expansion of the dense structure in the center of the cloud. This figure was obtained 0.1656 second after the water was released. All aspects of the structure observed in Figure 12C show an expanded form in Figure 12D.

A number of centers of cloud concentration are seen in the Vero Beach ROTI pictures of Figure 12 that show considerable similarity to the concentration centers in the Tech Lab TV Camera System pictures of Figure 9. Many of the structures observed by one camera system will not be recorded by the other due to the differences in the location of the observation sites.

Figure 13 shows the four (4) consecutive frames obtained following Figure 12D. The most distinctive feature of this series of frames is the small structure (cloudlet) that develops and moves out from the main body of the cloud. This small structure (cloudlet) is believed to be the same one observed in the lower right hand corner in the series of frames of Figure 9.

Figure 14A was obtained 0.0208 second after Figure 13D, and the remaining frames were acquired at intervals of 0.0832 second. Nearly all of the structures followed in Figures 11, 12, and 13 have expanded beyond the field of view. The motion of the curved structures (e.g., top center of Figures 14B and 14C) demonstrate the occurrence of turbulence in the expanding cloud.

3.4.3 Expansion Rate Velocities

One of the physical factors that can be measured from the photographs obtained on the High Water experiments is the expansion rate during the initial phases of the formation of the water-ice cloud. Using only simplified methods of measurement, the velocities obtained are minimal values, as they assume

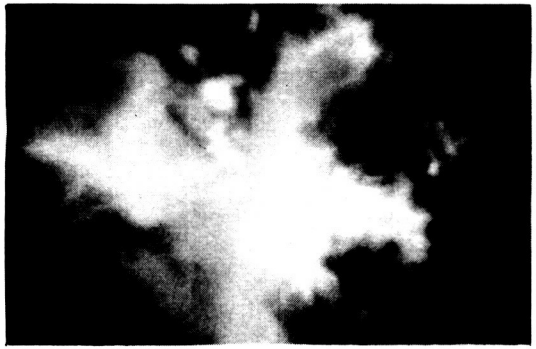

A

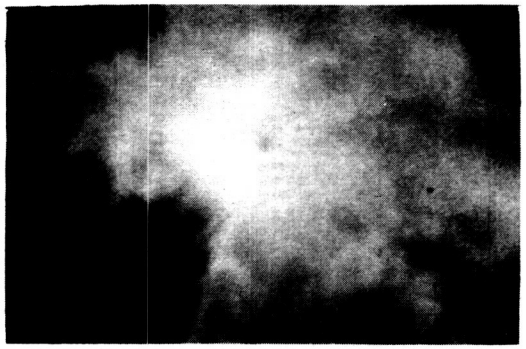

C

B

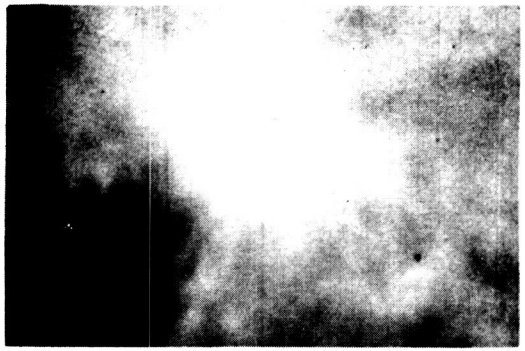

D

Figure 14: ROTI Camera Records of Project High Water - Fourth Series (4/48 second interval)

expansion only in the plane perpendicular to the line of sight. By combining the velocities of portions of the cloud identifiable in photographs from both camera locations and utilizing the angle of sight, a more exact evaluation of the expansion velocities can be determined.

Expansion rate velocities of the main portions of the cloud could be evaluated for approximately 200 milliseconds following the release. After 200 milliseconds substantial portions of the cloud were beyond the field of view of the optical systems. However, the velocity of the small cloudlet observed at both camera sites (cf. Figures 9 and 13) was obtained at a later time than 200 milliseconds (after the water release). The measured expansion rate velocities are summarized in Table III, and the variations of the first

Table III

Water-Ice Cloud Expansion Rate Velocities

Structure	Average Velocity	Maximum Velocity
General Cloud	1.05 km/sec	1.83 km/sec
Upward Spike	2.26 km/sec	3.16 km/sec
Sideward Spike	2.64 km/sec	3.60 km/sec
Cloudlet	1.28 km/sec	1.83 km/sec

three (3) structures are shown in Figure 15.

3.5 OCCURRENCE OF ONBOARD FIRE

An unexpected phenomena was observed shortly after the Project High Water cloud had dissipated. The colored motion picture of the tumbling Saturn vehicle sections show the development of a bright orange "glow" at the end of the tankage section. This glow can be due to one of two physical phenomena. Solar glint reflected by the tumbling body could

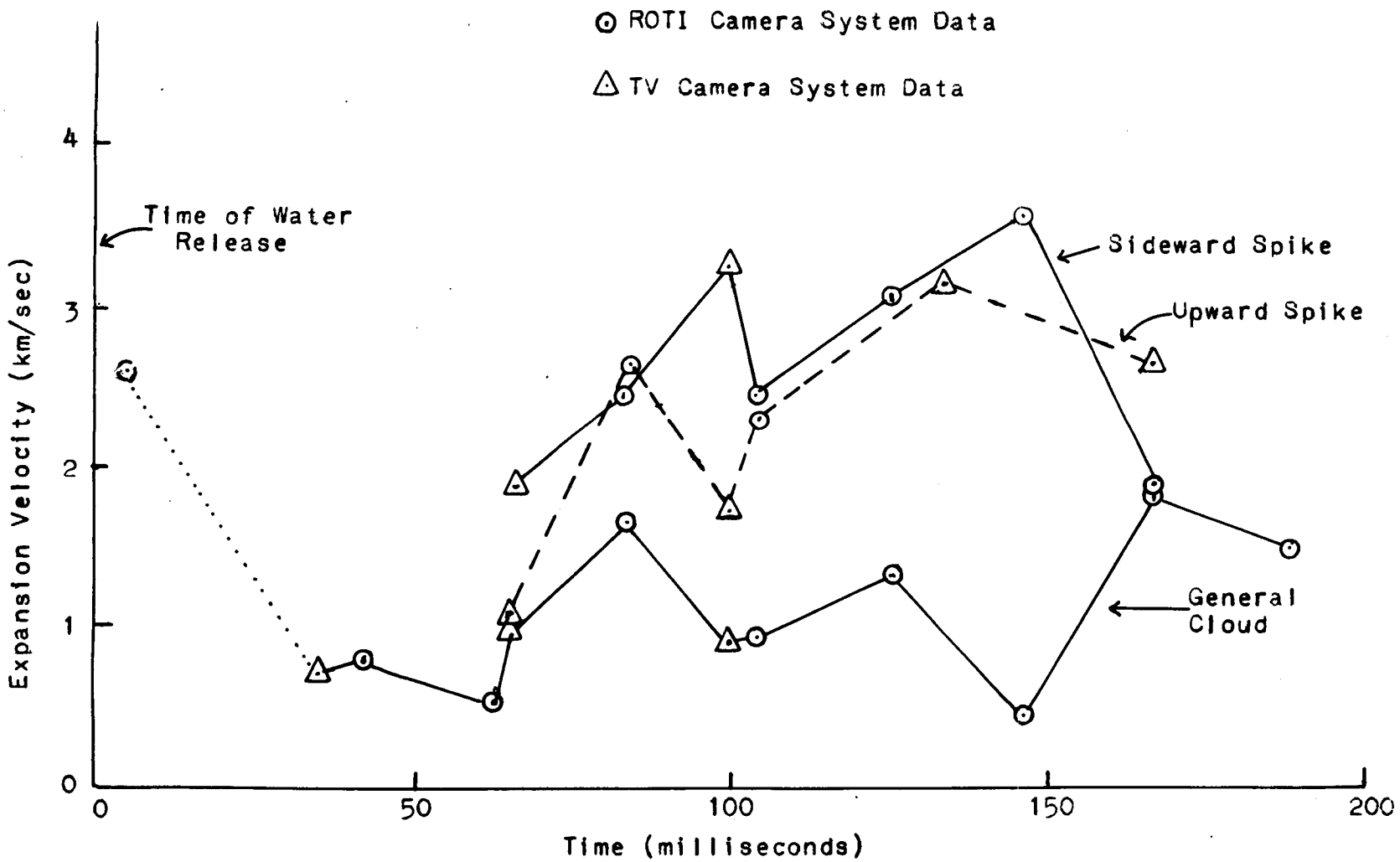

Figure 15: Expansion Rate Velocities of Water-Ice Cloud Structures

produce a sudden enhanced spot on the surface of the body, or a fire within the body which pulsates and at times extends outside the body could produce the enhanced glow. However, color analysis of the photographs obtained of the glow and geometric considerations of the occurrence of the enhanced glows show that this phenomena resulted from a pulsating fire on the interior of the vehicle rather than from glint.

If only the color of the glow is considered, some doubt can exist as to the cause of the glow. While the color was characteristic of a hydrocarbon flame, sun glint from the anodized interior of the vehicle could produce a similar color. However, considering both the various orientations of the vehicle at the times the orange colored glow was observed and the fact that the enhanced glow was simultaneously recorded by the TV camera (Tech Lab) and the ROTI Camera System (Vero Beach), the solar glint concept is considered impossible. All of the glows were associated with a single end of the vehicle section. Glows were recorded when this end of the vehicle section was oriented directly toward the camera, at an acute angle to the camera, at 90° to the camera, at an obtuse angle to the camera, and directly away from the camera. In one case, a sustained glow persisted for 0.625 second. Before this extended glow period, the rotation period of the vehicle was 7.17 seconds. After this extended glow period, the rotation period was lengthened to 7.92 seconds. Thus, some type of impulse was applied to the vehicle during the time of the sustained glow.

A series of four pictures showing the prolonged existence of the glow is shown in Figures 16 through 19. Figure 16 shows the vehicle just as the flame starts to develop. At this point the glow end of the vehicle has passed through a nearly end-on position and is pointed downward. Figures 17 and 18 show the flame at times when the flame is well developed. A close examination of Figures 17 and 18 also shows a small jet occurred in the direction of rotation. Figure 19 shows the last motion picture frame displaying the orange color during the sustained glow period. (Unfortunately, a large portion of the orange color has been lost in the reproduction.)

One of the problems associated with the occurrence of a fire onboard the launch vehicle after engine burnout is the physical cause of the combustion. Because the burnout process is the result of oxygen starvation, there is fuel left in the tanks. Apparently there was gaseous oxygen also left in the tanks. The color of the fire indicates it was an oxidizer-deficient hydrocarbon flame, and a flame of this type would have a very low thrust. At the time of the explosion, holes were created in the fuel and oxygen tanks so that the oxygen gas seeped into an area in which there was fuel. The mixture was ignited either from the explosion or from the flashback from the hot engine. Insufficient data exist to definitely identify the ignition mechanism.

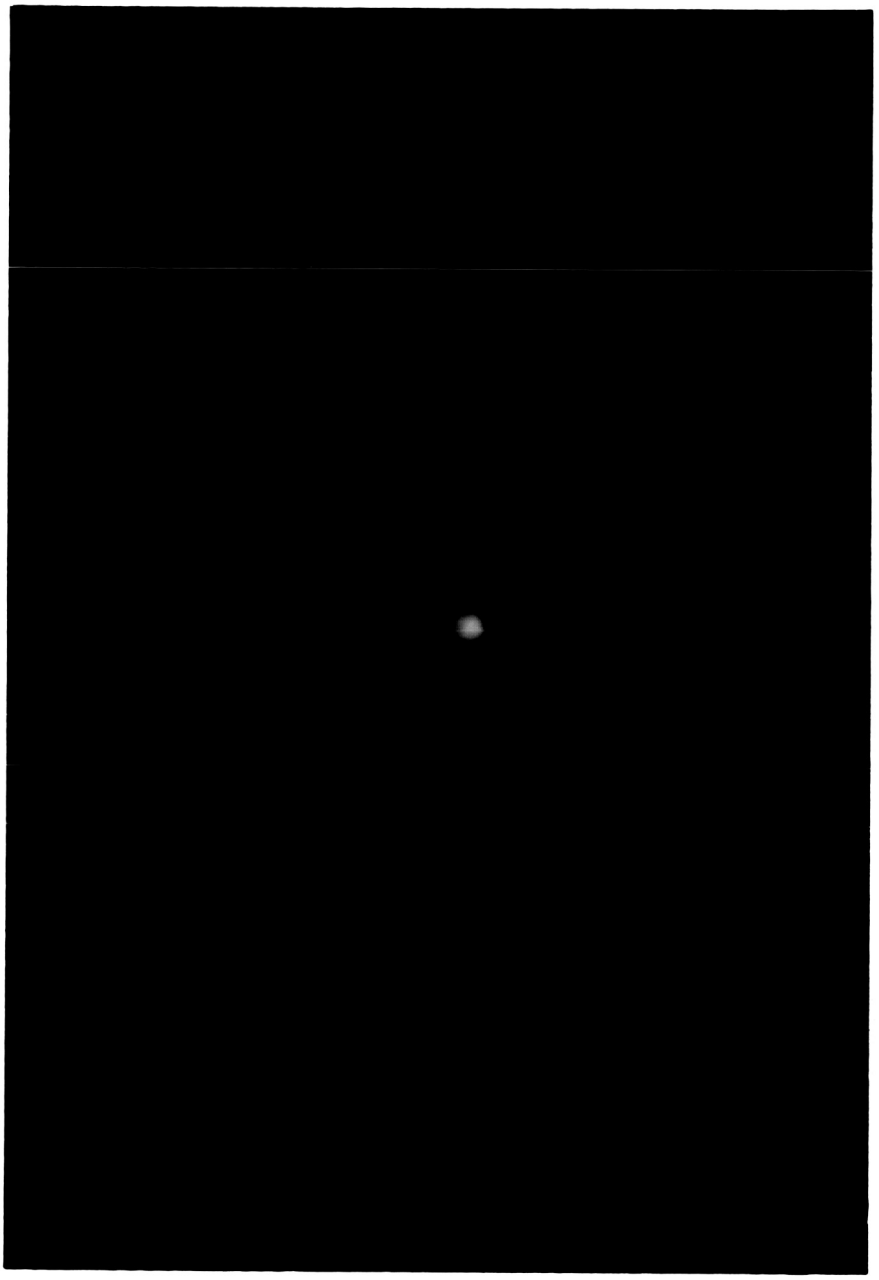

Figure 16: First ROTI Camera Frame Showing Persistent Glow (T+355 sec)

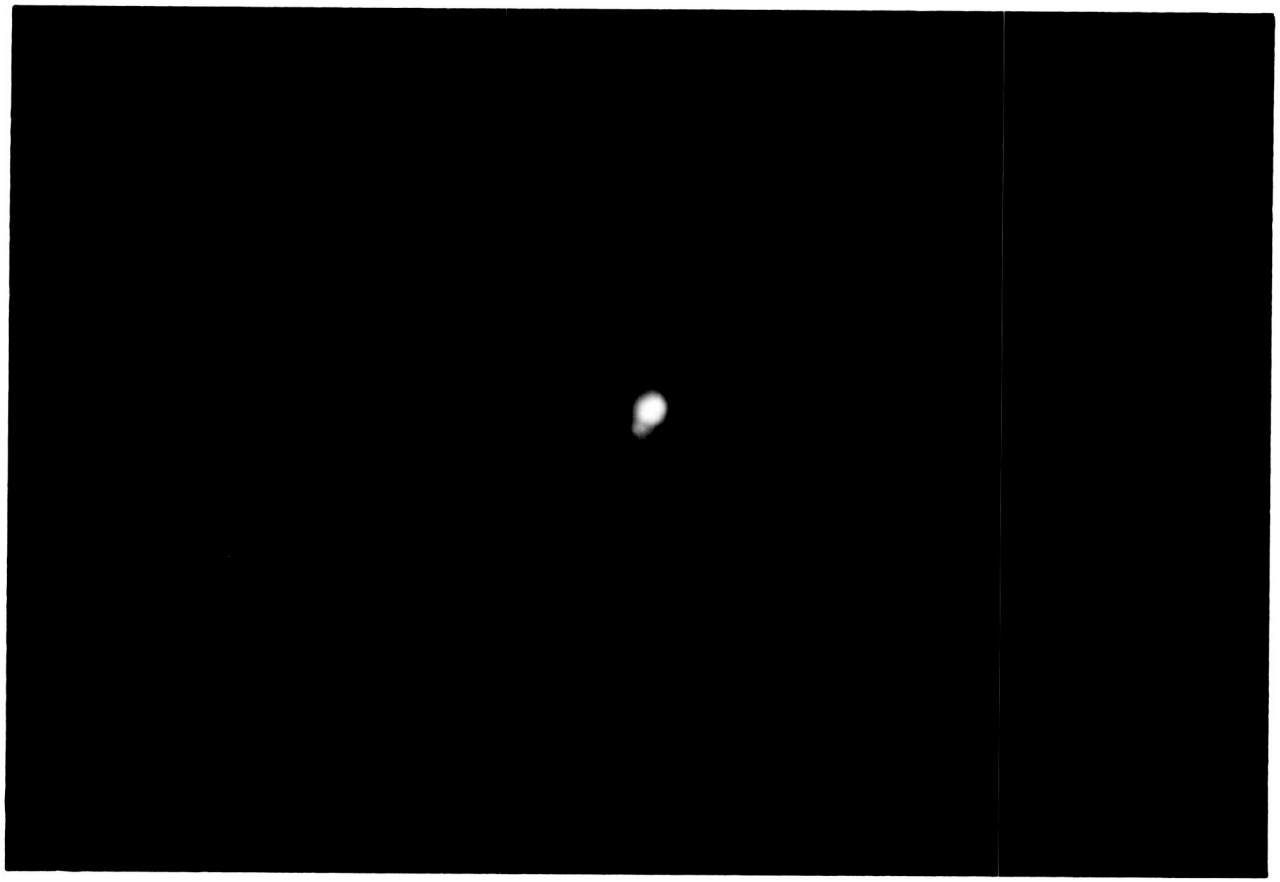

Figure 17: ROTI Camera Frame Showing Jet Structure to Persistent Glow

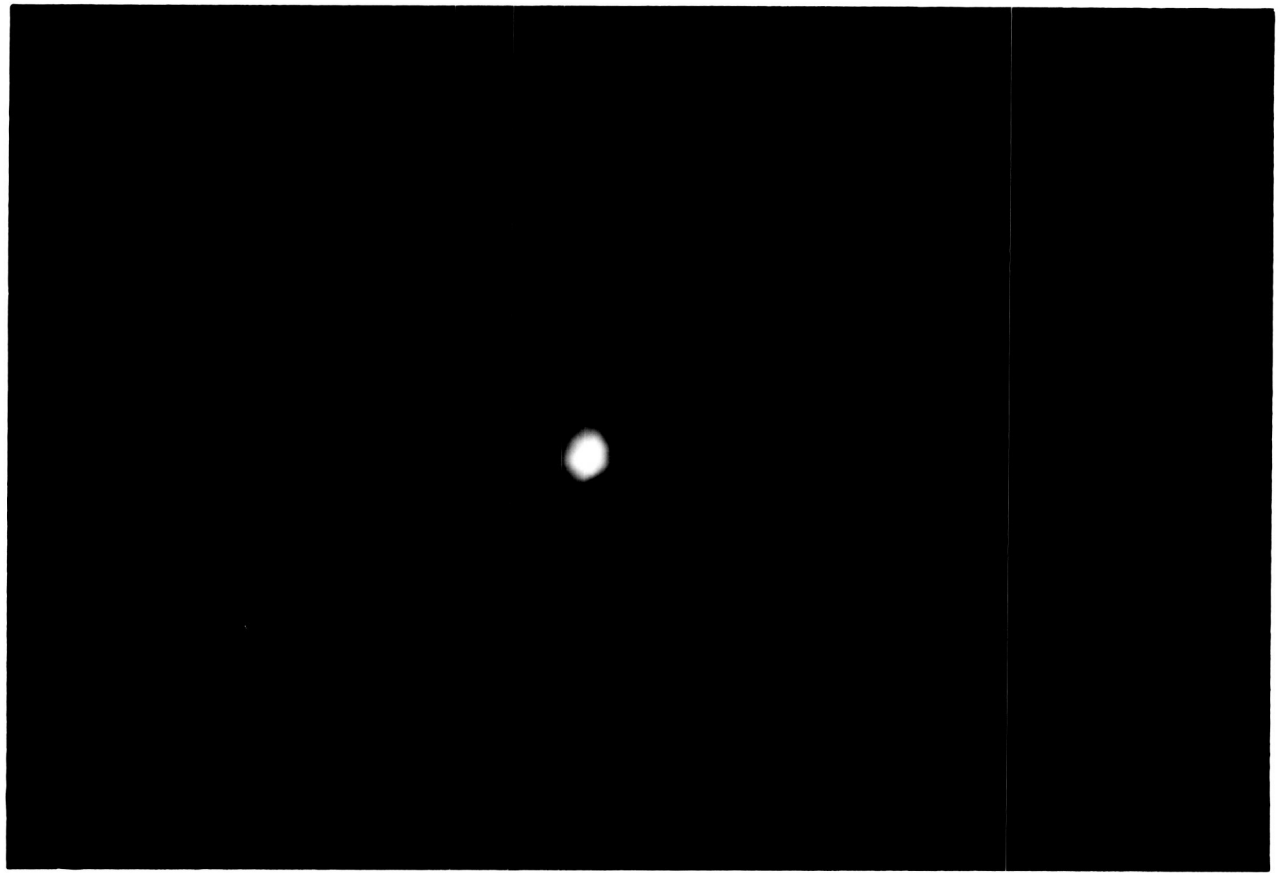

Figure 18: ROTI Camera Frame showing Maximum of Persistent Glow (with jet structure)

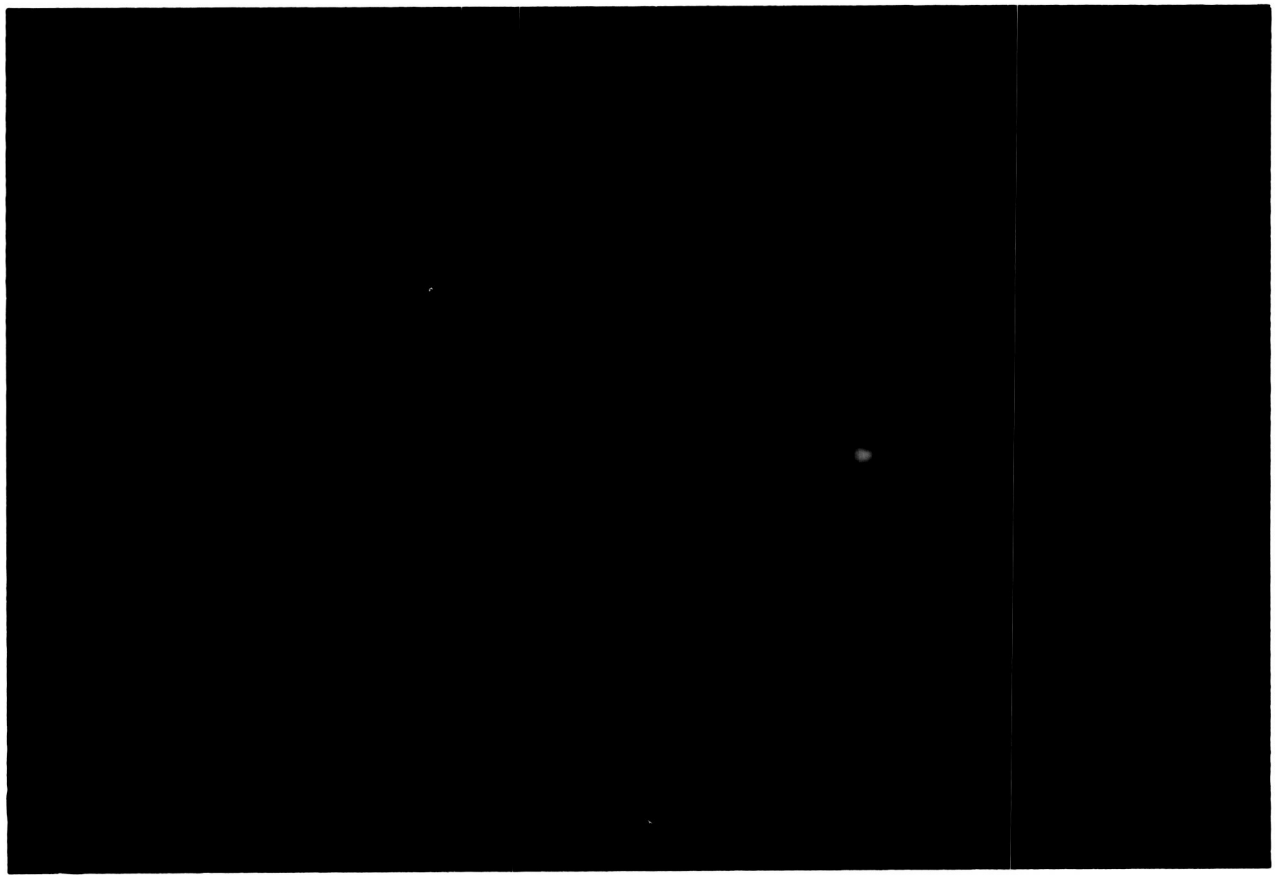

Figure 19: ROTI Camera Frame showing End of Persistent Glow

4.0 ELF-VLF SPECTRAL ANALYSIS

ELF-VLF spectral measurements in the frequency range of 855 cps to 2385 cps during the launch operation of the SA-3 vehicle (Project High Water) were obtained by ISC. The ISC high-resolution ELF-VLF Spectrometer was located approximately 4 miles northwest of Playalinda Beach, Florida ($28^{o}43'N$, $80^{o}40.8'W$) or approximately 15 miles north, northwest of the SA-3 launch site (Complex 37). A detailed description of the ELF-VLF Spectrometer and field operational procedures have been given previously (Ref. 5).

4.1 SUMMARY OF ANALYSIS OF ELF-VLF DATA

A detailed analysis was made of the ELF-VLF spectral data obtained during the second Project High Water Experiment. These high-resolution spectral measurements were made in the frequency range of 855 cps to 2385 cps. Four (4) spectral lines were found that correlate with the water release and the subsequent onboard fire. The frequencies of these four (4) spectral lines were: 2120 cps, 2140 cps, 2150 cps, and 2210 cps. These four (4) spectral frequencies form the basis of the ELF-VLF analysis. The conclusions of the ELF-VLF analysis are summarized in two (2) phases as in the case of the optical data.

4.1.1 Summary of the Water Analysis (Phase I)

A distinct change in the amplitude of the four (4) spectral lines was observed the first time the Spectrometer scanned each of the frequencies following the release of the water. A change in the amplitude behavior of the spectral

lines occurred at the time the visible cloud disappeared.

The ELF-VLF data analysis yielded the following:

A. The release of water caused a perturbation of the ionosphere.

B. The perturbation of the ionosphere resulted in emissions at four (4) discrete frequencies. That is, the radiation was spectral in character, and broadband emissions were not observed in the ELF-VLF region of the electromagnetic spectrum.

C. The ELF-VLF record definitely shows that no electrical discharges of any significance occurred during the time the visible cloud was present. A total of only six (6) sferics were observed during the first eighty (80) seconds following the release. Only two (2) of these sferics were recorded during the first fifty-eight (58) seconds after the release. The lack of sferics is considered conclusive evidence that no electrical discharges were associated with the second Project High Water experiment.

D. A theoretical analysis of the spectral frequencies yielded a magnetic field intensity at the location of the water release of 4.97×10^{-5} Weber/m^2.

4.1.2 Summary of Glow Phenomena (Phase II)

The ELF-VLF spectral data analysis supports the optical evidence that an onboard fire developed in the tankage section of the Saturn vehicle following Project High Water. The analysis of the ELF-VLF data obtained after the visible cloud had dissipated yielded the following:

A. Enhancements and changes in the ELF-VLF spectral lines show a high degree of correlation with optical data of the onboard fire.

B. The ELF-VLF spectral records provide definite evidence the onboard fire persisted for a considerable time after the optical tracking was discontinued.

C. ELF-VLF spectral observations provide a technique for observing and evaluating perturbations of the ionosphere. The changes in the background level during the free flight of the vehicle may be expecially important.

D. The ELF-VLF spectral behavior provides evidence of the vehicle's traversing an inhomogeneous region of the ionosphere during the descent.

4.2 DATA REDUCTION AND ANALYSIS PROCEDURES

The data reduction and analysis procedures employed with the ELF-VLF data for Project High Water were identical with those utilized in the SA-3 launch operations analyses (Ref. 5). In the analysis of the SA-3 launch operations data, twelve (12) spectral lines were identified that correlated with launch events. A detailed examination of these same twelve (12) spectral lines during Project High Water, particularly during the period of the onboard fire, failed to establish the occurrence of any significant changes.

Further analysis of the ELF-VLF records revealed that four (4) spectral lines developed at the time of the release of the water (Project High Water). These same four (4) lines correlated with the onboard fire. These four (4) lines have frequencies which lie between the (SA-3) Spectral Line #11 (2095 cps) and Spectral Line #12 (2370 cps) and are listed in Table IV.

Table IV

Spectral Line Frequencies

Line	Tuner Rotation	Frequency
A	124.3^{o}	2120 cps
B	128.0^{o}	2140 cps
C	133.2^{o}	2150 cps
D	150.4^{o}	2210 cps

The above listed lines are the only spectral lines that demonstrated a consistent correlation with the water release and onboard fire.

The ELF-VLF Spectrometer is a scanning type device which selectively examines each frequency. Thus, the frequency of the instrument is continuously varied over its range (i.e., 855 to 2385 cps). A complete instrument cycle is referred to as a "scan". Each scan is accomplished in approximately 1.03 seconds, and the instrument traverses the frequency range twice during a single scan.

For identification purposes, the scan in progress at the time of Project High Water release was designated by the number 600. All scans preceeding Project High Water were designated by a negative number. A detailed analysis was made of the ELF-VLF records obtained from (Range Time) T+252 seconds to T+534 seconds, background data obtained fifteen (15) minutes prior to the launch of the SA-3 vehicle, and observations obtained twenty (20) minutes after the Project High Water release. A portion of the pre-Project High Water analyzed data was not included in the graphical presentations since it yielded no additional information. The ELF-VLF data presented are summarized in Table V.

Table V

ELF-VLF Data

Scan Designation	Data Classification	Approximate Time
-1011 to -1000	Pre-launch	1729:53 to 1730:07 Z
- 638 to - 630	Free Flight A	T+252 to T+261 sec
- 609 to 600	Free Flight B	T+282 to T+292 sec
600 to 841	Project High Water to Post Impact A	T+292 to T+543 sec
900 to 911	Post Impact B	1809:53 to 1810:07 Z

The measured amplitudes of the four (4) spectral lines observed during the above time intervals are presented in graphical form and discussed in the following sections.

4.3 WATER - ICE CLOUD EXPANSION

Pre-Project High Water background amplitudes of the four (4) spectral lines measured prior to the launch of the SA-3 vehicle (Spectral Scans -1011 to -1000) and during free flight of the vehicle in the ionosphere (Spectral Scans -638 to -630) are shown in Figure 20. There is a small but consistent increase in amplitudes of the spectral lines for the time the vehicle was in the ionosphere compared to the pre-launch level.

Figure 21 shows graphs of the four (4) spectral frequencies just before the release and during the water expansion. The first vertical dashed line indicates the time of the water release as determined by the ELF-VLF spectral analysis. The ELF-VLF data indicates the release time to be no later than T+291.920 seconds nor earlier than T+291.211 seconds. (Due to the scanning procedure, the amplitude of a given spectral frequency is not recorded continuously.) However, an ambiguity was noted in the ELF-VLF records at T+291.849 seconds. This ambiguity may be the detonation of the explosive used to rupture the tanks. A definite signal enhancement was recorded at all four spectral frequencies immediately after the water was released into the ionosphere. Moreover, the characteristic pattern of the fluctuations in signal amplitude changed. This change in the amplitude

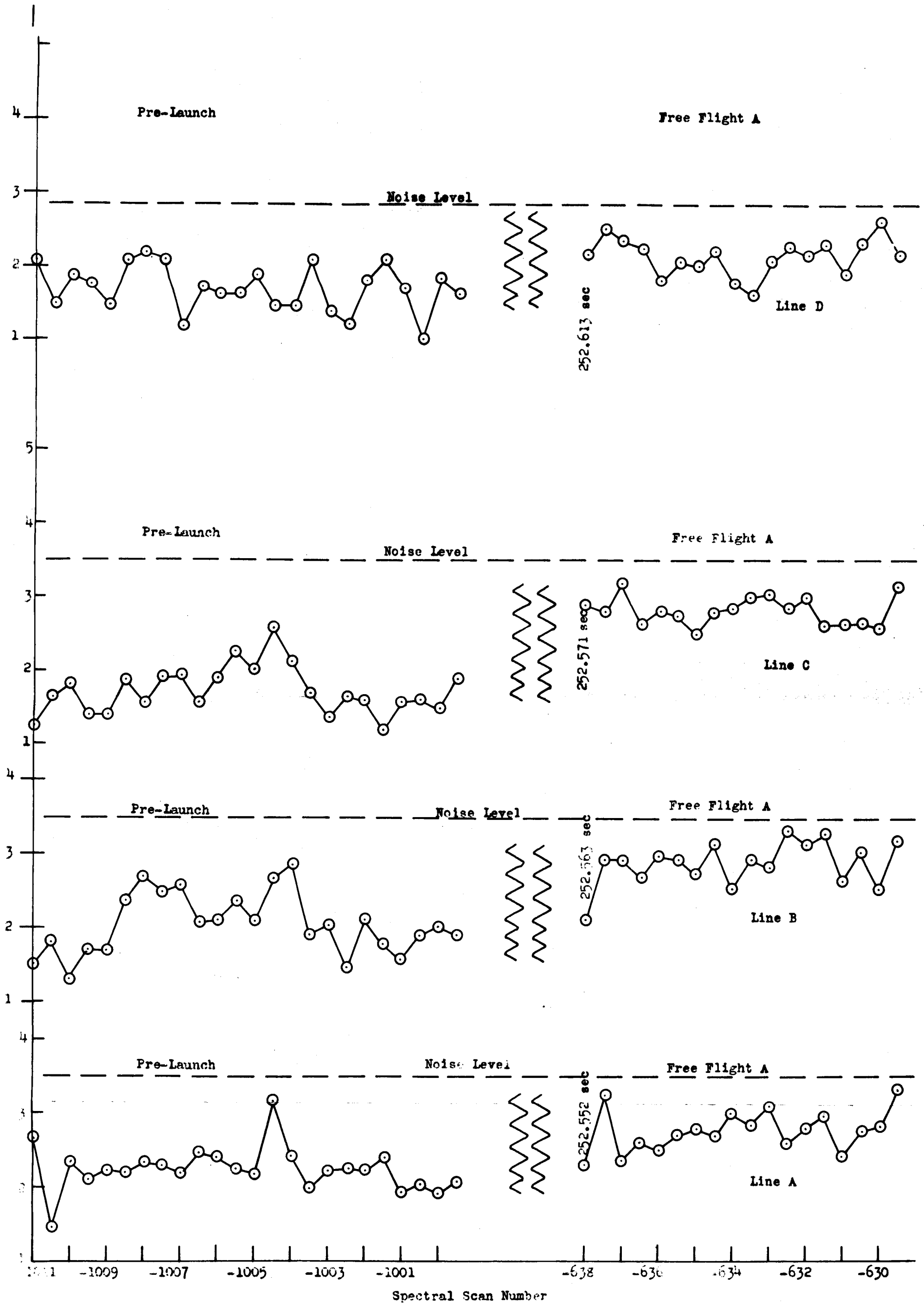

Figure 20: ELF-VLF Amplitude Variations; Spectral Scans -1011 to -630

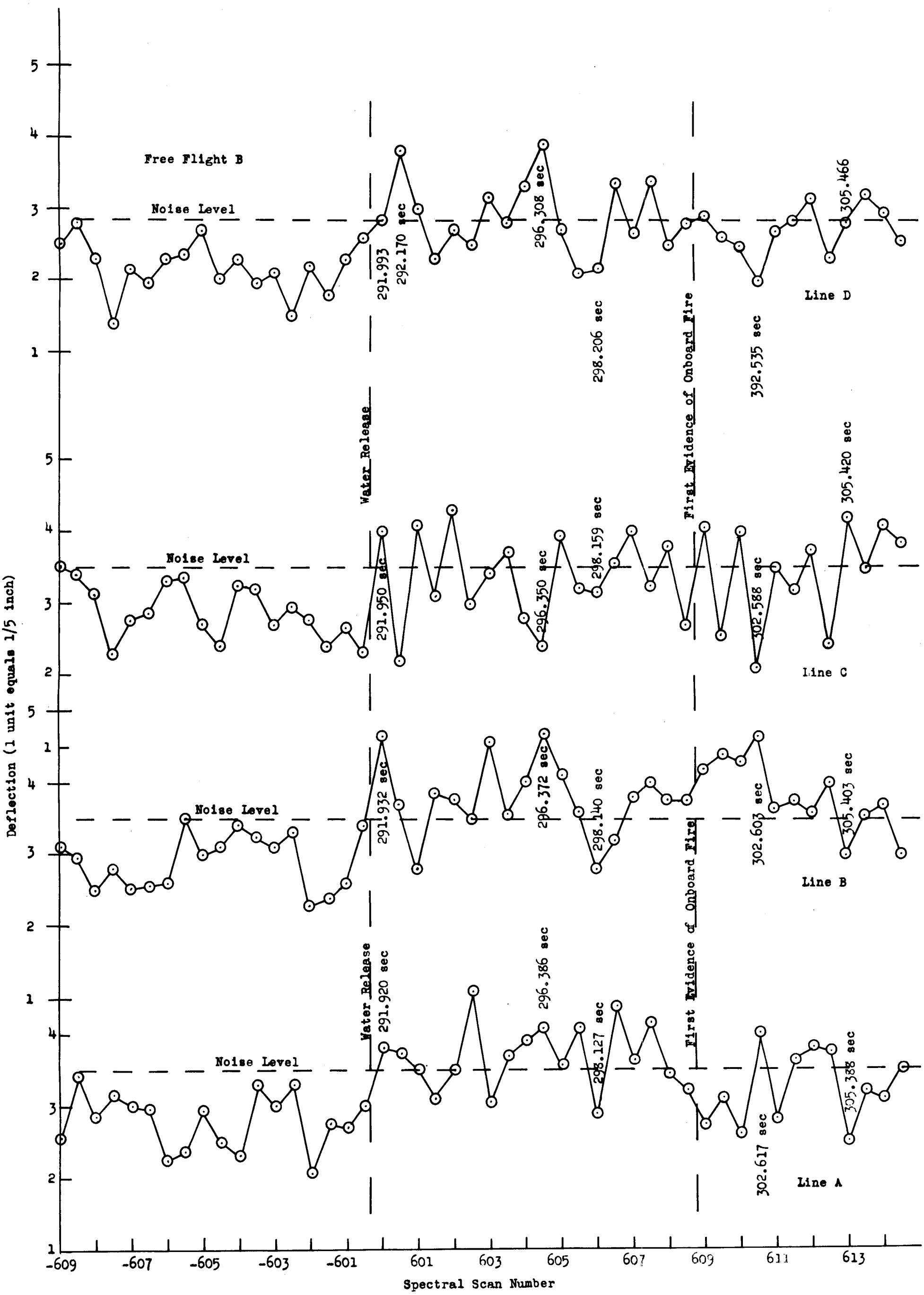

Figure 21: ELF-VLF Amplitude Variations; Spectral Scans -609 to 614

behavior of the spectral signals is especially evident for the 2150 cps frequency (Line C). Rapid fluctuations in the measured signal strength were recorded that were not observed prior to the release of the water. The horizontal dashed line represents the maximum level of background noise at each frequency during the acquisition of pre-release data. It is of importance to note that the level of the average signal strength after the release of the water becomes almost equal to the maximum pre-release background level.

Several features of the expansion of the water can be ascertained from both the optical and ELF-VLF spectral data. Photographically, the central core of the water-ice cloud formed by the release of the water into the ionosphere lasted for approximately seven (7) seconds. However, wide angle ground observations indicate that the outer ring of the cloud lasted for two (2) or three (3) seconds longer. The ELF-VLF spectral data shows a definite signal reduction at all four spectral frequencies seven (7) seconds after the water release. Following this reduction in signal strength, an increase in signal strength occurred for approximately three (3) seconds.

A rather consistent pattern of enhanced and reduced signals were recorded at all four (4) spectral frequencies during the cloud expansion. An initial enhanced signal was followed by an attenuated signal. This initially enhanced signal was followed by an attenuated signal. This initially enhanced signal appeared to last approximately one and one-half (1-1/2) seconds in three (3) of the four (4) spectral

lines (i.e., except for spectral line C). Spectral line C shows a sudden increase in the variations in signal strength during the initial expansion of the cloud. Variations in signal strength at the other three (3) spectral frequencies indicate a longer period of oscillation. All of these spectral signals are considered to be produced by perturbations produced in the ionosphere by the expanding water-ice cloud.

4.4 OCCURRENCE OF ONBOARD FIRE

Photographic data showed that a fire developed onboard the vehicle after the release of the water into the ionosphere. ELF-VLF spectral data acquired during the post water release flight of Saturn vehicle SA-3 supports this conclusion. The second vertical dashed line on Figure 21 represents the time when the first enhanced photographic signal was received by the TV Camera System. This TV Camera System was designed and developed by Mr. Walter Manning of the Air Force Missile Test Center, Patrick Air Force Base, Fla. At the time of the first appearance of the glow, several changes occur in the pattern of the signal strengths of the spectral lines. The change in the character of spectral line C (2150 cps) is particularly evident in that an oscillatory behavior developed. This oscillatory behavior is similar to that observed with the water release. Both spectral lines A and D exhibited a decrease in signal strength and spectral line B exhibited an increase in signal strength after the appearance of the glow.

The first photographic observations of an orange glow aboard the vehicle were obtained 14.563 seconds after the release of the water (i.e., T+306.5 sec). However, this

occurrence of the orange glow was acquired on only two frames of the motion picture film. A second observation of an orange glow started 17.542 seconds after the release of the water. This glow was recorded for 0.604 second. The first vertical dashed line on Figure 22 corresponds to the time of the beginning of this second occurrence of an orange glow. A change also occurred in the character of the variations in signal strength of each of the four (4) spectral ELF-VLF frequencies with this second orange glow observation. Spectral frequency 2150 cps displayed a short term oscillation similar to that recorded just after the water release and after the occurrence of the first enhanced glow that was recorded by the TV Camera System. Oscillations are established for a short period of time in the amplitudes of Spectral Lines A and D just after the second orange glow was observed by the color film. Only a single impulse was recorded at the spectral frequency 2140 cps (Line B) following the occurrence of the second orange flame. This characteristic signal pattern was similar to that recorded at this frequency following the water release and after the first enhanced optical signal was observed on the TV Camera System film. Enhanced photographic signals were also acquired by the TV Camera System (Tech Lab) during the same time interval the second orange glow was recorded by the ROTI Camera System (Vero Beach).

An orange glow was recorded by the ROTI Camera System (Vero Beach) which began 21.479 seconds after the release of the water. This glow had a duration of 0.117 second. An

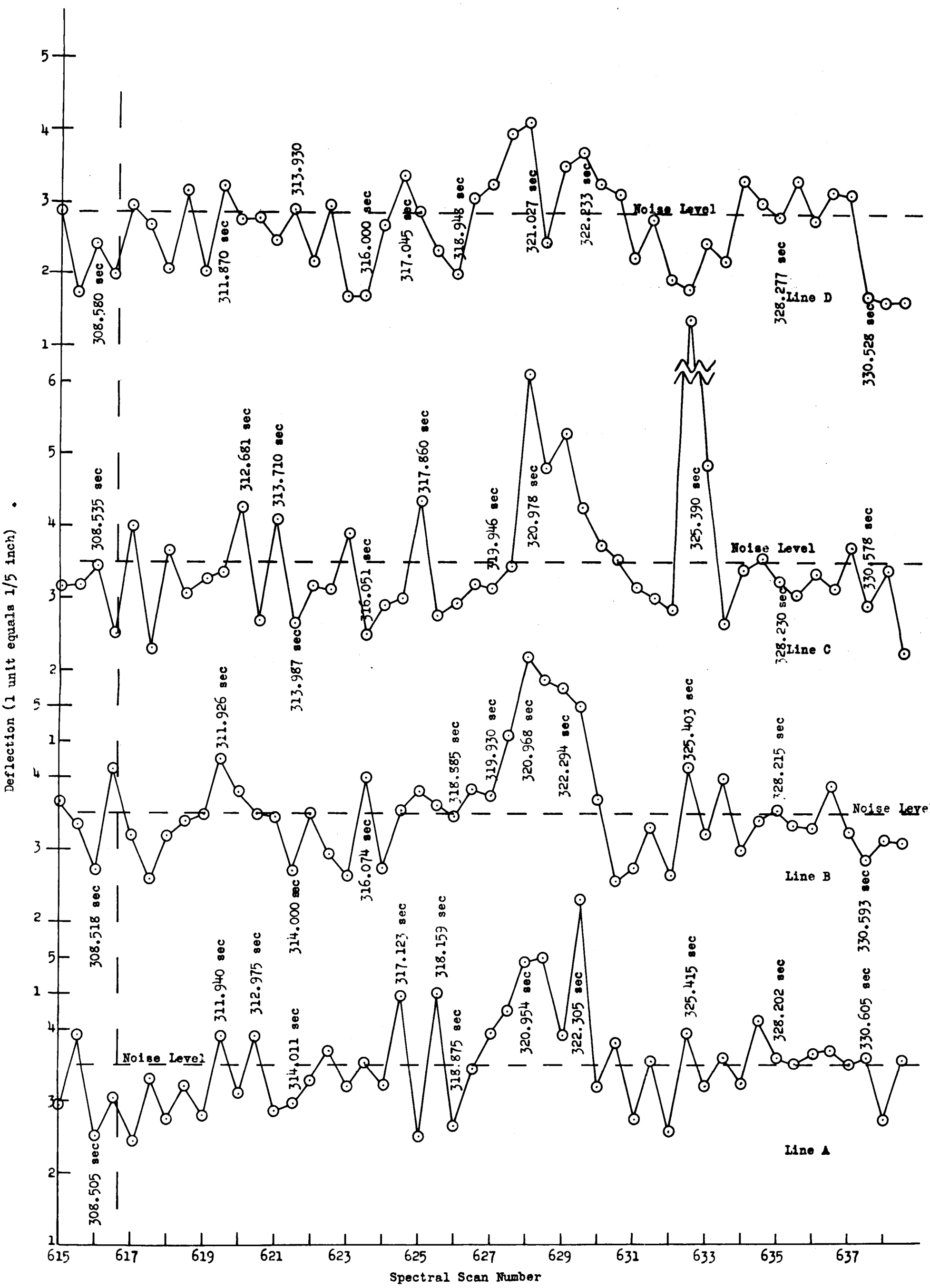

Figure 22: ELF-VLF Amplitude Variations; Spectral Scans 615 to 638

enhanced optical signal was also recorded by the TV Camera System (Tech Lab). The glow recorded by the TV Camera System commenced 0.179 second before the beginning of the one recorded by the ROTI Camera System. A change was also recorded in the ELF-VLF spectral data beginning about twenty-one (21) seconds after the release of the water. These changes in ELF-VLF spectral data indicate that there was increased action of the onboard fire before it was photographically observed. These conclusions are also justified because the flame was observed while the end of the vehicle was away from the cameras.

An enhanced optical image was recorded by the TV Camera System (Tech Lab) starting 25.467 seconds after the water release. No corresponding enhanced optical image was observed at this time from the Vero Beach tracking site. However, the occurrence of enhanced ELF-VLF spectral signals and the oscillations recorded at 2120 cps indicate that the onboard fire created a perturbation in the ionosphere at this time.

A prolonged large enhanced signal was recorded at all four (4) of the spectral frequencies between twenty-seven (27) seconds and thirty-one (31) seconds after the water release (Figure 22). No enhanced orange glow was recorded by the ROTI Camera System (Vero Beach) just before, during, or just after this time period. Beginning 28.800 seconds after the water release, an enhanced image was recorded by the TV Camera System (Tech Lab), but, unfortunately, the TV camera then lost track of the vehicle until just at the end of the period of the large enhanced ELF-VLF spectral signals. This large enhancement of the discrete spectral frequencies is considered to be

the result of two (2) effects:

1. The vehicle was passing through a region of inhomogeneities in the ionosphere.

2. The effects of the ionospheric inhomogeneities were intensified by the pulsation produced by the onboard fire.

These conclusions are in accordance with the results of ELF-VLF spectral measurements made during the launch of Saturn vehicles SA-3, SA-4 and of the Mercury-Atlas vehicle MA-9 (Ref. 5, 6, and 7). Analysis of the launch records showed that ELF-VLF spectral signals were enhanced when the launch vehicle passed through regions of atmospheric inhomogeneities. (i.e., regions of super gradients of the index of refraction).

A very large signal was recorded at 2150 cps, 33.470 seconds after the water release. Corresponding smaller enhanced signals were recorded at 2120 cps and 2140 cps. The spectral frequency 2210 cps exhibited an attenuation at this particular time. Three new ELF-VLF spectral signals were found to be enhanced during the two (2) seconds of the above-mentioned enhanced signal at 2150 cps. These new spectral signals (Table VI) were checked for the entire flight of Saturn vehicle SA-3 after the water release, and no equivalent enhancement was found to exist. In this particular

Table VI
Ephemeral Spectral Frequencies

Line	Tuner Rotation	Frequency
E	94.7^{0}	1134 cps
F	98.0^{0}	1150 cps
G	100.9^{0}	1165 cps

frequency range, the maximum noise level was about 2.00 units. Because of the short time of enhancement of these ephemeral spectral frequencies, no graphical plot of their intensity versus time was possible. Table VII shows the relative intensity of these lines during the short time period of their enhancement.

Table VII
Intensity of Ephemeral Frequencies

Spectral Scan	Line A	Line B	Line C
632 up	--	2.30	3.45
632 down	3.35	5.80	5.00
633 up	2.50	2.35	3.25
633 down	2.95	4.30	4.25
634 up	--	2.00	2.40

A definite change occurred in the amplitude behavior of all four (4) of the ELF-VLF spectral frequencies thirty-six (36) seconds after the water was released. Small oscillations were exhibited by the 2150 cps spectral frequency. These oscillations are similar to those noted previously at this frequency with other ionospheric perturbations (i.e., those created by the water release and the onboard fire). An enhanced optical image was recorded by the TV Camera System (Tech Lab), and an orange glow was observed by the ROTI Camera System (Vero Beach) at this time.

Two occurrences of an orange glow were observed by the ROTI Camera System during the thirty-ninth (39) second after the water release (T+331 sec). A prolonged enhanced optical image was observed by the TV Camera System (Tech Lab) from

38.800 seconds to 41.700 seconds after the water release. This time interval occurred during the last spectral scan of Figure 22 and the first two spectral scans of Figure 23.

Figure 23 shows two distinct regions which exhibit a completely different variation in the amplitude behavior for all four (4) of the spectral lines. These changes in the amplitude behavior correspond to the presence or absence of the orange glow. The first vertical dashed line (I) on Figure 23 is the time of the last frame (of the second occurrence during the 39th second after the water release) the orange glow was observed by the ROTI Camera System (Vero Beach). Beginning fifty-two (52) seconds (T+344 sec) after the water release, a series of pulsations of the onboard fire appeared to have developed. These pulsations were evident by the occurrences of a series of images of the orange glow recorded by the ROTI Camera System (Vero Beach) records. The onset of these pulsations are indicated by the second vertical dashed line (II) in Figure 23. The characteristic of all four (4) of the spectral frequencies also indicate the existence of pulsation in the ionosphere.

The time of the commensing of the prolonged flame that apparently produced a change in the rotation rate of the vehicle is indicated by the third vertical dashed line (III) (T+355 sec) in Figure 23. No pronounced change is evident in the ELF-VLF spectra at the beginning of this prolonged existence of the protruding flame. However, intensification of the oscillatory characteristic of the spectra becomes evident.

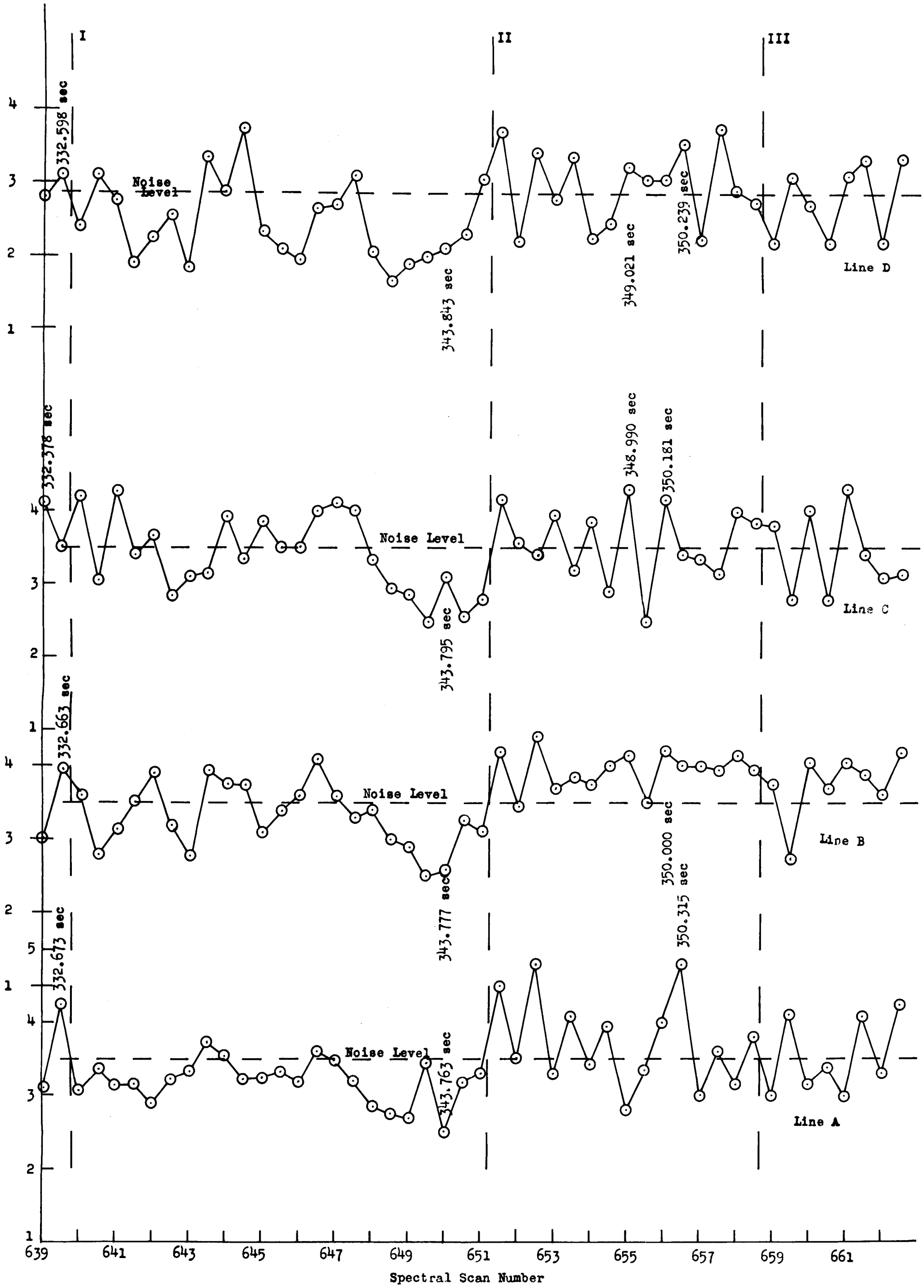

Figure 23: ELF-VLF Amplitude Variations; Spectral Scans 639 to 662

This lack of a pronounced change in the character of the spectral signals with the commensing of the prolonged flame is undoubtedly due to the series of flame pulsations that had just preceeded its occurrence.

Effects on the ionosphere of the onboard flame are shown in Figure 24. Optical data during this time interval was quite poor. The orange glow was photographed only two (2) times and for very short time intervals. However, the ELF-VLF data indicates the existence of ionospheric perturbations during the time interval encompassed by Figure 24.

The last optical image of the orange glow was obtained 97.083 seconds after the water release (T+389 sec). This time is indicated by the vertical dashed line on Figure 25. During the time interval (0.291 sec) that the orange glow was photographed, the orientation of the vehicle was nearly perpendicular to the line of sight of the ROTI Camera System (Vero Beach). Each of the four (4) spectral frequencies exhibited an increase in signal strength during the time the last pictures of the orange glow were obtained.

ELF-VLF spectral data indicate that ionospheric perturbations were still being produced after the cameras ceased to track the tumbling vehicle. Effects of these perturbations can be seen in Figures 25, 26, and 27. In these later figures, the apparent ionospheric impulses are of a different character than those discussed earlier. The possibility exists that these latter spectral signals were created by

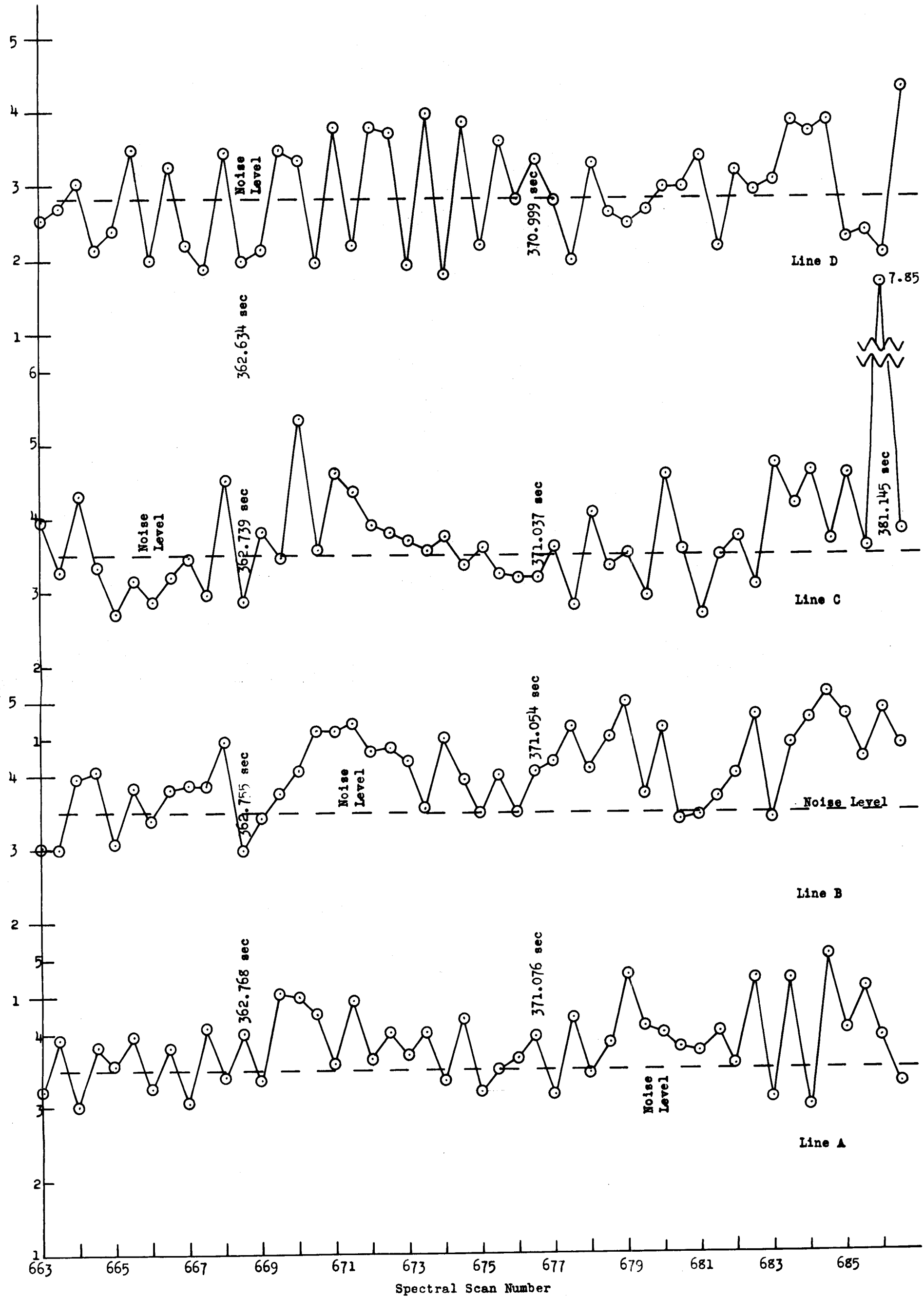

Figure 24: ELF-VLF Amplitude Variations; Spectral Scans 663 to 686

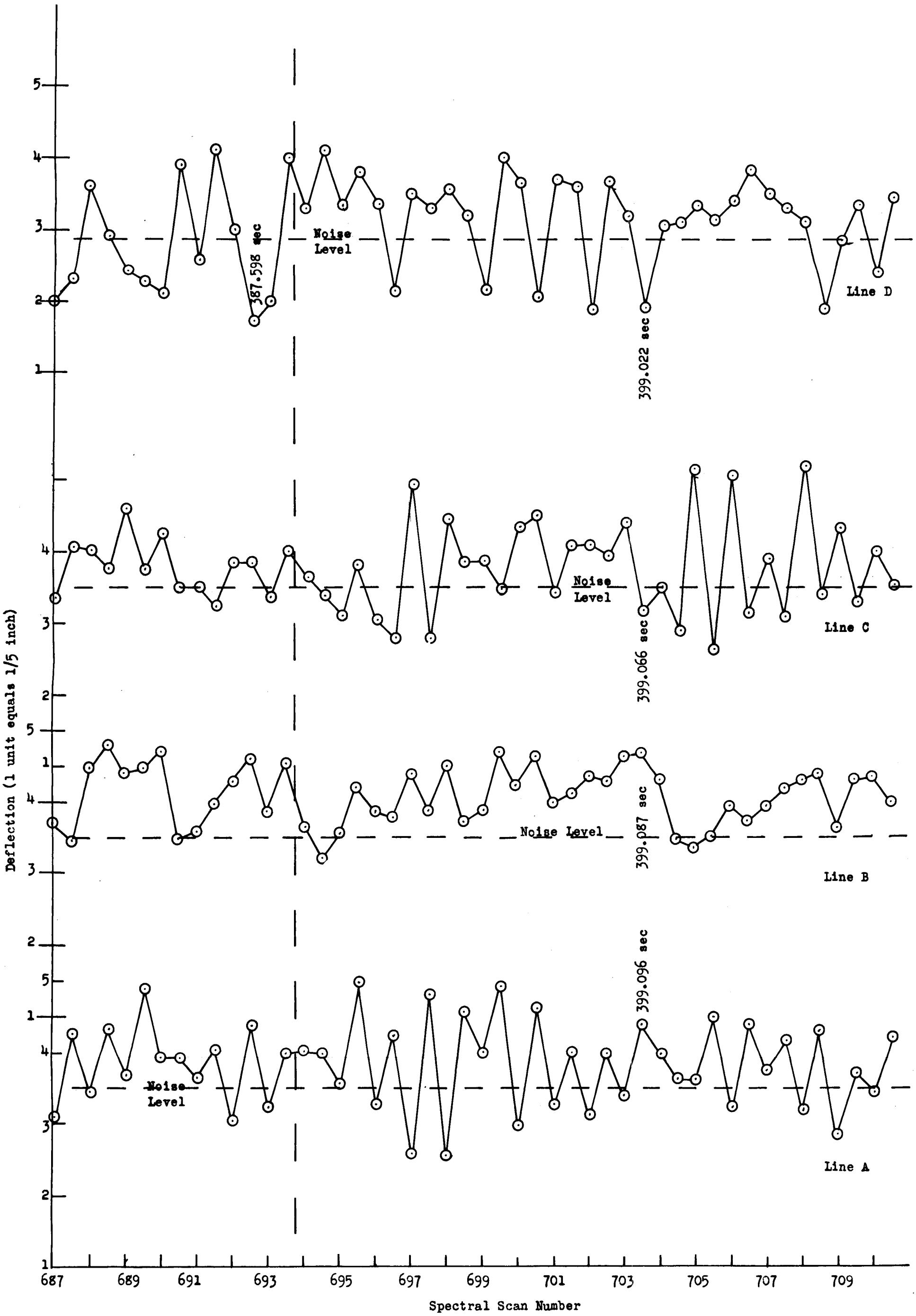

Figure 25: ELF-VLF Amplitude Variations; Spectral Scans 687 to 710

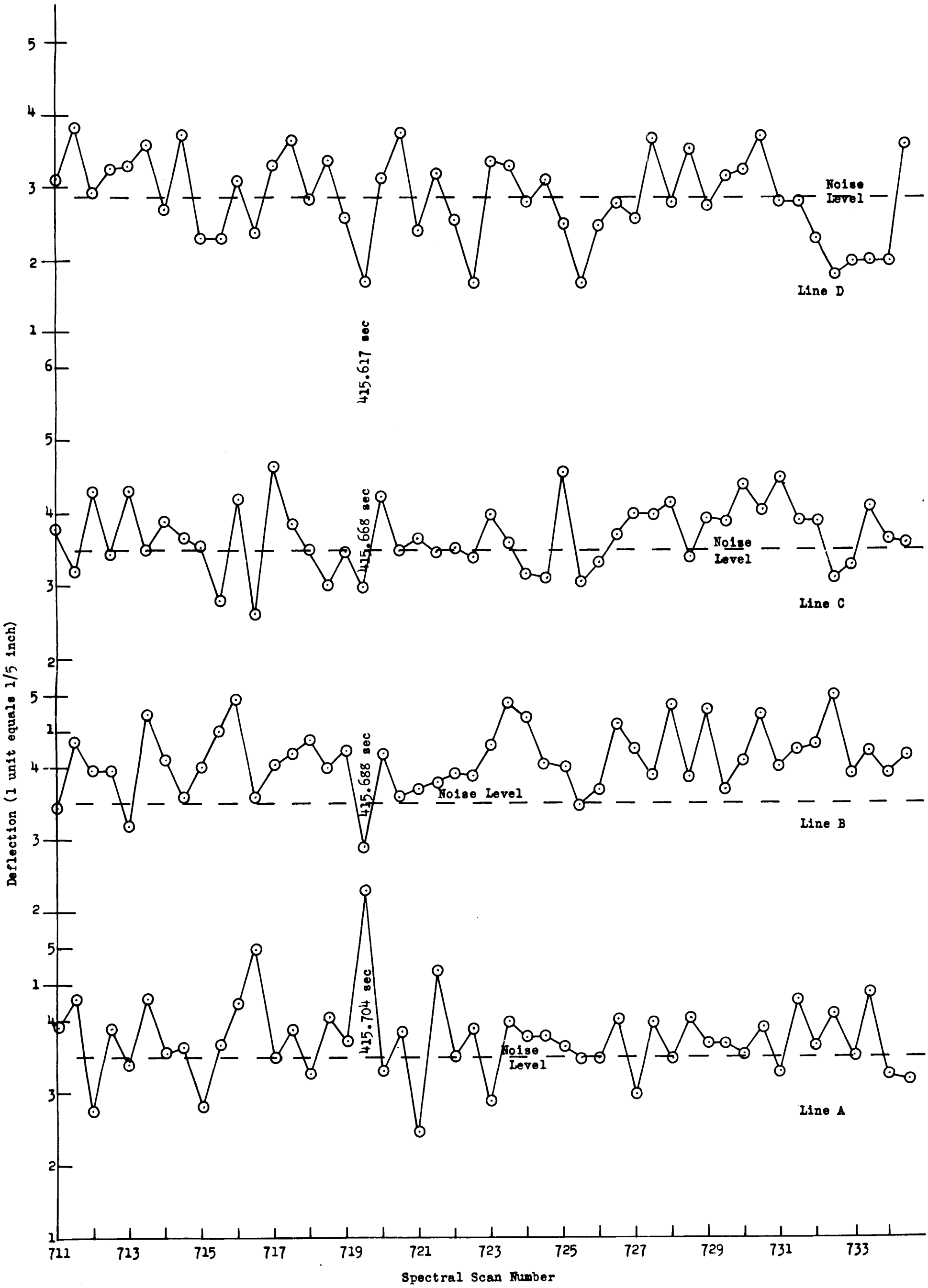

Figure 26: ELF-VLF Amplitude Variations; Spectral Scans 711 to 734

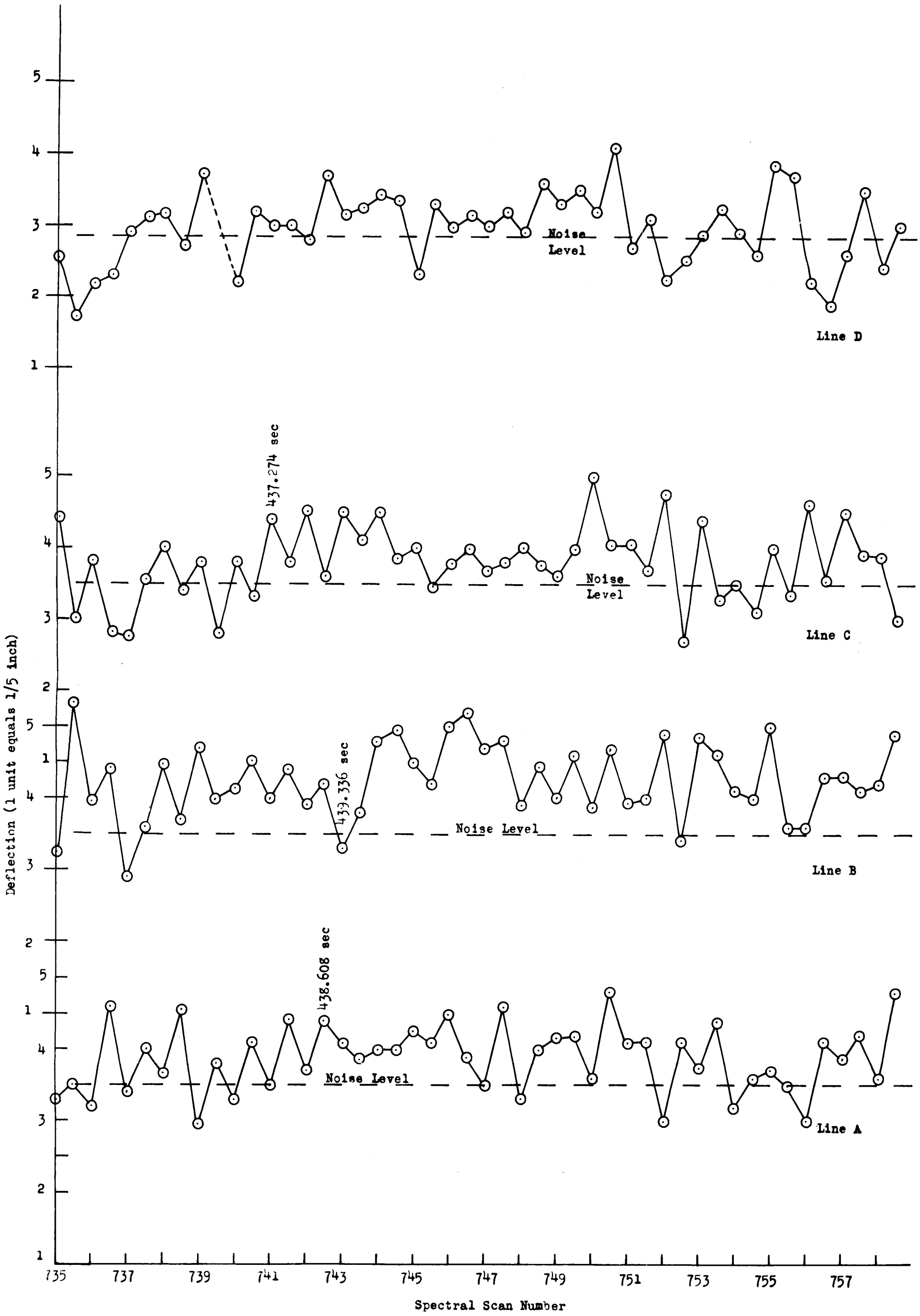

Figure 27: ELF-VLF Amplitude Variations; Spectral Scans 735 to 758

oscillations of the ionosphere which were generated by the release of the water and the fire aboard the tumbling vehicle.

The ELF-VLF data shown in Figures 28 and 29 has a considerably different character from that observed following the release of the water and the onboard fire. Although the amplitudes of the peak intensities measured by the Spectrometer are nearly as great as those observed after the water release, the distribution of the peaks is much more random. Impact occurred just before the 803rd spectral scan.

Post flight (Figures 30 and 31) ELF-VLF spectral signals are quite similar to those obtained just prior to water release (i.e., while the vehicle was in free flight through the ionosphere - spectral scans -638 to 600). The amplitude of the post flight signals are slightly higher than those observed just prior to the release of the water into the ionosphere. However, the fluctuations in signal strength are very similar. The post flight increased signal level is believed to be due to the residual distrubances created in the ionosphere by the passage of the vehicle, the release of the water and the pulsation from the fire aboard the tumbling vehicle.

ELF-VLF observations were continued until approximately 1825 Z. The amplitudes of the four (4) spectral lines over a twelve (12) second interval centered at 1820 Z are shown in Figure 31. The signal levels of all four (4) spectral frequencies have returned to approximately the same level observed prior to the launch of the SA-3 vehicle.

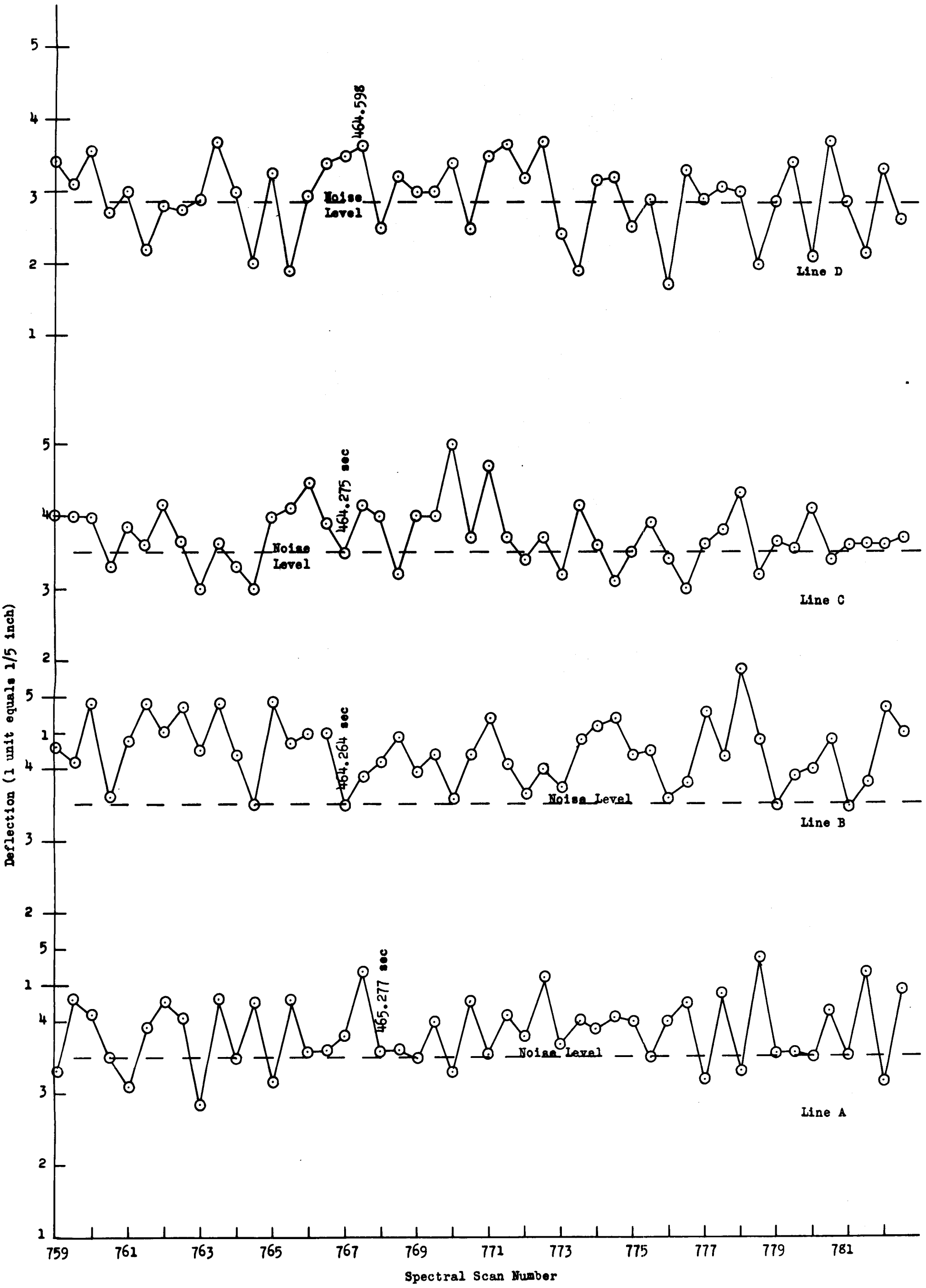

Figure 28: ELF-VLF Amplitude Variations; Spectral Scans 759 to 782

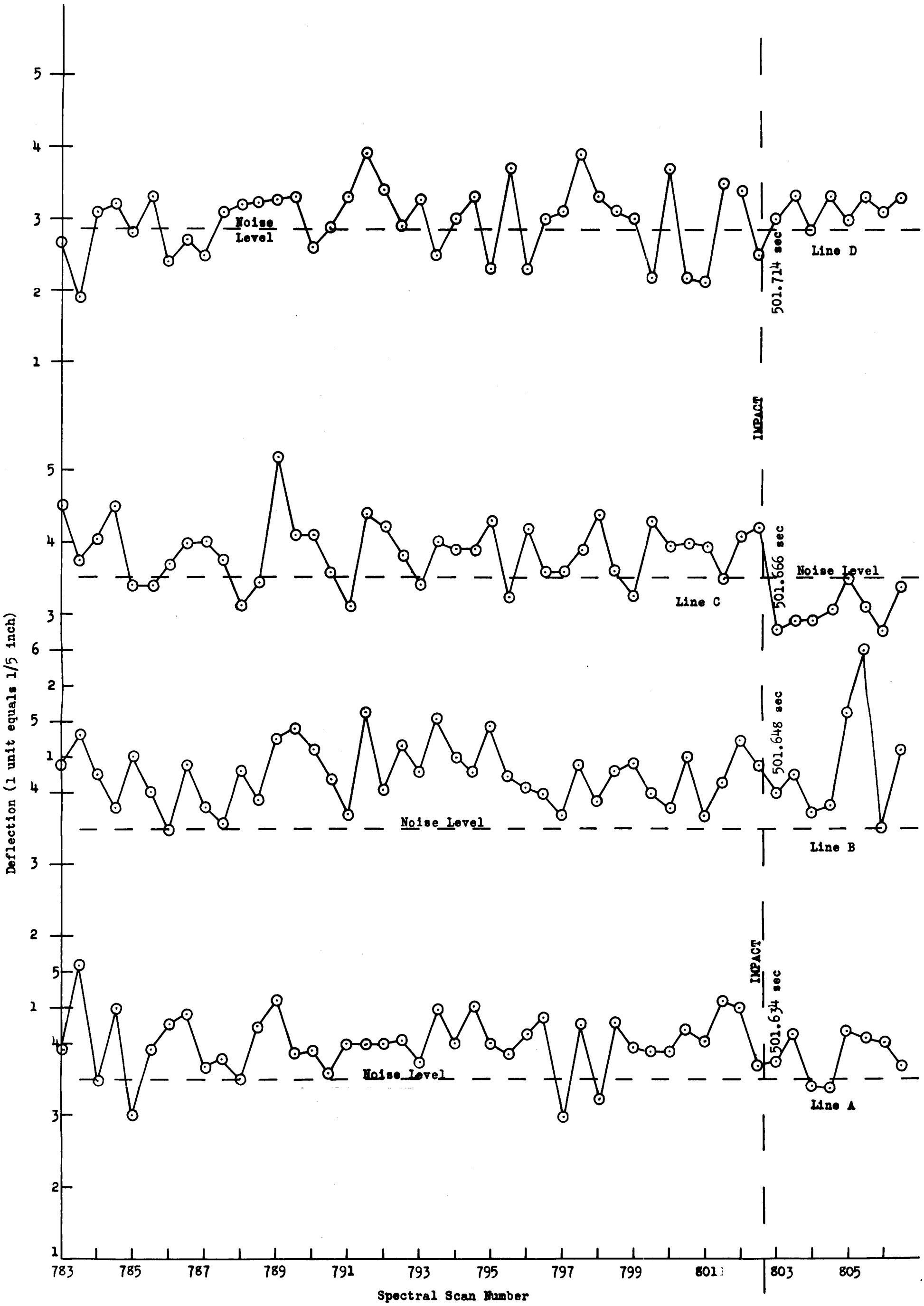

Figure 29: ELF-VLF Amplitude Variations; Spectral Scans 783 to 806

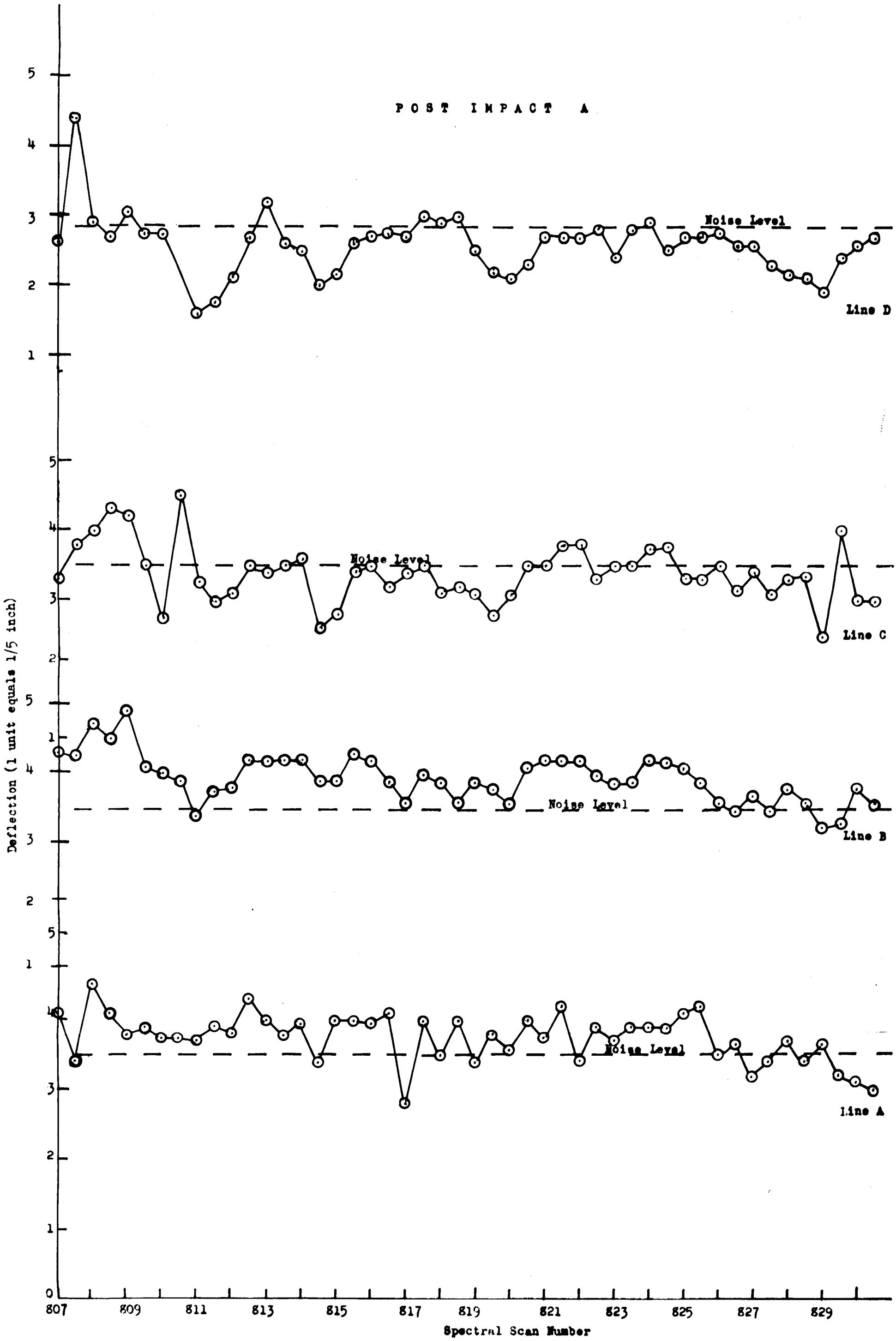

Figure 30: ELF VLF Amplitude Variations; Spectral Scans 807 to 830

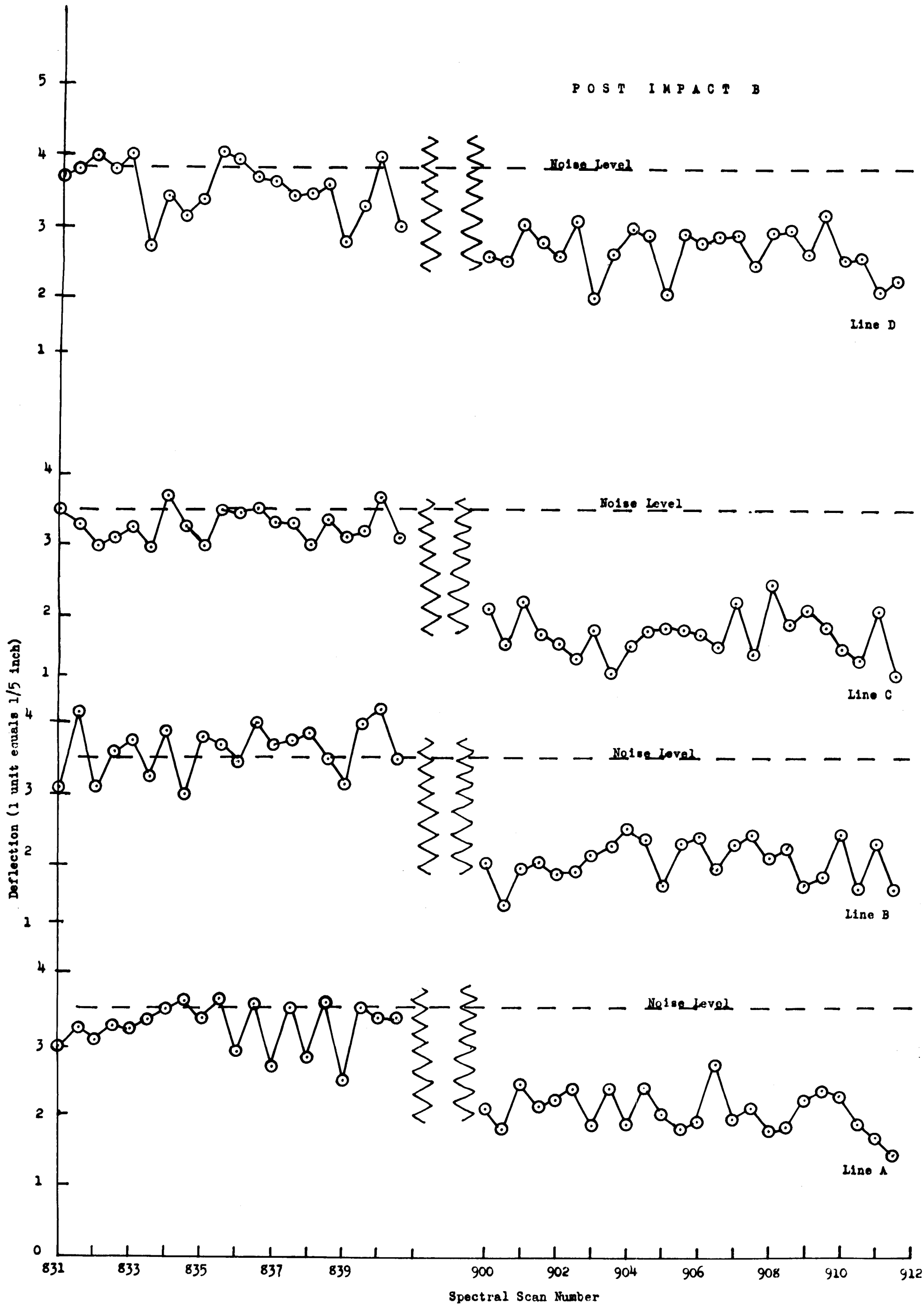

Figure 31: ELF-VLF Amplitude Variations; Spectral Scans 831 to 911

4.5 GENERAL ASPECTS OF THE ELF-VLF DATA

The ELF-VLF records obtained in conjunction with the SA-3 launch operation and Project High Water show that between 1630 Z and 1830 Z (on November 16, 1962) sferic (atmospheric noise) activity in the vicinity of Cape Canaveral was exceptionally low. A detailed examination of the ELF-VLF spectral records reveals that no sferics were observed during the time the visible cloud was present. A total of only six (6) sferics were observed in the eighty (80) seconds following the water release. The first post-water release sferic was recorded at (Range Time) T+305.823 seconds or approximately fourteen (14) seconds after the water release. The second post-release sferic was observed at T+307.457 seconds. The other four (4) observed in the 80 second period following the water release were observed at T+350.207 sec., T+363.202 sec., T+364.991 sec., and T+369.286 sec. The absence of sferics (or sferic-like signals) is virtually conclusive evidence that no electrical discharges were associated with the second Project High Water visible cloud. On the basis of available data, there is no evidence of any electrical discharges associated with the second Project High Water experiment.

The four (4) spectral frequencies found to correlate with the water release and the onboard fire are of considerable interest. All four (4) frequencies are within the general frequency range associated with spin state transitions of the proton. Using the assumption that the spin state transition is the radiation generation mechanism, the magnetic field

intensity can be calculated. The calculated magnetic field corresponding to each of the spectral frequencies is given in Table VIII.

Table VIII
Calculated Magnetic Field for Water Release

Line	Frequency	Calculated Magnetic Field
A	2120 cps	4.97×10^{-5} Webers/m^2
B	2140 cps	5.02×10^{-5} Webers/m^2
C	2150 cps	5.05×10^{-5} Webers/m^2
D	2210 cps	5.18×10^{-5} Webers/m^2

Since the magnetic field in the vicinity of Cape Canaveral has a value of 5.19×10^{-5} Webers/m^2, the magnetic field at the location of the water release will be a value below the Cape Canaveral value. There are two (2) factors that must be considered in comparing the magnetic field at the release location with that at Cape Canaveral. First, the release was nearer the earth's magnetic equator, and second, the release was made in the ionosphere. Both of these factors will cause the magnetic field to be less than it is at Cape Canaveral. On the basis of the presently available data, a magnetic field intensity of 4.97×10^{-5} Webers/m^2 is the preferred value. However, the magnetic field intensity may be as high as 5.05×10^{-5} Webers/m^2.

5.0 RADIOFREQUENCY AND RADAR OBSERVATIONS

Observations were made at selected locations in the radio-frequency (1 Kc/sec to 420 Mc/sec) and radar (C-band) portions of the electromagnetic spectrum during the High Water experiment. In addition, one record was made of WWV (10 Mc) reception during Project High Water. The principal observations in the radio frequency portion of the spectrum were "noise" recordings at thirteen (13) different frequencies. The specific frequencies employed for the noise measurements are summarized in Table IX. These noise measurements were made at two (2) locations. These were Patrick Air Force Base Technical Laboratory (Tech Lab) and the Cape Canaveral Frequency Control Analysis Building (FCA).

5.1 SUMMARY OF RADIOFREQUENCY AND RADAR DATA ANALYSIS

An analysis was made of the thirteen (13) "noise" observation records, the radar observations, and attenuations of WWV transmissions. Further support was found for the results obtained in the analysis of optical and ELF-VLF spectral data. These data combined with telemetry evaluations provided a valuable insight into the nature of the ionosphere and a proposed explanation for some of the telemetry and radar tracking problems. The results of this analysis are presented in three phases which are the water release analysis, the glow phenomena, and ionospheric attenuations of telemetry and radar.

5.1.1 Summary of Water Release Analysis (Phase I)

This analysis of the "noise" recordings, radar observations, (SA-3) telemetry evaluation, and WWV reception data

Table IX

R.F. Electromagnetic Noise Recordings

	Frequency	Receiver Bandwidth	Antenna	Receiver Location	Signals Correlate With High Water Release	Nature of Records
1	420 Mc/s	16 Kc	3.5 Turn Helix	Tech Lab PAFB	No	Low activity - amplitude variations generally confined to sharp enhancements.
2	232.4 Mc/s	16 Kc	Tri Helix	Tech Lab PAFB	Yes - not Unique	Moderate activity - amplitude variations consisted of both sharp enhancement & periods of sustained signals.
3	200 Mc/s	NL*	Vertically Polarized Dipole	Cape FCA Building	No	Extremely low activity - almost no amplitude variations.
4	160 Mc/s	NL*	Vertically Polarized Dipole	Cape FCA Building	No	Extremely low activity - almost no amplitude variations
5	136 Mc/s	16 Kc	Log Periodic Dipole	Tech Lab PAFB	Not significant	Low activity - amplitude variations primarily consisted of sharp enhancements with a few sustained signals.
6	89 Mc/s	16 Kc	Log Periodic Dipole	Tech Lab PAFB	No	Low activity - amplitude variations primarily sharp enhancements with a few sustained signals.
7	71 Mc/s	16 Kc	12 element yagi	Tech Lab PAFB	No	Low activity - amplitude variations limited to sharp enhancements.
8	20.973Mc/s	16 Kc	Log Periodic Dipole	Tech Lab PAFB	Yes - not Unique	High activity - amplitude variations of sharp enhancements and sustained signals.
9	16.8 Mc/s	NL*	Longitudinally Polarized Dipole	Cape FCA Building	No	Signals present at all times. Amplitude variations of 25 db. Receiver tuning changed after T+445 sec
10	5.5 Mc/s	NL*	Long Wire	Cape FCA Building	Yes	Moderate activity-sharp enhancements only until just prior to water release.
11	420 Kc/s	NL*	Whip	Cape FCA Building	Yes - not Unique	High activity-recorder driven into saturation several instances.
12	25 Kc/s	NL*	Long wire (North)	Cape FCA Building	Yes - not Unique	High activity-recorder frequently driven into saturation.
13	1 Kc/s	NL*	NL*	Cape FCA Building	No	Extremely low activity-amplitude variations rarely exceeded 2 db.

NL* This information not listed in data provided.

yielded the following:

A. Enhanced signals were recorded at five (5) of the thirteen (13) frequencies monitored (i.e., 232.4 Mc, 20.973 Mc, 5.5 Mc, 420 Kc, and 25 Kc) following the water release. Only the 5.5 Mc signals were unique. The 5.5 Mc signals have been identified as the fourth harmonic of the electron gyrofrequency.

B. The absence of enhanced signals at eight (8) of the frequencies monitored is strong evidence that the emissions observed at five (5) of the frequencies is spectral in character.

C. The release of the water caused the radar track of the vehicle to be lost. The time of this loss is believed to have been between ten (10) and seventeen (17) seconds.

D. Severe telemetry effects accompanied the water release. Loss of telemetry varied with receiver station and frequency. At some orientations and frequencies the telemetry loss exceeded sixty (60) seconds.

E. Approximately fifty-six (56) seconds after the water release, a dropout in the WWV (10 Mc) reception occurred. Other periods of marked attenuation were also experienced. The water release produced identifiable WWV reception effects for approximately three hundred (300) seconds.

F. The thirteen (13) "noise" recordings support the ELF-VLF evidence that no electrical discharges were associated with the second Project High Water experiment.

5.1.2 Summary of Glow Phenomena Analysis (Phase II)

A. Radar records show a definite change occurred in the tumble rate (i.e., a slowing down) of the SA-3 vehicle part. The time the tumble rate changed (T+353 to T+355 sec) correlates precisely with the optical data and the sustained period of the glow. Thus, all available data supports the evidence of an onboard fire.

B. Enhanced signals recorded at 5.5 Mc showed a high degree of correlation with the development of visible glows. Thus, a cross correlation was found between the optical data, 5.5 Mc data and the ELF-VLF spectral data.

5.1.3 Ionospheric Attenuation of Telemetry and Radar (Phase III)

A. A series of sharp spikes were recorded at 5.5 Mc during the time the SA-3 vehicle was traversing the E-layer of the ionosphere. These 5.5 Mc signals correlated timewise with the only significant signals observed at 160 Mc and signals observed at 420 Kc.

B. The physical basis for the above emissions at 5.5 Mc, 160 Mc, and 420 Kc is believed to be the result of encounters of the vehicle with inhomogeneities in the ionosphere.

C. Radar beacon dropouts occurred at all stations either during or just after the time the 5.5 Mc signals were observed.

D. Degredation of telemetry signals was experienced at several telemetry receiving stations shortly after the time the 5.5 Mc signals were observed. The telemetry degredation also displayed frequency dependency.

E. The above telemetry degredation and radar beacon dropouts are definitely believed to be a consequence of the presence of inhomogeneous regions in the ionosphere and that evidence of these regions was obtained from the 5.5 Mc observations.

5.2 NOISE RECORDINGS DURING PROJECT HIGH WATER

An examination of the noise recordings shows the occurrence of signals which correlated with the High Water release were observed at five (5) of the frequencies (i.e., 232.4 Mc, 20.973 Mc, 5.5 Mc, 420 Kc, and 25 Kc). Signals were observed at 136 Mc, but these signals do not appear to be of significance. The observations at 5.5 Mc are the only signals that display unique character. Although the signals observed at the other four (4) frequencies are considered to be associated with the High Water release, the character of the observed signals are quite similar to those which were observed both preceeding and well after the water release occurred.

A sketch of the unique 5.5 Mc signals is shown in Figure 32. The characteristics of these signals were as follows:

A. A sharp spike (26 db) was recorded at T+291.83 seconds.

B. A signal with a rising intensity followed the sharp spike at T+291.83 seconds.

C. The (rising) signal appeared to be composed of two signals with maximum amplitudes of 15 db and 36 db.

D. The maximum amplitudes were observed between T+295.0 and T+303.5 seconds.

E. An abrupt decrease in the 5.5 Mc signals occurred at the approximate time the visible cloud disappeared (T+299.5 sec). The signals returned to the same level at T+300.5 seconds.

F. The 5.5 Mc signal level returned to pre-release level at T+304.1 seconds.

No other 5.5 Mc signals were observed that showed resemblance to those which occurred following the High Water release during the time interval of the observations (i.e., from approximately T+10 sec to almost T+800 sec). Additional signals at a frequency of 5.5 Mc were observed at times other than those following the High Water release, but these additional 5.5 Mc signals do not show the same characteristics as those following High Water release. These additional 5.5 Mc signals will be considered later in this report.

Signals were observed at a frequency of 420 Kc which are also considered to be associated with the High Water release. At T+291.8 seconds, a sharp spike (16 db) was recorded. This spike is believed to have been generated by the explosive charge used to rupture the vehicle tanks. Before the recorder was able to return to the base line

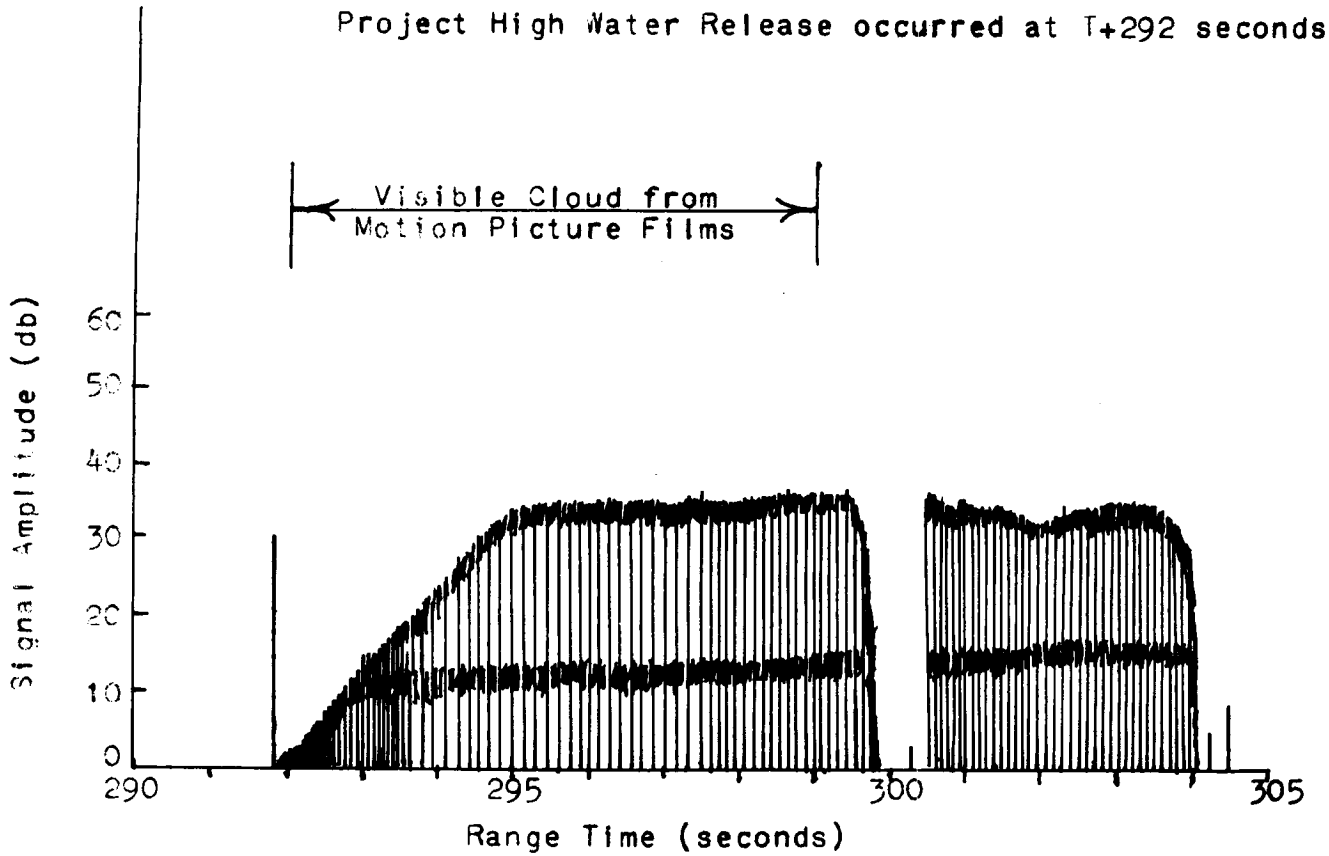

Figure 32: Sketch of 5.5 Mc Signals Observed Between T+290 and T+305 seconds

following the sharp spike (at T+291.8 sec), a second impulse was received and the recorder was driven to saturation. The recorder was saturated until T+296 seconds. A small enhancement (7 db) was recorded at T+303.2 seconds. Although these 420 Kc signals are not unique in the records for this frequency, their occurrence correlates timewise with the 5.5 Mc observations.

Signals were observed at 25 Kc during the time of High Water release. An impulse drove the recorder into saturation at T+291.0 seconds, and the recorder remained in saturation until T+293.5 seconds. A series of smaller spikes were recorded with the amplitude reaching a minimum value at T+303.5 seconds. The 25 Kc signals during the High Water release displayed no unique features, but their occurrence shows a reasonable degree of correlation with the 5.5 Mc and the 420 Kc signals.

Signals observed at 232.4 Mc consisted of an isolated spike (7 db) at T+293.1 seconds and a sustained signal (maximum value of 10 db) from T+294.9 to T+305.2 seconds. The only justification for considering these signals to be associated with the High Water release is the time of occurrence. There were no unique features to the 232.4 Mc signals noted above.

Signals at a frequency of 20.973 Mc consisted of a sharp spike (18 db) at T+293.1 seconds followed by a series of smaller amplitude signals terminating in a sharp spike (19 db) at T+293.3 seconds. A sustained signal (maximum

amplitude - 9 db) was present from T+298.5 to T+299.7 seconds. No unique features were associated with the above signals at a frequency of 20.973 Mc.

Signals at a frequency of 136 Mc consisted of an isolated spike (8 db) at T+293.9 seconds and a sustained signal (maximum amplitude - 6 db) from T+295.9 to T+301.5 seconds. This sustained signal (136 Mc) is very similar to a sustained signal which was recorded just prior to T=0.

Although signals were observed at five (5) (perhaps six (6)) of the frequencies monitored, the only signal that displays unique character following the High Water release was observed at 5.5 Mc. A possible theoretical mechanism for the generation of 5.5 Mc signals is the gyromagnetic motion of electrons. The gyromagnetic (or cyclotron) frequency $\underline{\nu_e}$ of an electron is a function of the magnetic field strength $\underline{H}$ (in Webers/m^2), or

$$\nu_e = 2.8 \times 10^{10} \, H \quad c/s \qquad (19)$$

In the analysis of the ELF-VLF spectral data, it was postulated that the intensity of the magnetic field at the water release location had an intensity of 4.79×10^{-5} Weber/m^2. If this value is used, the characteristic electron frequency is calculated to be:

$$\nu_e = 1.39 \text{ Mc/s} \qquad (20)$$

Thus, 5.50 Mc is 3.96 times the calculated characteristic frequency $\underline{\nu_e}$. Thus, it can be assumed that 5.5 Mc is the fourth harmonic of the electron gyrofrequency at the release point. The characteristic electron frequency is found to be 1.375 Mc which corresponds to a magnetic field of 4.93×10^{-5}

Weber/m^2 or a magnetic field intensity which is only 0.26×10^{-5} Weber/m^2 less than the mean value at Cape Canaveral and 0.04×10^{-5} Weber/m^2 less than the value obtained from the ELF-VLF data.

There are a number of additional aspects that lend some credulence to the hypothesis that the 5.5 Mc signals are a consequence of gyromotion of electrons. Two of the more important experimental facts are:

A. Plasmas have been shown to emit the characteristic frequency and harmonics of electrons (Ref. 8), and the ionosphere is a plasma (actually a pseudoplasma).

B. Charge separation (i.e., generation of electrons and ions) is a common phenomenon of water-ice systems, and there can be little doubt that a portion of the release water was converted into ice.

Unfortunately, there is insufficient information available at this time to confirm or reject the hypothesis that the 5.5 Mc signals were a consequence of gyromotion of electrons.

5.3 NOISE RECORDINGS PRIOR TO PROJECT HIGH WATER

Two (2) significant "bursts" of signals were recorded at 5.5 Mc prior to Project High Water. A series of sixteen (16) sharp spikes were recorded between T+164.1 seconds and T+188.0 seconds. A second series of fourteen (14) sharp spikes were recorded between T+273.6 seconds and T+284.2 seconds with a sustained signal recorded between T+277.8 to T+281.8 seconds. With the exception of these two "bursts", the 5.5 Mc records contained only an occasional spike in the time interval T+10 seconds to Project High Water. These two (2) "bursts" of signals showed virtually no similarity to

the signals recorded after T+292 seconds. It is noted that both "bursts" occurred well after burnout.

5.3.1 Noise Recordings between T+164 and T+188 seconds

The sixteen (16) 5.5 Mc spikes recorded between T+164 and T+188 seconds ranged in amplitude from 9.0 db to 34.5 db with ten (10) being 17 db or more. During this same time interval or T+165 to T+182 seconds, four (4) distinctive spikes were recorded at 160 Mc. These four (4) 160 Mc spikes range in amplitude from 5 db to 15 db, and they are unique in the (complete) records of the 160 Mc observations (i.e., T+10 sec to T+700 sec). The 160 Mc spikes do not correlate time-wise with the individual spikes at 5.5 Mc. Each of the 160 Mc spikes did occur 0.8 to 0.9 second prior to a 5.5 Mc spike. Signals were also recorded at a frequency of 420 Kc. The 420 Kc recorder was driven into saturation from T+164.5 seconds to T+172.0 seconds, and from T+175.0 seconds to T+179.5 seconds. Between T+180 and T+187 seconds, the 420 Kc signals were at a moderate level. A final sharp peak was recorded at T+188.0 seconds. The 420 Kc signals recorded between T+164 and T+188 seconds constituted the most sustained period of signal activity in the (total) 420 Kc records. No significant signals were recorded at the other ten (10) frequencies monitored (i.e., 420 Mc, 232 Mc, 200 Mc, 136 Mc, 89 Mc, 71 Mc, 20.973 Mc, 16.8 Mc, 25 Kc, and 1 Kc). A small amount of signal activity was recorded in the time interval T+164 to T+188 seconds at 25 Kc, 20.973 Mc, and 232 Mc, but the general character of these signals suggests that they are not of significance.

A physical basis must exist for the "noise" signals observed during the time interval of T+164 to T+188 seconds. Since definite signals were observed with three (3) independent receivers, it can be concluded that these signals were not a consequence of the receiver. Another possible source is ground-generated noise (e.g., electrical arcs, etc.). The ground-based noise source does not appear to be tenable. A noise source that generated signals at 160 Mc, 5.5 Mc, and 420 Kc would have also generated signals at other frequencies, and there were four (4) other receivers (i.e., 200 Mc, 16.8 Mc, 25 Kc, and 1 Kc) at the same location (FCA Building) which did not record significant signals in this time interval. The absence of signals in the records for 25 Kc and 1 Kc are considered especially significant since electrical arcs emit strongly at these frequencies. Therefore, it is logical to assume that the signals generated between T+164 and T+188 are associated with the flight of the Saturn (SA-3) vehicle.

The Saturn vehicle was at an altitude of 90 km at T+164 seconds and an altitude of 115 km at T+188 seconds. Therefore, the vehicle was traversing the E-layer of the ionosphere during the time the signals were recorded at 160 Mc, 5.5 Mc, and 420 Kc. A plausible explanation for the generation of these signals is that they are the consequence of the transit of the Saturn vehicle through varying inhomogeneities in the ionosphere. Varying inhomogeneities in the ionosphere would result in sharp gradients in the index of refraction. If the above model is representative of the physical conditions, then telemetry and radar effects should be experienced.

Distinct attenuations of the telemetry and radar beacon transmission were encountered.

One of the most obvious effects was the dropout of the radar beacon. These radar beacon dropouts are summarized in Table X.

Table X

Radar Beacon Effects
(Times referenced Range Zero)

Station	Time of Dropout (sec)
FPS 16 1.16	196.5
FPS 16 0.16	177
FPS 16 3.16	191.5
FPS 16 42.16	178

During the time interval T+196.5 to T+202.0 seconds (i.e., for 5.5 sec), the radar beacon was not received at any of the stations. Also, a sharp attenuation occurred in the records of FPS 16 42.16 between T+202.0 and T+203.5 seconds. A similar attenuation occurred in the records of FPS 16 3.16. The time could not be ascertained (poor time record), but it appears to be at a slightly later time than the preceeding case.

The telemetry effects varied depending on the location of the receiving station. Considerable degredation of the telemetry signals (242.0 to 258.9 Mc) were encountered at Hangar D between T+190 and T+227 seconds; however, the exact time interval was frequency dependent. Attenuations of telemetry signals during this same time interval were encountered by the stations located at New Smyrna Beach, Vero Beach, and Patrick Air Force Base. Three telemetry stations (Cape

Tel 2, Cape Tel 3, and Grand Bahama Island) did not experience telemetry signal degredations. The variation in the signal effects with stations is compatable with the proposed model since the effect depends on the relative orientation of the inhomogeneities with the transmission path.

5.3.2 Noise Recordings between T+273 and T+285 seconds

The second significant "burst" of signals recorded at 5.5 Mc prior to Project High Water occurred between T+273.6 and T+284.2 seconds. The amplitudes of the fourteen (14) 5.5 Mc spikes ranged from 15.0 db to 35.0 db with thirteen (13) having a value of 17 db or more.

A considerably different noise pattern (compared with the previous case) was observed at the other twelve (12) frequencies monitored. Persistent signals were recorded at four (4) other frequencies (420 Mc, 232.4 Mc, 136 Mc, and 8.9 Mc). Four (4) of the reacting receivers (420 Mc, 232.4 Mc, 136 Mc, and 8.9 Mc) were at the Tech Lab; whereas, the other receiver was located at the FCA Building. Since these two (2) locations are approximately 27 km apart, the probability of a ground-generated noise source being the cause of the response is remote.

Persistent signals were recorded at 232.4 Mc and 136 Mc from T+266 to T+284 seconds. The maximum amplitude of the 232.4 Mc signals was 11 db. The 136 Mc signals consisted of a general enhancement with 6 db and 13 db spikes superimposed.

Persistent signals with sharp spikes were recorded at 420 Mc and 8.9 Mc between T+270 and T+285 seconds. Unfortunately, the recorder was off briefly just after T+270 seconds so that the detailed behavior of the signals at 420 Mc and 8.9 Mc can not be ascertained.

A single sharp 25 Kc pulse (saturation) was recorded at T+284.5 seconds. A similar sharp 420 Kc pulse (saturation) was recorded at T+274 seconds. Some activity was noted at 71 Mc, 20.973 Mc, and 16.8 Mc, but these signals do not appear to be unique. At the other frequencies (200 Mc, 160 Mc, and 1 Kc) no discernable signals were recorded.

The Saturn vehicle was at an altitude of 164 km at T+273 seconds and an altitude of 166 km at T+284 seconds. Thus, the path of the vehicle was almost horizontally through the F_1 layer of the ionosphere. If the vehicle was traversing varying inhomogeneities in the F_1 layer, "noise" emissions would be generated. Only a limited amount of corraborating evidence is available from radar and telemetry data. One radar (station FPS 16 42.16) reported skin track to be noisy to off track between T+277 to T+325 seconds. Cape Tel 2 Telemetry Receiving Station noted signal degredations after T+291.9 seconds (253.8 Mc and 256.2 Mc), but this effect is considered to be due to Project High Water. Hangar D Telemetry Receiving Station noted considerable degredation of the 246.3 Mc signals between T+273.5 and T+275 seconds. The New Smyrna Beach Receiving Station noted considerable attenuation of the 253.8 Mc signals between T+273.4 to T+273.7 seconds.

The 5.5 Mc data indicates that approximately the same number of inhomogeneous regions were encountered between T+273 and T+285 seconds as were encountered between T+164 and T+188 seconds. The attenuation effects of the higher inhomogeneities were not as marked. In the first case, the inhomogeneous regions were between the vehicle and the receiving station (note that the earlier attenuations occurred a number of seconds after the vehicle encountered the inhomogeneities). In the second case, the inhomogeneities may have intervened for only a brief period of time. Another important consideration is the relative orientation of the inhomogeneity with respect to the transmission path. Attenuation effects are severe when the angle between the vector gradient and the transmission path is of the order of 70° to 90°.

The difference in the frequencies of the noise generated by the transit of the vehicle through the upper inhomogeneous regions as compared to the lower altitude case may be due to:

A. A change in the signal generation mechanism.

B. A shift in the frequencies of the emissions.

A change in the signal generation is considered improbable; however, the nature of the gradient may influence the particular frequencies emitted. A shift in the frequencies emitted is considered more probable. If the assumption is made that the amplitudes of the signals generated in the two cases are approximately the same, the data indicates the frequency of the signals recorded by the 5.5 Mc receiver were more nearly that of the receiver. This conclusion is based on the fact that the average amplitude of the spike of the

lower altitude case was 18.4 db compared to 26.9 db in the second case. A shift in frequency could result in a receiver recording one case and not the other particularly if the reception was near the frequency limit of the receiver (e.g., signals were recorded by the 420 Kc receiver for the lower altitude case but not the higher case).

A shift in frequency is compatable with the proposed model. The altitude and the ground tract of the vehicle were substantially different in the two (2) cases (i.e., T+164 to T+188 sec and T+273 to T+285 sec). The changes in altitude and the geographical position would result in the ambient magnetic field having a lower value in the second case compared to the first case.

5.4 NOISE RECORDINGS AFTER PROJECT HIGH WATER

Following Project High Water, a complex physical system was present in the ionosphere. In addition to the 87,400 kg of water released, the Saturn vehicle had been broked into three well-defined sections and a number of smaller ones. Although the visible water-ice cloud persisted for only approximately seven (7) seconds, the water as vapor was still present and expanding through the ionosphere. Also, a fire developed onboard the tankage section of Saturn vehicle. Therefore, the ionosphere was subjected to a variety of perturbations. The expanding water vapor constituted a continual but decreasing perturbation; whereas, the tumbling vehicle parts and the onboard fire were more of an impulse type. Consequently, a complex post-Project High Water noise pattern

is to be expected, and the observed noise will depend to a certain degree on the location of the monitority receivers. This dependency on the observation location is primarily a consequence of attenuation effects of the (High Water) vapor cloud. The monitoring receivers located at the Tech Lab (i.e., 420 Mc, 232.4 Mc, 136 Mc, 8.9 Mc, 71 Mc, and 20.973 Mc) experienced three (3) distinct periods of attenuation. The range times of these attenuations were approximately:

A. T+311 seconds to T+350 seconds

B. T+480 seconds to T+502 seconds

C. T+552 seconds to T+576 seconds

At the other times, most of these receivers showed considerable activity. An overall examination of the records clearly shows that a large number of spikes were present in the noise records during the nonattenuated periods. For example, eleven (11) spikes were observed to have occurred on all six (6) receivers between T+350 seconds and T+460 seconds. These eleven (11) spikes (on all six (6) receivers) in a one hundred ten (110) second interval is to be compared to ten (10) similar spikes observed between T=0 and T+292 seconds. The significance of these spikes (simultaneous) on all six (6) receivers is open to doubt due to the fact that an even greater spike density developed after T+600 seconds. The possibility does exist that these spikes are a consequence of the expansion and interaction of the Project High Water vapors cloud with the ionosphere, but the present data is insufficient to justify any definite conclusions in this regard.

In the post-Project High Water recording, the 5.5 Mc displayed a number of isolated spikes. However, the principal activity consisted of a series of six (6) spikes ranging from 14 db to 25 db during the time interval T+476.2 seconds and T+479.2 seconds. The 25 Kc receiver recorded three spikes (saturation) between T+471 and T+477 seconds. These three (3) 25 Kc spikes constituted the only significant activity between T+440 and T+500 seconds. The 420 Kc recorder saturated at T+478.6 and T+479.5 seconds. Enhanced signals were recorded at 89 Mc (T+465 to T+483 seconds), at 136 Mc (T+463 to T+470, and T+474 to T+483 seconds), and at 232.4 Mc (T+462 to T+483 seconds). Signals were also evident in the records at 20.973 Mc, 71 Mc, and 420 Mc, but these signals do not appear to be significant. No signals were evident in the records at 200 Mc, 160 Mc, and 1 Kc. (The 16.8 Mc receiver was being tuned; thus, the data has no significance.)

5.5 RADAR OBSERVATIONS

An excellent set of records were obtained by Radar Station FPS 16 3.16 (Grand Bahama Island). With the exception of the time interval T+191.5 to T+228 seconds, beacon track was accomplished from T+55 seconds to Project High Water. However, the radar operator classed the beacon performance as "poor" due to the shape of the pulse received.

An analysis of the beacon data indicates that the beacon dropout occurred at T+291.12 seconds. A similar examination of the skin track records shows a distinct change occurred at T+291.25 seconds. This change in the skin track records

persisted until T+302.43 seconds or for approximately ten (10) seconds after the water release. Between T+302.43 and T+309.25 seconds, the skin track records slowly returned to the pre-release conditions.

The FPS 16 3.16 operator made the following description of the radar observations for Project High Water: "After 292 seconds the skin return spread as anticipated over about 10K yds as viewed on the range indicator scope. The radar tracked this cloud for a short period until it dissipated into three well-defined targets and several smaller ones. The radar locked one of these and followed it to the horizon. The radar operator shifted to a couple of the other targets, but they seemed to follow the same trajectory. After completing track on these parts, the area of the trajectory was scanned and some very weak returns observed but not strong enough to track". A report of this quality appears to be an exception rather than the rule.

The FPS 16 3.16 records also provide clear evidence of the rotation of the vehicle part tracked. This rotation rate appeared constant over the time interval T+327 to T+353 seconds. Between T+353 and T+355 seconds, a change in the rotational rate occurred with the rotation being slower after T+355 seconds. This time of change in the rotation rate is precisely the same as obtained from (optical) photographic records. The photographic records displayed a gas jet expanding in the direction of rotation during the time the rotation rate changed. Thus, the radar records confirm that

an impulse was imparted to the vehicle part between T+353 and T+355 seconds.

5.6 WWV ATTENUATION RECORDS

WWV (10 Mc) time signals were recorded as part of the auxiliary data obtained while the ELF-VLF observations were being made (Location: Northwest of Playalinda Beach, Fla.). A total of 3556 seconds of recording at 10 Mc were made prior to Project High Water. Approximately 3264 seconds of the recordings were prior to T=0. This series of observations was initiated at 1630 Z, and three (3) of the observation periods were in excess of 1000 seconds. Reception was generally very good, and just prior to Project High Water (i.e., between 1749 Z and 1750 Z), the propagation conditions were classed as N-5 (no warning and fair conditions).

Only minor fluctuations were observed in the pre-Project High Water WWV records. Following the High Water release, no unusual variations in the WWV reception were noted until 1750:41 Z (i.e., 47 seconds after High Water release). The tick for 1750:41 Z (T+349 sec) was strongly enhanced. This enhanced tick was followed by a complete dropout of the WWV signals. A strongly enhanced tick at 1750:44 Z terminated the dropout. The WWV (10 Mc) receiver behavior between 1750:41 and 1750:44 Z was essentially identical to that during the time WWV was off the air (i.e., between 1745:17 Z and 1749:16 Z) which is the usual hourly quiet period. That is, the receiver rose sharply due to the lack of "quieting" produced by a received signal. A sustained period of

attenuation occurred from 1751:12 to 1751:19 Z (or 78 to 85 seconds after the release) with the maximum attenuation observed at 1751:16 Z (T+374 sec). A brief dropout also occurred between 1751:33.5 and 1751:34 Z. At 1752:49 (or T+471 sec) an attenuation was initiated with a marked attenuation recorded between 1752:53 to 1753:06 Z (179 to 193 sec after the release). A "pulsating" series of attenuations were observed to approximately 1755 Z (approximately 306 seconds after the release). Fluctuations after 1755 Z appeared to be of the same magnitude recorded prior to Project High Water. Observations were continued until just after 1825 Z, but no further significant variations were noted. The broadcast propagation conditions were classed as N-5 in the (WWV) transmission prior to 1820 Z.

It is emphasized that the anomalous behavior of the WWV reception after 1750:41 Z were unlike any of the variations encountered in the 3292 seconds of WWV signals recorded after 1755 Z. In particular, no WWV dropouts were observed other than those following Project High Water. A consideration of the relative locations of the WWV transmitter, the Project High Water cloud, the WWV receiver, and the general behavior of the received signal leads to the conclusion that the anomalous effects are a consequence of the Project High Water cloud acting as a secondary reflection/refraction "surface". When the (reflected/refracted) WWV signals from the Project High Water cloud to the receiver site were out of phase with the "normal" transmission path, cancellation of signals (by superposition) resulted. The

variations of the WWV reception provide a method of estimating the motion of the Project High Water cloud in the latter stages of its existence as a coherent entity.

5.7 EFFECT OF WATER RELEASE ON TELEMETRY SIGNALS

The release of the water in the second Project High Water experiment produced severe attenuations in a number of instances. The specific effects produced depended on the receiver station location and the telemetry frequency. The effects of the water release on telemetry signals are exemplified by the data for 253.8 Mc, 256.2 Mc, and 259.7 Mc (Ref. 9). These data are summarized in Table XI.

Table XI

Telemetry Signal Reception During Project High Water

Receiver Station	Range Time Interval (sec)	% of Signal Above Noise Level
	253.8 Mc	
Cape Tel 2	291.9 - 340	Less than 50
Cape Tel 3	291.9 - 458.8	95 to 100
Vero Beach	291.9 - 459	Less than 50
New Smyrna Beach	291.9 - 400	50 to 75
GBI	291.9 - 458.8	95 to 100
	256.2 Mc	
Cape Tel 2	291.9 - 321	75 to 95
Cape Tel 3	291.9 - 420.4	95 to 100
Vero Beach	291.9 - 420.5	Less than 50
GBI	291.9 - 420.5	95 to 100
	259.7 Mc	
Cape Tel 2	291.9 - 360	No signal
Cape Tel 3	291.9 - 359.8	No signal
Vero Beach	291.9 - 360	No signal
New Smyrna Beach	291.9 - 360	No signal
GBI	291.9 - 359.8	No signal

All stations were reporting excellent signals (i.e., 95 to 100% above noise) just prior to Project High Water for these frequencies (i.e., 253.8 Mc, 256.2 Mc, and 259.7 Mc). In the case of the 259.7 Mc signals, good to excellent signals (75 to 100% above noise level) were observed at three (3) receiving stations (Cape Tel 3, New Smyrna Beach, and GBI) while poor signals (less than 50% above noise) were received at the other two stations (Cape Tel 2 and Vero Beach) after T+360 seconds. The data presented above illustrates the various telemetry signal effects. Comparable effects were also found at the other telemetry frequencies. These data clearly demonstrate that severe telemetry attenuations will be produced by an abort/explosion in the ionosphere or space.

6.0 CONCLUSIONS

The data associated with the second Project High Water experiment has yielded a considerable amount of information concerning the behavior of liquids at reduced pressures and concerning ionospheric inhomogeneities. An unexpected occurrence (at the time of the experiment) was the development of an onboard fire following Project High Water. It has been found that an extensive number of cross correlations existed between the optical data, ELF-VLF spectral data, radar observations, and radio frequency "noise" observations. The analyses of the Project High Water have been combined with the laboratory data on the release of liquids at low pressures and with instrumentation operations analysis for the SA-3 test.

The results of this analysis may be placed in three (3) general categories. These are: the water release and expansion, the onboard fire, and the effects of ionospheric inhomogeneities on telemetry and radar. A number of the conclusions have engineering significance, and these aspects are also presented.

6.1 WATER RELEASE

Water released at an altitude of 165 km (or a pressure of the order of 2.4×10^{-6} torr) rapidly and turbulently expands over an enormous volume. In the second Project High Water experiment 87,414 kg of water were released, and the diameter of the visible cloud created was about 9 km. A substantial portion of the water released was converted into

ice, and extensive cooling of the environ occurred. It is estimated that the ice cloud had a temperature of the order of -110°C (163°K).

In a number of instances the optical data provided evidence of an increase in the density of the ice-cloud as the expansion progressed. This increase in density is believed to be the result of the "condensation" of water vapor on the ice particles. This effect was observed in the laboratory studies. However, its observation in the Project High Water cloud must represent this process occurring with a large number of particles within a small region of the expanding cloud. Thus, the Project High Water cloud displayed comparable behavior with the small scale laboratory studies.

During the initial phases of the expansion, the second Project High Water cloud was highly unsymmetrical. This asymmetry undoubtedly was a consequence of the procedure used to rupture the water tanks. However, the expansion approached greater symmetry as the expansion progressed. Due to the asymmetry and turbulence of the expansion, a considerable variation in the (measured) expansion rate velocities was encountered. The general cloud expansion rate velocities for the initial phases ranged from 0.417 km/sec to 1.83 km/sec with an average value of 1.05 km/sec. However, portions of the cloud displayed much higher expansion rate velocities. The maximum (measured) velocity of a cloud portion was 3.60 km/sec. Evidently the expansion rate decreased as a function of time, but the overall expansion rate velocity (maximum diameter) for the visible cloud was of the order of 0.65 km/sec.

The injection of the water created a large perturbation of the ionosphere. This perturbation produced extensive electromagnetic effects. These effects include both emissions of electromagnetic radiation at selected frequencies and attenuations of transmitted signals. No evidence was obtained of any significant (lightning-like) electrical discharges or other broad bandwidth emissions.

The most significant emissions were spectral in character (i.e., narrow bandwidth). Four (4) spectral lines were found in the ELF-VLF portion of the electromagnetic spectrum at frequencies of 2120 cps, 2140 cps, 2150 cps, and 2210 cps. The behavior of these four (4) spectral lines displayed excellent correlation with events as determined from optical coverage of the water release. Spectral emissions were also observed at 5.5 Mc. These 5.5 Mc emissions are believed to be the fourth harmonic of the electron gyrofrequency. From these spectral emissions, the magnetic field present in the expanding water-ice cloud was calculated to be between 4.97×10^{-5} and 5.05×10^{-5} Weber/m^2 with the preferred value of 4.97×10^{-5} Weber/m^2. While the electromagnetic emissions observed with the release of the water were restricted to a select group of frequencies, the induced ionospheric perturbation resulted in attenuations of electromagnetic transmissions over a wide frequency range (i.e., from 10 Mc to C-band radar). These attenuation effects persisted well beyond the presence of the visible cloud. The attenuation effects of the water perturbation on electromagnetic transmissions were found to have both a directional

and a frequency sensitivity. Radar (C-band) attenuation effects persisted for approximately seventeen (17) seconds with loss of track from between ten (10) to seventeen (17) seconds. The frequency and directional aspects of the (perturbation) attenuation were especially evident from the telemetry records. Degredation of telemetry signals was not experienced at some frequencies (e.g., 253.8 Mc and 256.2 Mc) and at selected receiving stations (Cape Tel 3 and GBI), whereas, loss of signals was experienced at other frequencies (e.g., 249.9 Mc and 259.7 Mc) and at all receiving stations. The time interval of the loss of telemetry signals was up to sixty-eight (68) seconds (e.g., 259.7 Mc).

From an engineering standpoint, the second Project High Water data provides experimental results that are particularly useful for first order estimations of the effects of an abort and/or explosion in space. The second Project High Water experiment clearly demonstrates that the release of substantial quantities of any liquid at reduced pressures will form a "cloud" that expands with a high velocity and produces the extensive cooling effects. (In the case of water, velocities up to 3.61 km/sec were measured, and the temperature was estimated to be $-110^{\circ}C$.) This cloud will also cause telemetry and radar tracking dropouts. The turbulent character of the expansion will result in large concentration gradients to be developed, but it will also cause a mixing of liquid propellants to occur. The asymmetrical expansion demonstrates that the initial rate of mixing (of propellants) will depend on the destruct

procedures employed. The second Project High Water data can also be employed to make first order calculations of pressure effects and the size of the fireball associated with an explosion in the ionosphere or space. It will be necessary to employ a number of scaling factors in order to make the pressure effects and fireball size calculations; however, it is evident that the pressure effects and the fireball size will be considerably different from those associated with a surface of low altitude explosion. In particular, the fireball will be several orders of magnitude larger than a comparable surface explosion.

6.2 ONBOARD FIRE

The combined optical, ELF-VLF and radar data provides conclusive evidence that a fire developed aboard the tankage section of the SA-3 vehicle following Project High Water. Specifically, the optical data considered pertinent was:

A. Glow Color: The color of the glow was that of an oxidizer-deficient hydrocarbon flame.

B. Orientation Angle: The glow is believed to have developed from only one end of the vehicular section, and the glow was recorded with this end at various angles with respect to the cameras.

C. Simultaneous Observations: Simultaneous observations of the glow were recorded by the two (2) widely separated cameras (i.e., at the Tech Lab and Vero Beach which are over 40 miles apart).

D. Change in Tumble Rate: A distinct change in the tumble rate (i.e., from a rotation period of 7.17 sec to 7.92 sec) occurred at Range Time T+355 seconds. This change in tumble rate was associated with a persistent glow. A discontinuous change in the tumble rate

requires an impulse being imparted to the vehicular part.

E. Gas Jet: An examination of the photographs of the glow noted above (D) shows a jet extending in the direction of rotation of the vehicular part. A gas jet would impart an impulse to the vehicular part.

The ELF-VLF spectral data provides further support to the onboard fire. A high degree of correlation was found between changes in the behavior of the ELF-VLF spectra and appearances of the glow. The ELF-VLF spectra also shows that the onboard fire persisted for a considerable length of time beyond the time optical tracking was terminated. The radar data also shows a discontinuous change in the tumble rate at Range Time T+355 seconds. Thus, the radar data directly supports the evidence that an impulse was imparted to the vehicular part at about T+355 seconds. Therefore, the combined optical, ELF-VLF, and radar data definitely eliminates the possibility that the glow was sun glint and shows that the glow was produced by an onboard fire.

6.3 EFFECTS OF IONOSPHERIC INHOMOGENEITIES ON TELEMETRY AND RADAR

Signal attenuations which were found to be associated with the perturbation, synthetically created by the injection of water into the ionosphere, experimentally demonstrate that inhomogeneous regions in the ionosphere can cause degredation of electromagnetic transmissions. Although the water release created a perturbation in the ionosphere, this perturbation, when compared to the surrounding ionospheric regions, was simply an inhomogeneity in the ionosphere. Therefore, if synthetically created, inhomogeneities can cause degredation

of signal transmissions, naturally occurring ionospheric inhomogeneities can produce a similar degredation providing these inhomogeneities are of sufficient size and magnitude. The pre-Project High Water data yielded strong evidence that inhomogeneous regions exist in the ionosphere and that these inhomogeneities are of sufficient size and magnitude to cause degredation of telemetry and radar transmissions.

During the time the SA-3 vehicle was traversing the E-layer of the ionosphere (90 to 115 km), a series of signals were recorded by the 5.5 Mc receiver. The generation of these 5.5 Mc signals are believed to be a consequence of acceleration of electrons in inhomogeneous ionospheric regions (i.e., regions with sharp gradients in the index of refraction). An examination of radar and telemetry records revealed that:

A. Dropouts of signals from the SA-3 vehicle's radar beacon were experienced by all receiving stations either during the time the vehicle was traversing the inhomogeneities or just after the transit was accomplished (i.e., the regions were between the beacon and the receiving stations). There was a time interval of 5.5 seconds where reception of the radar beacon was not achieved by any of the receiving stations.

B. Degredation of telemetry signals were experienced by most of the receiving stations for an extended time interval shortly after the vehicle traversed the inhomogeneities. The attenuations of the telemetry signals depended on the direction and frequency of the transmitted signals.

The striking similarity between the radar and telemetry effects observed after the vehicle had traversed the E-layer of the ionosphere and those produced by the synthetically created inhomogeneity (Project High Water) is considered strong evidence

that the attenuations of the telemetry and radar signals were a consequence of ionospheric inhomogeneities. The 5.5 Mc signals are definitely believed to identify the physical location of the inhomogeneous regions.

Knowledge of the physical causes of anomalous attenuations of telemetry and radar signals is an absolute necessity before improved performance and/or reliability can be achieved. Thus, the Project High Water data yielded the first "controlled" experimental evidence on a physical cause of anomalous ionospheric attenuation effects. In addition, the pre-Project High Water data provides the basis for determining the location of ionospheric inhomogeneities.

The development of techniques and procedures for improved telemetry and radar tracking is one of the critical problems in the development of high performance space vehicles. Data from the second Project High Water experiment provides clear evidence that a cause of radar and telemetry attenuations is inhomogeneities in the ionosphere.

6.4 CONCLUDING COMMENTS

The analyses of Project High Water data put forth in this report is limited in scope primarily because of the data available and the types of available data. This report is general in nature, and its ultimate purpose is to endeavor to put forth those specific events that are of major importance with regard to the overall Project High Water. This report attempts to present the essential features of each significant event in a concise manner. The description of each event

(including relevant data and cross correlations) could easily be expanded into a much more detailed presentation.

Further experiments of the Project High Water type are essential to the development of:

A. An understanding of the phenomena associated with the release of large quantities of liquids into the ionosphere or space.

B. An adequate representation of the ionospheric propagation of electromagnetic transmissions.

The Project High Water type experiments offer one of the best possible procedures for obtaining the required engineering parameters on the behavior of liquids at reduced pressures and in ionospheric propagation of electromagnetic radiation. It is recommended that future experiments of the Project High Water type include studies:

A. With various volumes of liquids.

B. With other types of liquids (e.g., JP-4, LOX, etc.).

C. At other altitudes (i.e., both lower and higher than those already performed).

The recommended experimental effort is technologically feasible, and the data obtained from this effort will materially contribute to the solution of problems encountered in space.

This analysis of the second Project High Water data has shown the desirability for additional instrumentation to be employed in future Project High Water type experiments. Specifically, the instrumentation should include the following:

A. Temperature probes in the vicinity of the tanks containing the liquids.

B. Additional RF electromagnetic observations at spectral frequencies (e.g., harmonics of electron gyrofrequency).

C. Wide angle of view photographic coverage of the event.

The scientific importance and engineering value of the data that can be obtained from fully instrumented Project High Water type experiments should not be underestimated.

REFERENCES

1. Saturn Flight Evaluation Working Group, "Saturn SA-3 Flight Evaluation", MPR-SA7-63-1.

2. D. D. Woodbridge, R. A. Knezek, and J. B. Temple; "Ionospheric Water Dumping", Vought Astronautics Report No. 00.35, Feb. 5, 1962.

3. J. A. Lasater; "Dispersal of Liquids in the Upper Atmosphere", Vought Astronautics Report No. 00.54, 16 May 1962.

4. J. A. Lasater; "Radiation from Plasmas", International Space Corporation Report No 00.03, 13 March 1963.

5. D. D. Woodbridge, J. A. Lasater, and R. E. Clark; "ELF-VLF Spectral Radiation Associated with the SA-3 Launch Operation", ISC Report No. 01.01 Contract NAS 10-468, 18 June 1963.

6. J. A. Lasater, D. D. Woodbridge and R. E. Clark; "ELF-VLF Spectral Radiation Associated with the SA-4 Launch Operation", ISC Report No. 01.02 Contract NAS 10-468 8 Aug 1963 (Conf.).

7. J. A. Lasater, D. D. Woodbridge, R. E. Clark, and B. M. Fultz; "ELF-VLF Spectral Radiation Associated with the MA-9 Launch Operation", ISC Report No. 01.03 Contract NAS 10-468 29 Aug 1963 (Conf).

8. J. E. Drummon; "Plasma Power Absorption" Symposium of Plasma Dynamics, 293-353 Addison-Wesley, Reading, Mass. (1960).

9. N. F. Hines; "Instrumentation Operations Analysis Part 11b of the Firing Test Report Saturn Vehicle SA-3", NASA LOC Report LTR-1-8.2.b December 18, 1962.

APPENDIX "A"

THE TV CAMERA SYSTEM

Mr. Walter H. Manning, Jr. of the Air Force Missile Test Center used an Image Orthicon tube coupled with a long focal-length telescope to obtain data during the flight of Saturn vehicle SA-3. Thus, he obtained a series of pictures of the Project High Water cloud as shown in Figures 8 through 10 of the text. This system also produced data that assisted in determining the existence of the onboard fire following the water release.

Development of the TV telescope grew out of an investigation into how the detection sensitivity and resolution capability of the ultra-sensitive image orthicon TV tube could be applied to the detection, acquisition, and tracking of space vehicles. Recording high-resolution images of orbiting space vehicles with long focal-length optics is difficult due to tracking errors and atmospheric turbulence. Electronic image intensification, which gives an effective exposure index of the order of 10^4 has greatly enhanced the probability of obtaining clear images under the above conditions by allowing short exposures. Light from an object is focused on the photocathode of the image orthicon.

The image orthicon photocathode is biased with a negative voltage with respect to the target-mesh combination. Photoelectrons are ejected from the photocathode in proportion to the light intensity variations contained in the original image. These electrons are accelerated toward

the target by the electric field due to the potential differences of the photocathode (-300 to -500 v) and the target-mesh combination which is near ground potential.

The photoelectrons are electrically focused onto the target in the same relationship as in the original image which appeared on the photocathode. When the electron hits the target, secondary electrons (the number depends on the secondary emission efficiency of the target film) are emitted from the target and are conducted to ground by a wire mesh screen close to the target. The target is a very thin film usually MGO in ultra-sensitive orthicons, which has a very high resistance in the plane of the target (side to side) and a very high conductivity through the target.

At this point, a replica of the original image exists in the form of an effective positive charge on the target, the magnitude of the charge being proportional to the brightness of the image at that point and the secondary-to-primary gain of the target material. A low-velocity electron beam scans the target and neutralizes this positive charge, and the electron beam is turned around by suitable fields and returns to an electron multiplier system of dynodes which amplifies the return-beam current variations. This becomes the video output signal for the closed-loop TV system. Hence the video signal consists of a beam current which is reduced in magnitude in proportion to the original light intensity.

The orthicon's resolution capabilities can be explored by target under-scanning, which, in fact, places more scan

lines across a smaller portion of the target at the expense of narrowing the field of view, since the whole target is no longer being scanned. Such experiments clearly show that the orthicon's resolution increases in direct proportion to the under-scan ratio. Ratios of three to one (with an 875-line system) indicate that resolution upward of 2500 lines can be expected.

A 1000-line resolution system has the equivalent resolution of 200 line-pairs/mm while 2500 lines yield 50 line-pair/mm. These resolutions are comparable to film ASA with ratings of 800 to 200.

Since the orthicon has approximately 1000 times the sensitivity of such films, image information that requires greater resolution can be recorded by increasing the focal length, thereby producing a larger but less bright image. This decrease in brightness is more than compensated for by the tremendous sensitivity of the image orthicon.

To overcome image motion due to tracking errors and to circumvent possible image smear by wave-front distortion due to atmospheric turbulence, the TV system was coupled to a 24-in. aperture, 240-in. focal-length Gregorian telescope. The telescope and associated TV system is shown in Figures A1 and A2.

The telescope was equipped with a relay lens system to provide variable focal lengths from 240 to 2400 in. The TV system is capable of resolving approximately 30 TV lines/mm

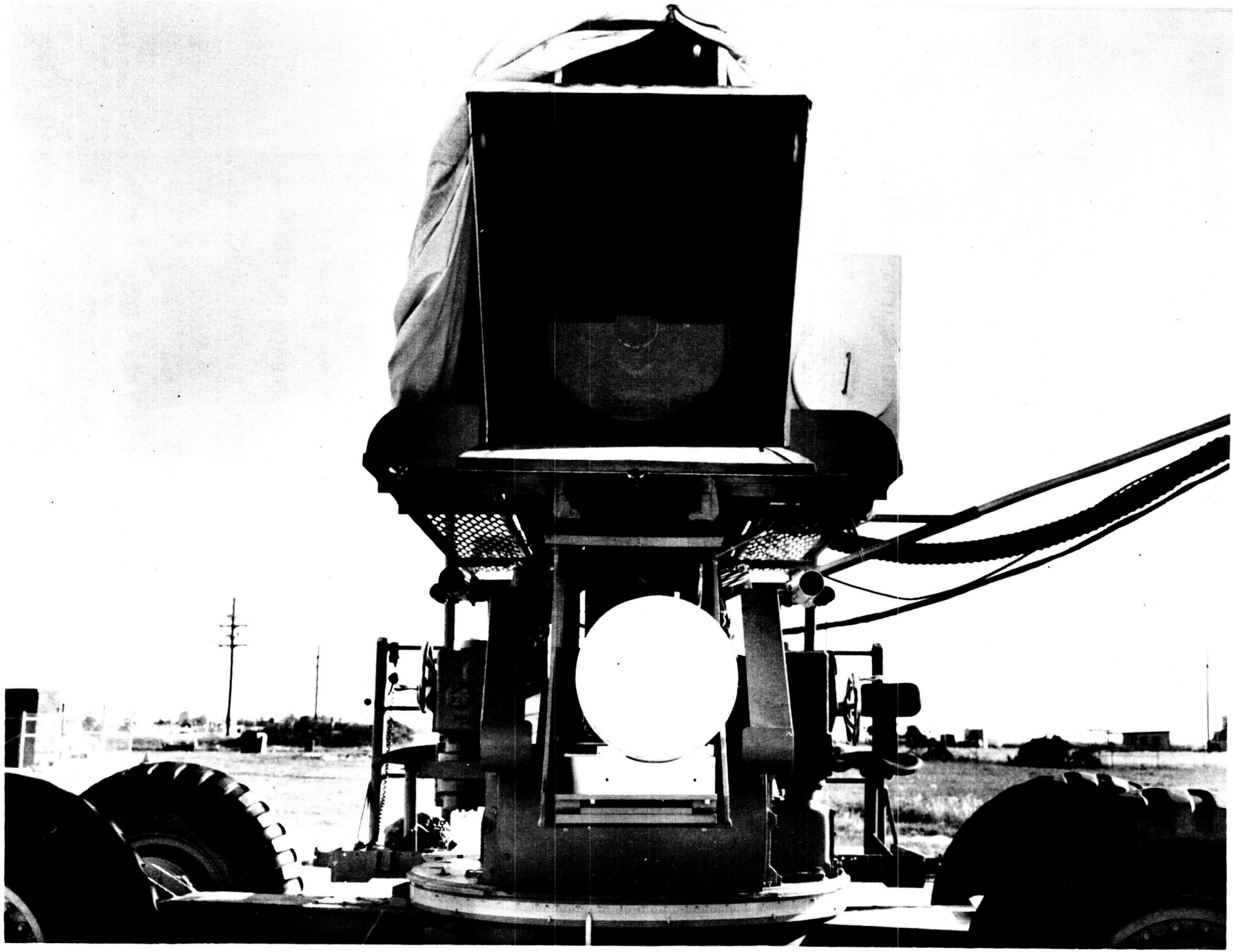

Figure A2: Front View of Telescopic TV Camera System

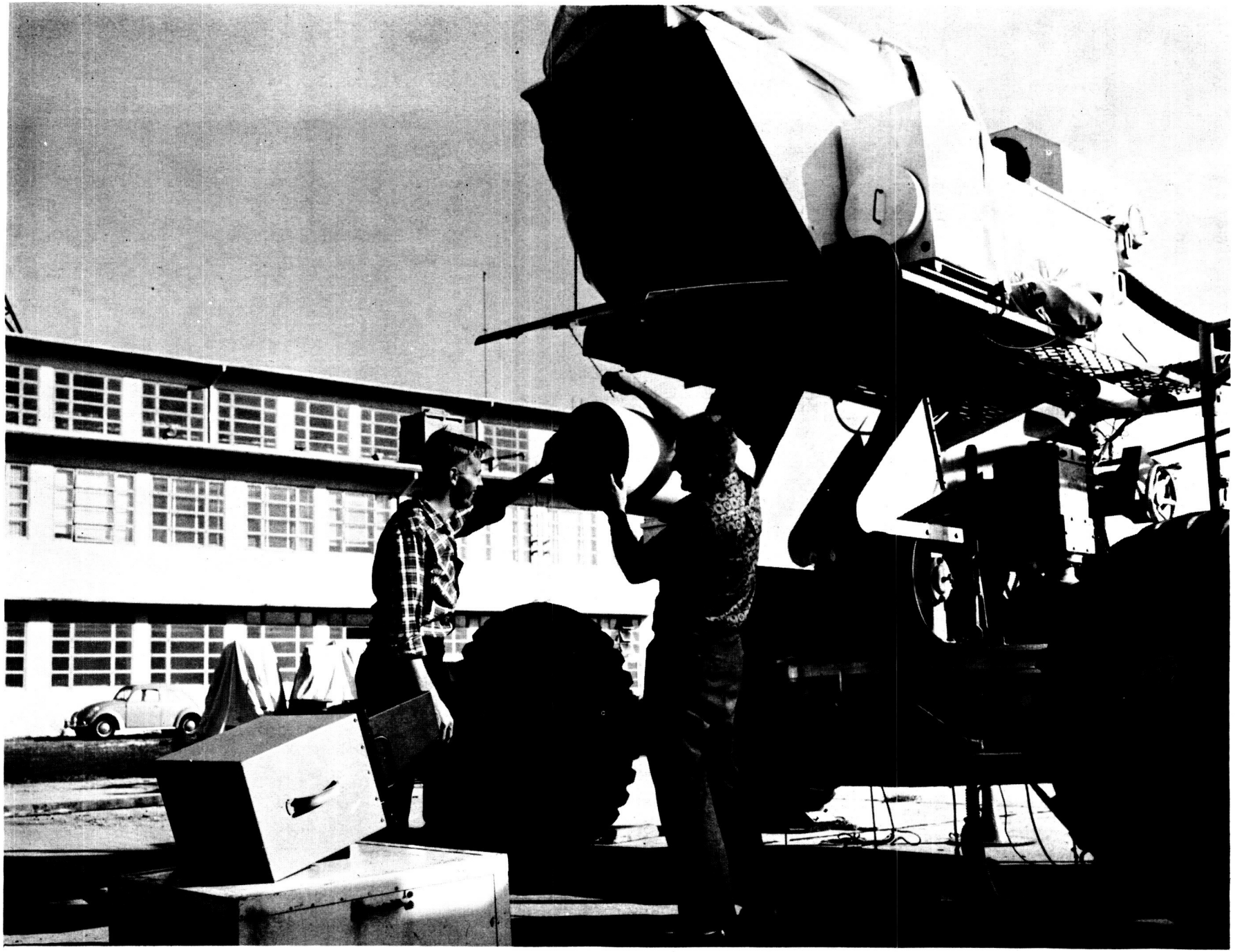

Figure A1: Oblique View of Telescopic TV Camera System

on a 1.12 by 0.84-in. format at the target of the image orthicon. Permanent recording of the image produced on a TV monitoring screen is made with a high-quality 35-mm motion picture camera synchronized to the TV scan of 30 frames/sec. The television scans at 875 lines (interlaced) at 30 frames/sec.

Additional information on the capabilities of the telescopic TV Camera System have been presented in the literature (e.g., W. H. Manning, Jr. "The TV Telescope" Astronautics and Aerospace Engineering, pp 36-40, July 1963).

REFERENCES

1. Saturn Flight Evaluation Working Group, "Saturn SA-3 Flight Evaluation", MPR-SA7-63-1.

2. D. D. Woodbridge, R. A. Knezek, and J. B. Temple; "Ionospheric Water Dumping", Vought Astronautics Report No. 00.35, Feb. 5, 1962.

3. J. A. Lasater; "Dispersal of Liquids in the Upper Atmosphere", Vought Astronautics Report No. 00.54, 16 May 1962.

4. J. A. Lasater; "Radiation from Plasmas", International Space Corporation Report No 00.03, 13 March 1963.

5. D. D. Woodbridge, J. A. Lasater, and R. E. Clark; "ELF-VLF Spectral Radiation Associated with the SA-3 Launch Operation", ISC Report No. 01.01 Contract NAS 10-468, 18 June 1963.

6. J. A. Lasater, D. D. Woodbridge and R. E. Clark; "ELF-VLF Spectral Radiation Associated with the SA-4 Launch Operation", ISC Report No. 01.02 Contract NAS 10-468 8 Aug 1963 (Conf.).

7. J. A. Lasater, D. D. Woodbridge, R. E. Clark, and B. M. Fultz; "ELF-VLF Spectral Radiation Associated with the MA-9 Launch Operation", ISC Report No. 01.03 Contract NAS 10-468 29 Aug 1963 (Conf).

8. J. E. Drummon; "Plasma Power Absorption" Symposium of Plasma Dynamics, 293-353 Addison-Wesley, Reading, Mass. (1960).

9. N. F. Hines; "Instrumentation Operations Analysis Part 11b of the Firing Test Report Saturn Vehicle SA-3", NASA LOC Report LTR-1-8.2.b December 18, 1962.